

SYNTHESIS AND NITROGEN DOPING OF GRAPHENE BY CHEMICAL VAPOR DEPOSITION

**A Thesis Submitted to
Graduate School of Engineering and Sciences of
İzmir Institute of Technology
in Partial Fulfillment of the Requirements for the Degree of
MASTER OF SCIENCE
in Materials Science and Engineering**

**by
Alper YANILMAZ**

**May 2017
İZMİR**

We approve the thesis of **Alper YANILMAZ**

Examining Committee Members:

Assoc. Prof. Dr. Cem ÇELEBİ

Department of Physics, İzmir Institute of Technology

Assist. Prof. Dr. Gökhan UTLU

Department of Physics, Ege University

Assist. Prof. Dr. Mehmet Z. BAYKARA

Department of Mechanical Engineering, Bilkent University

31 May 2017

Assoc. Prof. Dr. Cem ÇELEBİ

Supervisor, Department of Physics,
İzmir Institute of Technology

Assist. Prof. Dr. Umut ADEM
Co-Supervisor, Department of
Material Science and Engineering,
İzmir Institute of Technology

Prof. Dr. Mustafa Muammer DEMİR

Head of the Department of Materials
Science and Engineering

Prof. Dr. Aysun SOFUOĞLU

Dean of the Graduate School of
Engineering and Sciences

ACKNOWLEDGEMENTS

Firstly, I would like to thank my parents for all their patience and support through the whole process of my study.

I would like to thank my advisor Assoc. Prof. Dr. Cem Çelebi for all his help, patience and detailed reviewing all of my study.

I would like to express my appreciations to the committee members of my thesis Assist. Prof. Dr. Gökhan Utlu and Assist. Prof. Dr. Mehmet Z. Baykara for their participation.

I would like to acknowledge and thank all of my colleagues and friends who helped me through the whole process of my study. Especially, I would like to thank Hasan Aydın for KPFM measurements and also Elif Özçeri for XPS measurements. I would also like to thank to Hasan Aydın, Elif Özçeri and Ozan Arı for their help in CVD setup. I would like to thank to Assist. Prof. Dr. Hadi M. Zareie and Aysel Tomak for STM/STS measurements. I would like to thank Barış Akbalı, Cihan Bacaksız and Assoc. Prof. Dr. Hasan Şahin for their great contributions and theoretical calculations.

I would like to give my dearest thanks to all of my friends and colleagues who helped me through my study with their collaborations and gave me motivation with their kind friendships. Thanks for being a second family to me.

I would like to thank to Dilce Özkendir who always supported and encouraged me through this whole process.

I wish to acknowledge AQuReC facilities at IZTECH for XPS and Raman measurements. In addition, I would like to thank TUBITAK and IRMAM for financial and technical support.

A special mention goes to my late advisor, Assoc. Prof. Dr. Yusuf Selamet who always believed in me. Without his support and guidance, I would never have been able to complete this study. To him I dedicate this thesis.

ABSTRACT

SYNTHESIS AND NITROGEN DOPING OF GRAPHENE BY CHEMICAL VAPOR DEPOSITION

Controllable carrier transport due to charged impurities in the graphene lattice is still lacking. Doping of graphene by foreign atoms leads to modify its band structure and electro chemical properties. Among numerous potential dopants, nitrogen (N_2) is considered to be an excellent candidate to form strong valence bonds with carbon atoms, which would provide n or p-doping according to bonding character of charged-impurity atom. Exposure of graphene lattice to nitrogen gas leads to a change in the carrier concentration and opens a bandgap due to symmetry breaking. Furthermore, this seems to be an effective way to customize the properties of graphene and exploit its potential for various applications.

This thesis focuses on the growth of graphene by low pressure chemical vapor deposition (LPCVD) and doping it with N_2 by using N_2 plasma treatment. Here, copper foil was used as the catalytic substrate to grow large area graphene at LPCVD system. The grown graphene was transferred onto SiO_2 , Au (111) and Sapphire substrates. The effect of different plasma time and power on doping process was investigated while keeping the N_2 flow rates constant by using N_2 plasma. The nitrogen doped graphene (N-graphene) was characterized via Raman Spectroscopy, X-ray photoelectron spectroscopy (XPS), scanning tunneling microscopy/spectroscopy (STM/STS), Kelvin probe force microscopy (KPFM). Raman mapping of N-graphene was also conducted to show the homogeneity of N_2 incorporation into graphitic lattice. STM results were theoretically modelled by using density functional theory (DFT). Our results provide the opportunity to produce N-graphene with homogenous and effective doping which would be valuable in electronic and optoelectronic applications.

ÖZET

KİMYASAL BUHAR BİRİKTİRME İLE GRAFENİN SENTEZLENMESİ VE AZOT İLE KATKILANMASI

Grafen örgüsünde yüklü safsızlıklar ile kontrol edilebilir elektriksel taşınım hala sağlanamamaktadır. Grafenin yabancı atomlar ile katkılanması bant yapısının ve elektrokimyasal özelliklerinin değişmesine neden olur. Karbon atomu ile aralarında güçlü valens bağı oluşturması ve bu yüklü safsızlıkların bağ karakterine göre grafeni hem n hem de p tipi katkılayabilmesi, nitrojenin birçok potansiyel katkılayıcı arasından mükemmel bir aday olmasını sağlamıştır. Bir grafen örgünün nitrojen gazına maruz kalması, taşıyıcı konsantrasyonunda değişikliğe ve simetrisinin bozulmasından dolayı bant aralığının açılmasına neden olmaktadır. Ayrıca bu yöntem sayesinde, grafenin özelliklerini ihtiyaca göre uyarlamak ve potansiyelinden farklı şekilde yararlanmak mümkündür.

Bu tezde, grafenin kimyasal buhar biriktirme yöntemi ile büyütülmesine ve azot plazma ile katkılanmasına odaklanılmıştır. Düşük basınçlı kimyasal buhar biriktirme sisteminde geniş alanlı grafen üretmek için katalitik alt katman olarak bakır levha kullanılmıştır. Üretilen grafen, SiO₂/Si, Au (111) ve Safir alt katmanlara transfer edilmiştir. Nitrojen plazma sistemi ile, nitrojen gazı akış oranı sabit tutularak farklı plazma gücü ve zamanının katkılama sürecine etkisi araştırılmıştır. Nitrojen ile katkılanan grafen (N-grafen) Raman spektroskopisi, X-ışını fotoelektron spektroskopisi (XPS), taramalı tünelleme mikroskopisi/spektroskopisi (STM/STS), Kelvin probe kuvvet mikroskopisi (KPFM) kullanılarak karakterize edilmiştir. Aynı zamanda N-grafenin Raman haritalandırması ile grafitli örgüdeki nitrojen homojenliği de araştırılmıştır. STM sonuçları, yoğunluk fonksiyoneli teorisi kullanılarak kuramsal olarak da modellenmiştir. Elde edilen sonuçlar, etkili ve homojen bir şekilde katkılanan N-grafenin, elektronik ve optoelektronik uygulamalarda kullanılmasına olanak sağlamaktadır.

TABLE OF CONTENTS

LIST OF FIGURES	viii
LIST OF TABLES.....	xii
LIST OF ABBREVIATIONS.....	xiii
CHAPTER 1. INTRODUCTION	1
1.1. What is Graphene ?	1
1.2. Crystal Structure of Graphene	3
1.3. Properties of Graphene	4
1.3.1. Electronic Properties of Graphene	4
1.3.2. Vibrational Properties of Graphene	7
1.3.3. Other Properties of Graphene	8
1.4. Graphene Production Methods	9
1.4.1. Mechanical Exfoliation.....	10
1.4.2. Thermal Decomposition of SiC	11
1.4.3. Chemical Vapor Deposition.....	12
1.5. Doping of Graphene.....	15
1.5.1. The Production of N-doped Graphene.....	17
CHAPTER 2. CHARACTERIZATION TECHNIQUES.....	19
2.1. Optical Microscopy.....	19
2.2. Raman Spectroscopy.....	20
2.3. X-Ray Photoelectron Spectroscopy	24
2.4. Scanning Tunneling Microscopy and Spectroscopy.....	26
2.5. Kelvin Probe Force Microscopy	27
CHAPTER 3. EXPERIMENTAL.....	29
3.1. Materials	29
3.2. Sample Preparation	29
3.2.1 Synthesis of Large Area Graphene by CVD.....	29
3.2.2 Graphene Transfer Procedure	33

3.2.3 Nitrogen Plasma Treatment of Graphene	34
CHAPTER 4. RESULTS AND DISCUSSION.....	36
4.1. Characterization of CVD grown Graphene	36
4.1.1. Optical Microscopy and Raman Spectroscopy Results	36
4.2. Characterization of N-doped Graphene	44
4.2.1. Raman Spectroscopy Results.....	44
4.2.2. XPS Results	50
4.2.3. STM-STs Results	52
4.2.4. Methodology of DFT Simulations.....	56
4.2.5. Kelvin Probe Force Microscopy (KPFM) Results.....	58
CHAPTER 5. CONCLUSIONS	62
REFERENCES	64

LIST OF FIGURES

<u>Figure</u>	<u>Page</u>
Figure 1. Representation of some carbon allotropes: (a) 3D graphite (side view), (b) 2D graphene, (c) 1D carbon nanotubes, and (d) 0D carbon fullerenes (top view), respectively ⁸	2
Figure 2. Schematic illustration of sp^2 hybridization in graphene unit cell.....	3
Figure 3. (a) Unit cell and (b) Brillouin zone of graphene ²⁰	4
Figure 4. (a) 3D and (b) 2D display of energy band structure of graphene in the 1 st BZ ²⁴ . The three most symmetrical points (Γ , K and M) are noted.....	6
Figure 5. (a) Atomic motions of C atoms in graphene can be along the out-of-plane (Z), in-plane transverse (T), and in-plane longitudinal (L) direction. (b) The phonon dispersion branches for a graphene sheet, plotted along high symmetry directions ²⁹ . The phonon frequency versus the momentum space representation of the dispersion relation of out-of-plane modes (c) and in-plane modes (d) of graphene ³⁰	8
Figure 6. Schematic representation for the mechanical exfoliation of graphene from graphite using Scotch tape ³⁷	11
Figure 7. Schematic illustration of the graphene growth by thermal decomposition of SiC ³⁸	12
Figure 8. Schematic illustration of CVD set up for the graphene synthesis ⁴⁵	13
Figure 9. Different crystalline orientation of Cu surface after annealing procedure, as mapped by the EBSD ⁵²	14
Figure 10. Schematic diagram of a N-graphene ⁹²	17
Figure 11. Schematic representations of (a) direct synthesis ¹⁰² (b) post treatment methods ⁷² used in production of N-graphene.....	18
Figure 12. Optical image of the exfoliated graphene layers on SiO ₂ (~290 nm)/Si substrate ¹⁰⁶	19
Figure 13. (a) Optical microscope images of graphene domains on Cu foil and (b) Raman spectra of graphene collected from different Cu faces. The fluorescence effect caused by Cu was subtracted from total spectra ¹⁰⁸	20
Figure 14. Schematic diagram of the energy transitions including Rayleigh, Stokes and Anti-Stokes scattering processes.....	21

Figure 15. (a) Phonon dispersion relation and main Raman peaks of graphene which are corresponding to these phonon modes. Raman spectra of (b) pristine and (c) damaged or defect induced graphene with Raman active bands ¹¹²	22
Figure 16. Illustration of the main Raman processes in defect induced graphene. (a) D band (peak) double resonant process containing a scattering from a defect (horizontal dotted line), (b) G band (d) G' band engendered through a second-order process that is either double resonant or triple resonant, (c) and (f) two intra-valley double resonance Raman bands, 2D'and D' ¹¹² . Here 'q and d' stands for the magnitude of the phonon and defect wave vector, respectively.....	23
Figure 17. The XPS measurements of (a) C1s peaks of N-graphene and pristine graphene, (b) N1s peak of N-graphene and (c) schematic structure of N-graphene ⁷¹	25
Figure 18. (a) Large-scale STM topographic image of graphitic N dominated graphene on Cu foil showing the presence of pointlike N dopants (Vbias = - 0.015 V, Iset = 0.3 nA), (b) High-resolution STM image of graphitic N dopant (Vbias = - 0.015 V, Iset = 0.3 nA), (c) Large-scale STM topographic image of pyrrolic N dominated graphene on Cu foil (Vbias = - 0.02 V, Iset = 0.3 nA) and (d) High-resolution STM image of pyrrolic N dopant (Vbias = - 0.02 V, Iset = 0.3 nA) ¹²⁶	26
Figure 19. Band diagram of tip and sample in KPFM, V.L. represents the vacuum level.....	28
Figure 20. A picture of LPCVD setup at the department of Physics, IZTECH.....	30
Figure 21. Heating (1), annealing (2), growth (3) and cooling (4) stages of graphene growth process on Cu foil with schematic representations by LPCVD.	30
Figure 22. Graphene growth scheme under ethylene atmosphere and its associated formation mechanisms ⁴⁹	31
Figure 23. Schematic illustration of the graphene transfer procedure.....	33
Figure 24. (a) Representation of N ₂ plasma process, (b and c) schematic illustrations of N doping on graphene lattice.	35
Figure 25. Change in grain size and formation based on different annealing temperatures; (a) 700 °C, (b) 850 °C and (c) 990 °C viewed by using 10x optical microscope.....	37

Figure 26. (a) and (b) Raman Spectra of graphene samples which were grown at different temperatures on Cu foil, (c-e) represents the center positions and FWHM values of fitted G' peaks of samples.....	39
Figure 27. (a) and (b) Raman Spectra of graphene samples which were grown for different growth time on Cu foil, (c-e) represents the center positions and FWHM values of fitted G' peaks of samples.....	40
Figure 28. (a) and (b) Raman Spectrum of graphene samples which were grown for different growth time on Cu foil, (c-e) represents the center positions and FWHM values of fitted G' peaks of samples.....	42
Figure 29. (a) Optical image and (b-c) Raman spectra of pristine graphene on Cu foil after optimizing of the growth parameters. Circles indicate where the Raman spectra were collected.	43
Figure 30. (a) Optical image and (b) Raman spectra of pristine graphene on SiO ₂ substrate. As shown with black circle, greeny particles represent FeCl ₃ residues and white circles indicate where the Raman spectra were collected.	45
Figure 31. Raman spectra of N-graphene doped with different plasma times. The duration of plasma doping was varied between 5 and 79 min.	46
Figure 32. Raman spectra of N-graphene doped with different plasma powers. The intensity ratio of characteristics peaks was enclosed herewith.	47
Figure 33. (a) Raman spectra of pristine graphene (GRP) and N-graphene (NGRP). Images (b), (c) and (d) show the Raman mapping of I _G /I _G , I _D /I _D and I _D /I _G of NGRP on SiO ₂ /Si substrate with the selected region of 20 μm x 20 μm, respectively. N doping parameters: N ₂ gas flow 10 sccm, effective RF-Power 10 W, plasma time 15 min, N ₂ pressure 890 mTorr.	48
Figure 34. Raman spectra of N-graphene doped with different plasma powers and plasma times.....	50
Figure 35. The XPS measurements of C1s and N1s band in N-graphene films on SiO ₂ /Si treated by N ₂ plasma during (a-b) 15 min with RF-power of 10 W and (c-d) 20 min, with RF-power of 7W, respectively. The N ₂ gas flow rate at plasma chamber was kept constant as 10 sccm.	51

Figure 36. STM images of graphene (a-b) and N-graphene (c-f) on Au (111) substrate. In Figure f, simulated N and C atoms are shown as black and white colors, respectively. The STM images were recorded under constant-current mode with bias voltage varying between 25 and 70 mV and a 1 nA tunneling current.....	53
Figure 37. STS curves of (a) pristine and (b) N-graphene, respectively.	54
Figure 38. dI/dV characteristics of pristine (red line) and N-graphene (blue line) on Au (111).	55
Figure 39. (a, d) The top and side views, (b, e) the energy band structure, and (c, f) density of states of N substituted and N adsorbed graphene, respectively. ...	57
Figure 40. Surface potential differences of graphene (GRP) and N-graphene (NGRP) with various doping parameters. N-graphene films on SiO ₂ /Si treated by N ₂ plasma during (red color) 15 min with RF-power of 10 W and (blue color) 20 min with RF-power of 7W, respectively. The N ₂ gas flow rate at plasma chamber was kept constant as 10 sccm. HOPG (green color) is used as reference	60

LIST OF TABLES

<u>Table</u>	<u>Page</u>
Table 1. Properties of graphene obtained by different methods ³⁵	10
Table 2. Graphene growth parameters on Cu foil by LPCVD.....	32
Table 3. Growth parameters of N-graphene.	34
Table 4. Average Raman peak analysis of N-graphene.....	49
Table 5. The values of mean CPD and mean Φ	60

LIST OF ABBREVIATIONS

CPD	Contact Potential Difference
CVD	Chemical Vapor Deposition
DFT	Density-Functional Theory
DOS	Density of States
FFT	Fast Fourier Transform
FLG	Few Layer Graphene
FWHM	Full Width at Half Maximum
HOPG	Highly-Oriented Pyrolytic Graphite
KPFM	Kelvin Probe Force Microscopy
LPCVD	Low Pressure Chemical Vapor Deposition
MLG	Multilayer Graphene
NGRP	Nitrogen Doped Graphene
PR	Photoresist
RF	Radio-Frequency
SiC	Silicon Carbide
SLG	Single Layer Graphene
STM	Scanning Tunneling Microscope
STS	Scanning Tunneling Spectroscopy
XPS	X-Ray Photoelectron Spectroscopy

CHAPTER 1

INTRODUCTION

1.1. What is Graphene ?

Since its experimentally discovered by Geim and Novoselov in 2004¹⁻², graphene has become hot topic for researchers in material science and physics³⁻⁴. The word graphene is derived from the word graphite and the suffix -ene which is used for polycyclic aromatic hydrocarbons like ferrocene, anthracene and benzene⁵. Thus, graphene refers to one-atomic layer thick material that carbon (C) atoms are sp^2 bonded and densely packed into two-dimensional (2D) honeycomb lattice, namely a single layer of graphite.

Graphene sheets are comprised of C atoms connected in hexagonal shapes with each C atom covalently bonded to three other C atoms. Since C is an incredibly versatile element, depending on how atoms are arranged they can combine easier with themselves to form allotropes⁶. Depending on nanoscale range (<100 nm), carbon materials can be examined as zero-dimensional (0D), one-dimensional (1D), two dimensional (2D) and three-dimensional (3D)⁷. For instance, when graphene sheet is wrapped up; fullerenes (0D) and when it rolled into cylindrical shape carbon nanotubes (1D) are formed. The multilayered graphene sheets are also named as graphite (3D) (Figure 1). The separation of C atoms in graphene is 0.142 nm and in graphite, individual graphene layers are bounded weakly from one another with separation of 0.335 nm.

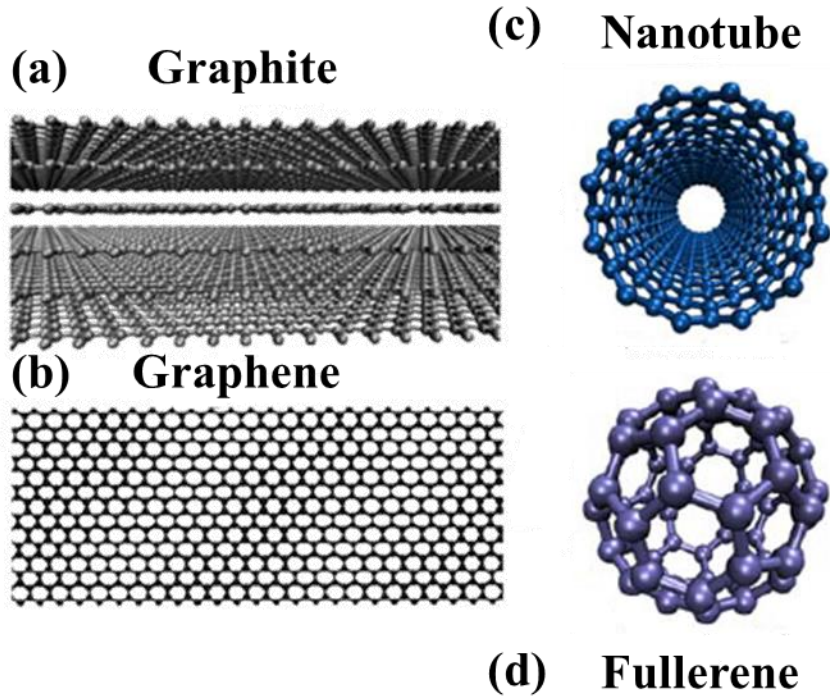


Figure 1. Representation of some carbon allotropes: (a) 3D graphite (side view), (b) 2D graphene, (c) 1D carbon nanotubes, and (d) 0D carbon fullerenes (top view), respectively ⁸.

Graphene has honeycomb lattice structure that can be thought of two equivalent triangular sub-lattices A and B with inversion symmetry and corresponding energy bands of them coincide at zero energy at Dirac points; K points of reciprocal lattice. The velocity of the electrons near K point is 10^6 m/s and the dispersion relation near Dirac points is linear which is similar to a system of relativistic particles with zero effective mass. Thus, due to the zero band-gap, graphene is called as zero band gap semiconductor or semimetal. When the number of the graphene layers increase, the energy bands start to overlap and gap is occurred. For instance the overlap between energy bands is 1.6 eV for bilayer graphene ⁹. This consideration gives a very small band overlap but at larger energies the bilayer graphene can be treated as the gapless semiconductor ¹⁰. Due to its sp^2 hybridization and one atom thickness, graphene breaks so many records in terms of electrical ¹¹, optical ¹², thermal ¹³ and mechanical ¹⁴ properties. At room temperature graphene also has anomalous quantum Hall effect and charge carrier mobility ($\sim 230,000$ cm²/Vs) in graphene is extremely high than in silicon ¹⁵⁻¹⁶.

Since it has such unique properties mentioned above, graphene is very convenient for especially in field-effect transistor, capacitor, energy storage, ultrafiltration, sensor and photovoltaic applications. Another use area of graphene is optical electronics. Since graphene has highest transparency and flexibility, it can be used instead of indium tin oxide (ITO) in photovoltaic, liquid crystal displays (LCDs) and organic light emitting diodes (OLEDs) ¹⁷.

1.2. Crystal Structure of Graphene

As mentioned previously, graphene consists of sp^2 -bonded C atoms that are intensely packed in a hexagonal shaped crystal lattice. A neutral C atom has a total of six electrons, but not all six electrons are located in the same energy level. Two of them are located in the first (inner) shell, while the remaining four are located in the second (outer) shell with an electron configuration of $1s^2 2s^2 2p^2$. In outer shell, valence electrons are filling the s electrons and 3p states where 3p electrons can be specified as p_x , p_y and p_z . In graphene, the sp^2 bonding is occurred with the hybridization of s electron with two p_x and p_y electrons in 2D ¹⁸. Bonding between the p_x and p_y electron is called σ bonding and p_z electrons is called π bonding. The angle between sigma bonds is 120° which takes the form of hexagonal structure. Due to the strong covalent bonding of sigma bonds, graphene has excellent mechanical stiffness ($\sim 130\text{GPa}$) ¹⁹.

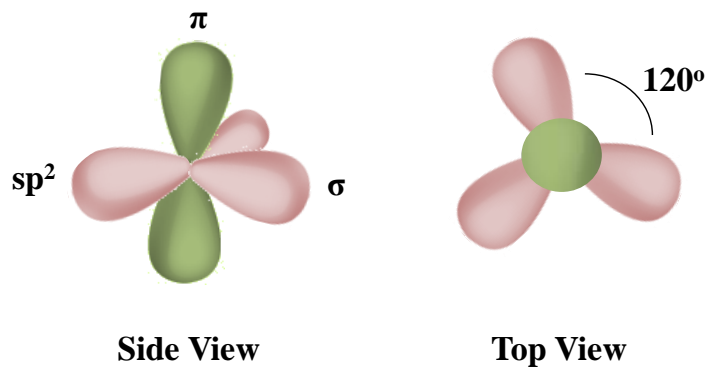


Figure 2. Schematic illustration of sp^2 hybridization in graphene unit cell.

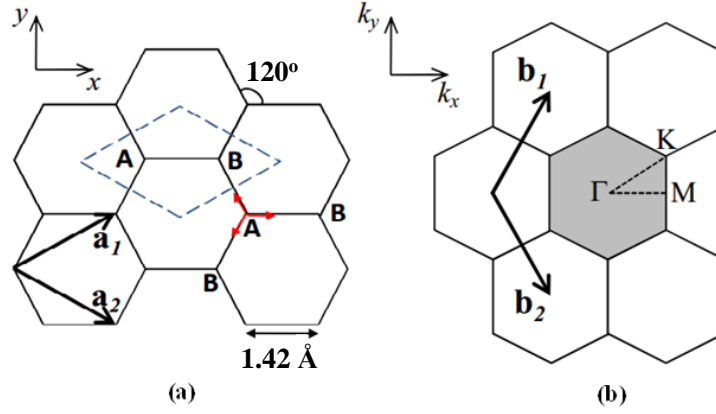


Figure 3. (a) Unit cell and (b) Brillouin zone of graphene²⁰.

1.3. Properties of Graphene

1.3.1. Electronic Properties of Graphene

Graphene's unique electronic properties are explained by tight binding theory²¹. According to this theory, the graphene lattice consists of two equivalent sub lattices of C atoms. The unit cell of the graphene has two atoms A and B. As shown in Figure 3a, \vec{a}_1 and \vec{a}_2 are the basis vectors of the real space crystal structure where $\vec{a}_1 = (1, \sqrt{3})\mathbf{a}_0$ and $\vec{a}_2 = (-1, \sqrt{3})\mathbf{a}_0$ in which \mathbf{a}_0 is the lattice constant of 2.46 Å. Reciprocal space also has hexagonal structure with the vectors of \vec{b}_1 and \vec{b}_2 . Due to the relation of $\mathbf{a}_i \cdot \mathbf{b}_i = 2\pi$;

$$\mathbf{b}_1 = 2\pi/\mathbf{a}_1 = 2\pi/\sqrt{3}\mathbf{a}_0 (\sqrt{3}, 1) \quad (1.1)$$

$$\mathbf{b}_2 = 2\pi/\mathbf{a}_2 = 2\pi/\sqrt{3}\mathbf{a}_0 (-\sqrt{3}, 1) \quad (1.2)$$

The first Brillouin zone is shown in Figure 3b. Center point is represented with Γ and corner points are shown as K and K'. M point represents the center of the edge of the hexagonal Brillouin zone (BZ). Corners of the first BZ are K and K' and their positions in reciprocal space are given by

$$\mathbf{K} = 2\pi/3a_0 \left(\mathbf{1}, \mathbf{1}/\sqrt{3} \right), \quad \mathbf{K}' = 2\pi/3a_0 \left(\mathbf{1}, -\mathbf{1}/\sqrt{3} \right) \quad (1.3)$$

According to tight binding approximation, only the nearest neighbor atoms in primitive cell can contribute to the energy band. Therefore, electron hopping is directed from A to B and also from B to A. From the E-k relation, we can see that the valence band touch conduction band at K and K' positions. Consequently, the electronic structure of graphene can be solved nearly as a function of k_x and k_y .

$$E(k_x, k_y) = \pm\gamma \sqrt{1 + 4\cos\left(\frac{\sqrt{3}k_x a_0}{2}\right) \cos\frac{k_y a_0}{2} + 4\cos^2\left(\frac{k_y a_0}{2}\right)} \quad (1.4)$$

where γ ($\approx 2.7\text{eV}$) is the nearest neighbor hopping energy²². This dispersion relation is linear at all the six corners of the Brillouin zone. Therefore, at K point overlapping in energy states and touching of bonding π and antibonding π^* states make graphene zero band gap semiconductor²³.

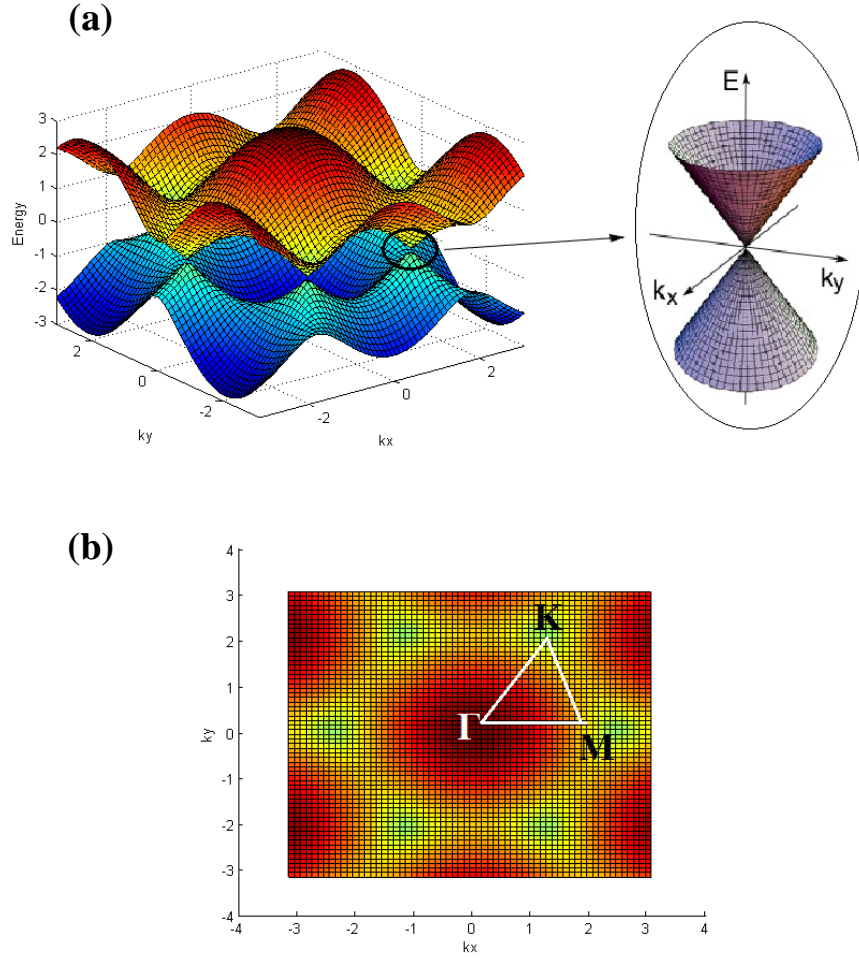


Figure 4. (a) 3D and (b) 2D display of energy band structure of graphene in the 1st BZ²⁴. The three most symmetrical points (Γ , K and M) are noted.

Due to the linear dispersion relation of graphene, charge carriers (electrons and holes) in graphene lattice have zero effective mass and these charge carriers are regarded as Massless Dirac Fermions in analogy to relativistic massless particles like phonons and they move with Fermi velocity ($\sim 10^6$ m/s) in hexagonal structure²⁵.

Interlayer interactions between the layers of multilayer graphene or between the substrate and graphene layer can induce symmetry breaking. Energy band gap can be obtained with some perturbation or symmetry break such as inducing inequivalent atoms of A and B in the unit cell. It was observed in Ref.²⁶ that applying external electric field opens a gap in bilayer graphene.

The outstanding electronic properties of graphene have been focal point in such electronic applications from its discovery. These properties can be mentioned in a comprehensive manner. For instance, at room temperature, graphene shows high

electron mobility that surpasses $2000 \text{ cm}^2/\text{V.s}$ ²⁷. Such processes like annealing process after the post-fabrication of graphene and oxidation of graphene enhances mobility value from 25,000 to 40,000 $\text{cm}^2/\text{V.s}$ due to the lattice vibrations of the substrate at room temperature ²⁸ and this electron mobility value for suspended graphene can be achieved as $\sim 230,000 \text{ cm}^2/\text{V.s}$ ¹⁵⁻¹⁶. This high mobility value makes graphene an important alternative to use in electrical devices such as field effect transistors.

1.3.2. Vibrational Properties of Graphene

The vibrational modes of graphene are directly related with its phonon dispersion relation. As discussed in the previous section, the phonon dispersion relation has very assimilated shape with its electronic band structure. The two sub-lattices A and B atoms in unit cell could vibrate in all three dimensions. Due to the fact that graphene has 2 atoms in unit cell, there are six branches of phonon modes; three of them are acoustic and the other three are optical phonon branches. There are two out-of-plane modes (atomic vibrations are perpendicular to the plane) and four in-plane phonon vibration modes. Out-of-plane modes can be named as acoustic (ZA) and optical (ZO) and in-plane modes are denominated as transverse acoustic (TA), transverse optical (TO), longitudinal acoustic (LA) and longitudinal optical (LO). The modes represented as out-of-plane (Z), in-plane longitudinal (L), and in-plane transverse (T) atomic motions and phonon branches in graphene are shown Figure 5a and b.

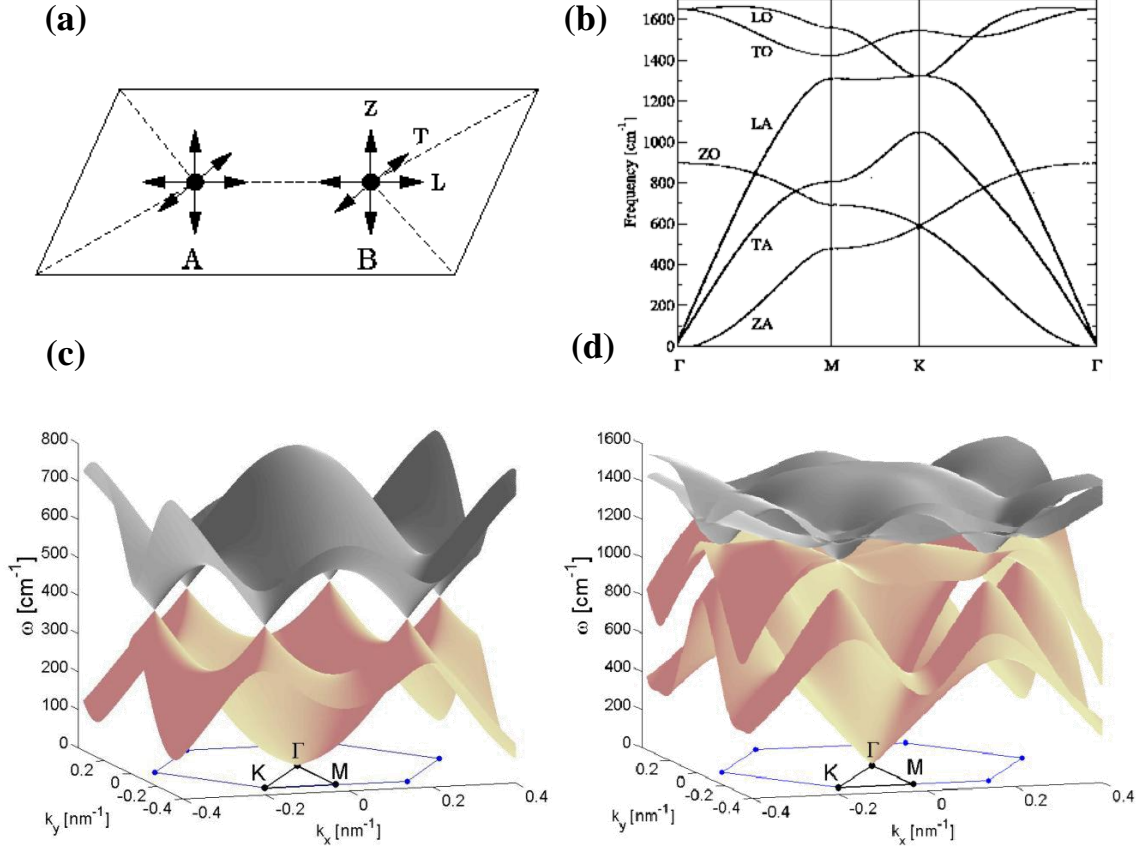


Figure 5. (a) Atomic motions of C atoms in graphene can be along the out-of-plane (Z), in-plane transverse (T), and in-plane longitudinal (L) direction. (b) The phonon dispersion branches for a graphene sheet, plotted along high symmetry directions²⁹. The phonon frequency versus the momentum space representation of the dispersion relation of out-of-plane modes (c) and in-plane modes (d) of graphene³⁰.

Figure 5c shows the out-of-plane modes; gray surface corresponds to the ZO mode. The ZA mode is also shown as the pink surface. The dispersion is quadratic at the Γ point. The in-plane modes are indicated in the Figure 5d. The dispersion have cone shape at the K and K' points. The gray surface signifies the optical modes; TO and LO, whereas the pink surface infers the acoustic modes; TA and LA.

1.3.3. Other Properties of Graphene

Besides having extraordinary electrical properties, graphene has unique optical properties. It exhibits very high transparency. The transparency of the graphene layer

increases with the decreasing in number of layer. For instance, five, two and one layer of graphene film absorbs 11.5, 4.6 and 2.3% white light, respectively ³¹. Despite the fact that graphene is highly transparent it is also flexible material. Nowadays ITO materials are used in electronic and optical device technology but it has some drawbacks in production and use area. Especially, instead of ITO, graphene can be used for device technology owing to its high flexibility and transparency in electrodes ³²⁻³³.

Another unique property of graphene is mechanical durability. Single layer graphene is the strongest material due to its C bonds with Young's modulus of ~ 1100 GPa and tensile strength of 130 GPa ³⁴. On the other hand, graphene is very light (0.77 mg/m²). These extraordinary properties of graphene make it a suitable material for wide range of engineering applications.

1.4. Graphene Production Methods

In the use of practical applications designed for graphene, including microelectronics, optoelectronics, super-capacitors etc., uniform and high quality (which is defined by the lack of intrinsic defects) graphene is needed. In accordance with this purpose, numerous methods are developed to ensure the controllability of graphene production in order to achieve reproducible results. The most used graphene production methods are: mechanical exfoliation of atomic layers from highly oriented pyrolytic graphite (HOPG), thermal decomposition of silicon carbide (SiC) and chemical vapor deposition (CVD) growth of graphene on transition metals. General comparisons of these methods are shown in Table 1.

Table 1. Properties of graphene obtained by different methods ³⁵.

Method	Crystallite Size (nm)	Sample Size (mm)	Charge Carrier Mobility (cm ² /V.s) (at ambient temperature)	Applications
Mechanical Exfoliation	>1,000	<1	>2x10 ⁵ and <10 ⁶ (at low temperature)	Research
Thermal Decomposition of SiC	50	100	10,000	High-frequency transistors and other electronic devices
Chemical Vapor Deposition	1,000	~1000	10,000	Nanoelectronics, transparent conductive layers, sensors, bioapplications

According to Table 1, high quality graphene based on crystallite size and mobility can be achieved by mechanical exfoliation method, however, sample size is limited. Although crystallite size is similar for thermal decomposition of SiC and chemical vapor deposition, in terms of transferring process of graphene on another substrate makes CVD method more practical and also CVD synthesized graphene has high quality and production of large area and defect free graphene is possible with this method.

1.4.1. Mechanical Exfoliation

Graphite is formed by overlapping graphene layers that are kept together by Van der Waals force. It is easy and feasible to separate graphene flakes from a graphite sheet by using mechanical or chemical energy thanks to these weak bonds ³⁶. In this method, a fresh piece of Scotch tape is taken, and then adhesive side of Scotch tape is pressed onto the HOPG (Figure 6a). The tape is gently peeled away with thick shiny layers of graphite attached to it. The part of the tape with layers from the HOPG was refolded upon a clean adhesive section of the same piece of the tape and then the tape is unfolded (Figure 6b,c). This process is repeated several times until the end of the tape is no longer shiny but becomes dark/dull and grey. As seen in Figure 6d, graphite layers on the tape are transferred onto the desired substrates such as Si/SiO₂ wafers with the

oxide thickness of 90 nm or 300 nm by gently pressing them onto the tape for some time and then peeling off ³⁷.

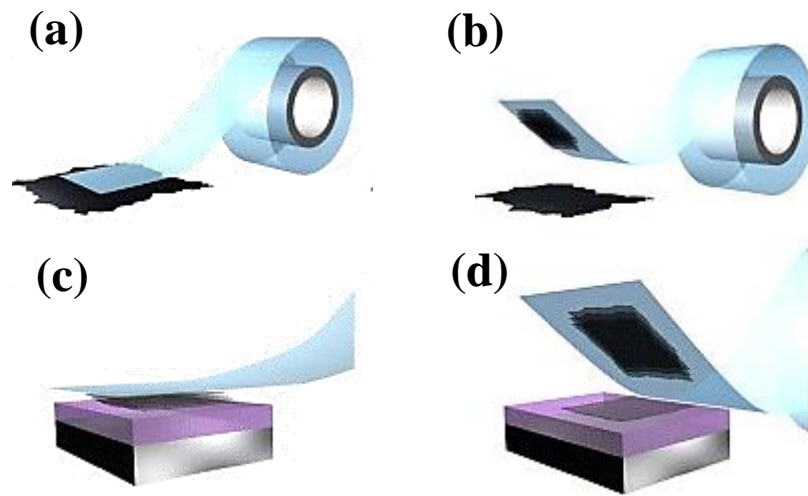


Figure 6. Schematic representation for the mechanical exfoliation of graphene from graphite using Scotch tape ³⁷.

Although this method is very reliable and easy technique and graphene flakes can be distinguished under an optical microscope in visible range, exfoliated graphene has lots of defects and limited in small sizes. Another drawback of this method is that graphene flake control is also hard and graphene has irregular shape. For the use of graphene in commercial applications, large-area and defect-free graphene are needed.

1.4.2. Thermal Decomposition of SiC

The main concept behind the thermal decomposition of SiC method is that the vapor pressure of silicon is higher; as a result on heating the SiC wafer, the Si evaporates leaving behind the graphene layers on the SiC. This process occurs in ultrahigh vacuum (UHV) environment and ordinarily by going up to temperatures between 1000- 1500 °C for a short time ~1 to 20 minutes ³⁶.

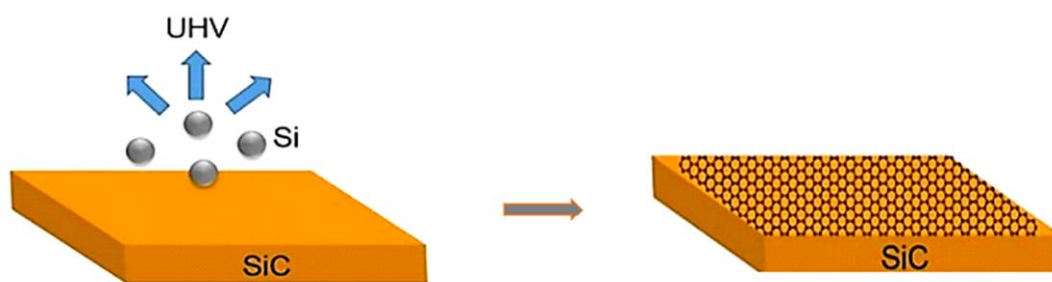


Figure 7. Schematic illustration of the graphene growth by thermal decomposition of SiC³⁸.

UHV technique hinders the uniform growth of multi-layer graphene (MLG) and favors to control C layers on the substrate. The SiC substrate is heated at a temperature (around 1200 °C) and the conditions of the chamber are set accordingly. The Si atoms evaporate due to thermionic emission leaving behind the C atoms on the remaining substrate (Figure 7). Layer controlled graphene can be grown on the SiC substrate by controlling various parameters such as SiC temperature and pressure³⁹. Since SiC has two polar faces to c-axis, graphene can be grown on these Si and C faces which shows different growth behaviors and electronic properties⁴⁰.

Although this method produces graphene in larger scale with a high quality than exfoliation method does, high temperature, high cost of production and lacking of transferring graphene on another substrate are limited this method for applications.

1.4.3. Chemical Vapor Deposition

Chemical vapor deposition (CVD) is the mostly favored method in graphene synthesis with the advantage of producing high quality mono-layer graphene. This method leans on the chemical reaction of a vapor on a heated surface. In CVD furnace, as seen in Figure 8, gas phase C source precursor (CH₄, C₂H₄ etc.) is decomposed on a transition metal film like Cu⁴¹, Ni⁴², Pt⁴³ or Ir⁴⁴ under various temperatures (between 800 °C and 1100 °C) and, then graphene layers are obtained by thermal cracking of C atoms on substrates.

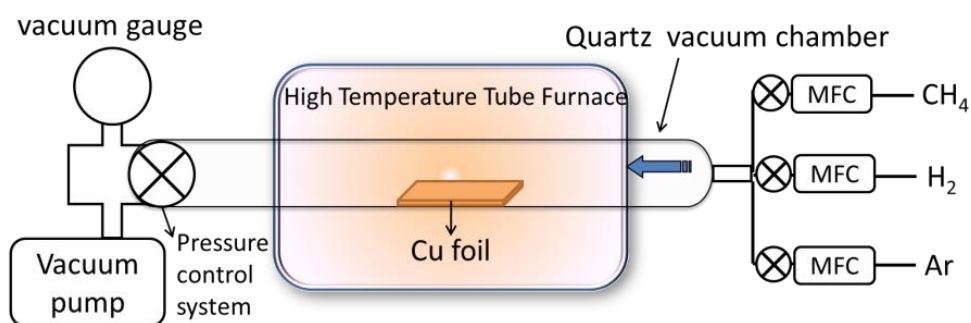


Figure 8. Schematic illustration of CVD set up for the graphene synthesis ⁴⁵.

Since deposition of C on metals is easy due to the deposition mechanism, desired substrates are generally chosen as metallic substrates. Concordantly, for production of uniform graphene films, transition metals play an important role in CVD technique. Owing to the highest film quality and ease of processing in transfer, copper (Cu) and nickel (Ni) have become the most preferred transition metals for graphene growth process by CVD. The mechanism for C deposition on these metals has been shown to depend on the C solubility, the electronic structure, and the crystal structure of the metal. However, graphitic films grown on Ni substrate are more quality of crystallinity with respect to Cu ⁴⁶, Ni has higher dehydrogenation ability and C solubility ⁴⁷. Owing to high C solubility, graphene layer control in large area is hard in growth process. Therefore, nearly zero C solubility, low cost and ease of graphene transfer compared to others ⁴⁸ makes Cu an ideal catalyst to grow graphene. Surface catalysis and the lack of bulk-C help to achieve self-terminated reactions under desired growth conditions and finally, single layer graphene (SLG) can be grown in large area ⁴⁹.

Intrinsically, oxidation of Cu ⁵⁰ is easy when compared with other transition metals used in graphene growth. For this reason, reduction process is done to remove native oxide, often using acetic or hydrochloric acid pretreatments ⁵¹. Another method to eliminate native oxide on Cu is high-temperature annealing at 900-1000 °C is the main furnace process before growth step. Additional coatings or solvent impurities from substrate may lead the formation of nanometer-sized impurities during growth. These impurities are hard to remove from the surface and can be attached to graphene even after transferring to other substrates ⁴⁹.

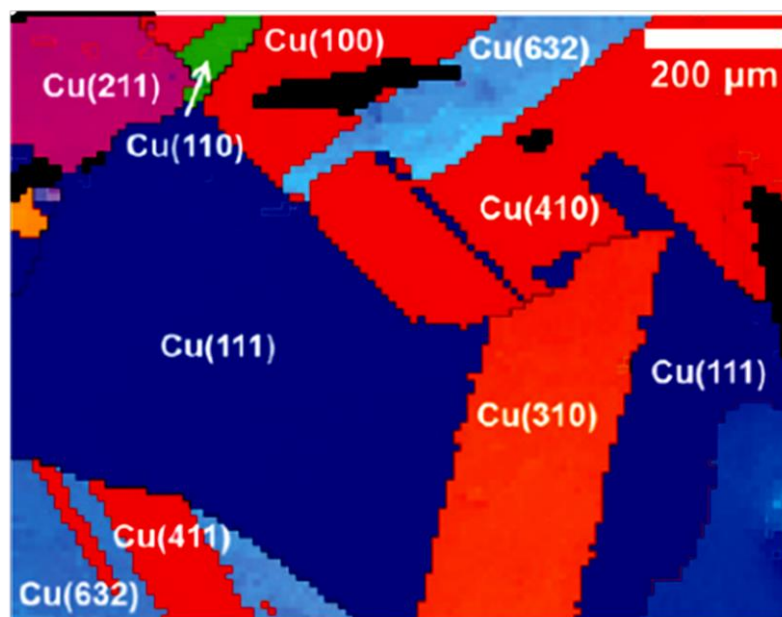


Figure 9. Different crystalline orientation of Cu surface after annealing procedure, as mapped by the EBSD ⁵².

Graphene can be grown on single or polycrystalline Cu foils or thin films. Studies have shown that the grain size increment in Cu foils, sizing up to hundreds of nanometers, is more dramatic than Cu films by annealing at 900-1000 °C ⁵³⁻⁵⁴. As seen in Figure 9, this information is determined by using electron back-scattering detection (EBSD). With annealing process, crystalline orientation can also renew on the surface. It is reported that the dominant surface orientation becomes (200) for Cu foils; while for Cu films, annealing crystallizes the mostly amorphous film to have a (111) surface with EBSD mapping of Cu surface ⁵⁴. This results indicate that low-index Cu facets is more likely to yield SLG with less defects ⁵².

A typical growth on Cu starts with reducing the oxides on the surface by high-temperature annealing, followed by exposure to the C precursor at the similar temperatures. The graphene nucleates and enlarges by consuming the reactants catalyzed on Cu from the C precursor. Generally, methane has become the most popular C precursor for the surface catalysis on Cu but it requires higher temperatures for pyrolysis. This temperature is very close to the melting point of Cu (~1085°C), and then creates intense Cu evaporation and then condensation fluxes upon cooling, which can influence the reproducibility of graphene growth and also reduce the quality of graphene and the reactor lifetime ⁵⁵. Being more reactive and able to synthesize carbon nanomaterials at much lower temperatures, acetylene and ethylene can easily lead to

deposition of undesired amorphous carbon and degradation of the nanomaterial quality. This amorphous carbon structures can be decomposed with the atomic hydrogen. Additional H₂ flow and the catalytic activity of Cu surface and H₂ also acts as etching reagent that controls the size and morphology of the graphene domains⁵⁶. Compared to acetylene and methane, ethylene can be a preferable carbon precursor because it is cheap and easy to handle. In addition, ethylene has a lower reactivity and promises an easier control for the lower temperature growth on Cu^{48, 57}. Owing to these benefits, ethylene was chosen as a C precursor in this study. Details of sample preparation and deposition were mentioned in experimental section.

In CVD technique, such parameters like flow rates of inert gases, chamber temperature, heating and cooling rates and thickness and quality of the metal substrates play an important role to obtain large scale and defect free graphene. After achieving these parameters, graphene can be synthesized easily and producing wafer scale graphene in economical way is possible.

Since the production process is self-limiting, a highly uniform and predominantly single layer graphene film can be produced even at low temperature and transferring of graphene onto desired substrates such as silicon (Si), silicon oxide (SiO₂) and glass for electronic or optic applications is possible, these benefits make CVD technique the most preferred technique when compared with previous graphene growth techniques.

1.5. Doping of Graphene

The most important feature of graphene is its linear energy dispersion relation with no energy gap¹. Due to the fact that graphene is a zero band-gap semiconductor for electrons (holes) in the conduction (valence) bands, it is not favorable for electronic applications.

This result shows that its Fermi level lies on the top of its valance band, where it touches the conduction band. Although zero-gap feature makes graphene a unique material and gives the interesting perspectives to the graphene, for several applications including energy conversion and storage, sensors and electronics, graphene based materials can be effectively modified by doping in order to improve electronic properties⁵⁸.

These novel properties of graphene open a wide range of applications in nanodevices such as field effect transistors (FETs), transparent electrodes, transistors and supercapacitors. However, for some applications such as a high on/off ratio of FETs, and an increase in conductivity of transparent electrodes, semiconducting graphene is essential⁵⁹⁻⁶⁰. Transport behavior of graphene is strongly relevant to the nature of disorder because of scattering mechanism^{4, 61-62}. Thus, doping of graphene by foreign atoms is of particular interest⁶³⁻⁶⁵ because doping leads to modify the band structure and electro chemical properties of the graphene⁶⁶⁻⁶⁷ further extending the potential applications including lithium batteries⁶⁸⁻⁶⁹, bio applications⁷⁰, field-effect transistors⁷¹, supercapacitors⁷², and oxygen reduction reaction in fuel cells⁷³⁻⁷⁴.

Doping is an especially remarkable attitude to invent and control the semiconducting properties of graphene. This can be supported by the modulation of Fermi level of graphene through doping. Metal doping⁷⁵, electrochemical doping⁷⁶ and chemical doping⁷⁷ are simple ways to control electronic, structural and optical properties. The effect of chemical doping in terms of change in physical and chemical properties of carbon based materials has been proved effectively in the doping of carbon nanotubes (CNTs)⁷⁸.

Chemical doping of graphene can be done in two ways: one is the adsorption of gas⁷⁹ or organic molecules⁸⁰ to the graphene surface and other is substitutional doping which means to introduce heteroatoms, such as boron (B)⁸¹, sulfur (S)⁸², potassium (K)⁸³ or nitrogen (N)⁸⁴⁻⁸⁵ into the C lattice of graphene. These methods can alter the electronic, optical and chemical features of graphene.

Among various potential dopants, N is considered to be an excellent candidate because of its similar atomic size and the presence of five valence electrons available to form strong valence bonds with C atoms, which would provide n-^{59, 86-87} or p-⁸⁸⁻⁸⁹ doping according to bonding character of charged-impurity atom⁸⁹⁻⁹⁰. According to theoretical studies, N doping to graphene improves electron density, and adjusts Fermi level (E_f) and chemical reaction properties^{66, 91}.

When N atom is introduced to C lattice, it usually has three common bonding configurations, including quaternary N (or graphitic N), pyridinic N, and pyrrolic N. To be more precise, pyridinic N bonds with two C atoms at edges or defects of graphene and gives one p electron to the π system of graphene lattice. N atoms donated two p electrons to the π system and bonded with five-membered ring, as in pyrrole are named

as pyrrolic N. N atoms that substitute for C atoms in the hexagonal ring refer to quaternary N. Furthermore, there is sp^2 hybridization in, pyridinic N and quaternary N, while sp^3 hybridization is occurred in pyrrolic N configuration. Additionally, three usual N types, N oxides of pyridinic N have also been occasionally realized in the nitrogen-doped graphene (N-graphene) samples (Figure 10) ⁷⁴.

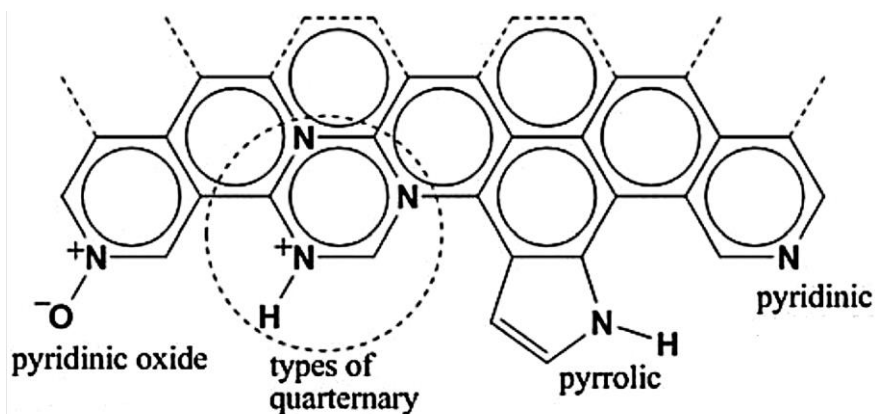


Figure 10. Schematic diagram of a N-graphene ⁹².

1.5.1. The Production of N-doped Graphene

A number of approaches have been reported to synthesize N-graphene. The production methods of N-graphene can be categorized as direct synthesis ^{71, 84, 86-87, 93} and post treatment methods ^{67, 70, 72, 74, 94}. Direct synthesis methods are chemical vapor deposition (CVD) or plasma enhanced chemical vapor deposition (PECVD) approach, segregation growth approach, solvothermal approach and arc-discharge approach with N content in graphitic lattice, ; 4–9 at.%, 0.3–2.9 at.%, 4.5 at.% and 0.5–1.5 at.%, respectively. Post treatment methods are thermal treatment, hydrazine hydrate (N_2H_4) treatment and plasma treatment. By using these methods, N doping in graphitic lattice can be reached up to 19.7 at.% ⁷⁴.

A widely used direct synthesis method is chemical vapor deposition (CVD) growth with solid ^{73, 89} or liquid ^{68, 93} C sources and doping precursors, and also with hydrocarbon and N containing gases ^{84, 86, 89, 95} (Figure 11a). Chemical doping is an efficient way to adjust the semiconducting features of carbon materials but it is reported that the environmental stability of chemically doped graphene is inadequate ⁹⁰.

Additionally, these methods are limited by the N doping percentage and a lack of uniformity⁹⁶.

Thermal treatment^{69, 97-98} and plasma treatment^{67, 70, 99-100} are some of the most outstanding post treatment methods to obtain semiconducting graphene. By thermal treatment methods N doping is more likely to occur at the defects and edge of graphene. Thus, N content is low in N-graphene by these methods^{74, 97} due to the lack of defects in the high quality graphene and exposure to high temperatures break C-N bonds¹⁰¹. Plasma treatment leads to defects and oxygen-containing groups in N-graphene^{70, 100} (Figure 11b). To easily bind N atoms to defects and edges of graphene⁵⁹ and with a delicate optimization of plasma process conditions provide to avoid excess ion induced defects.

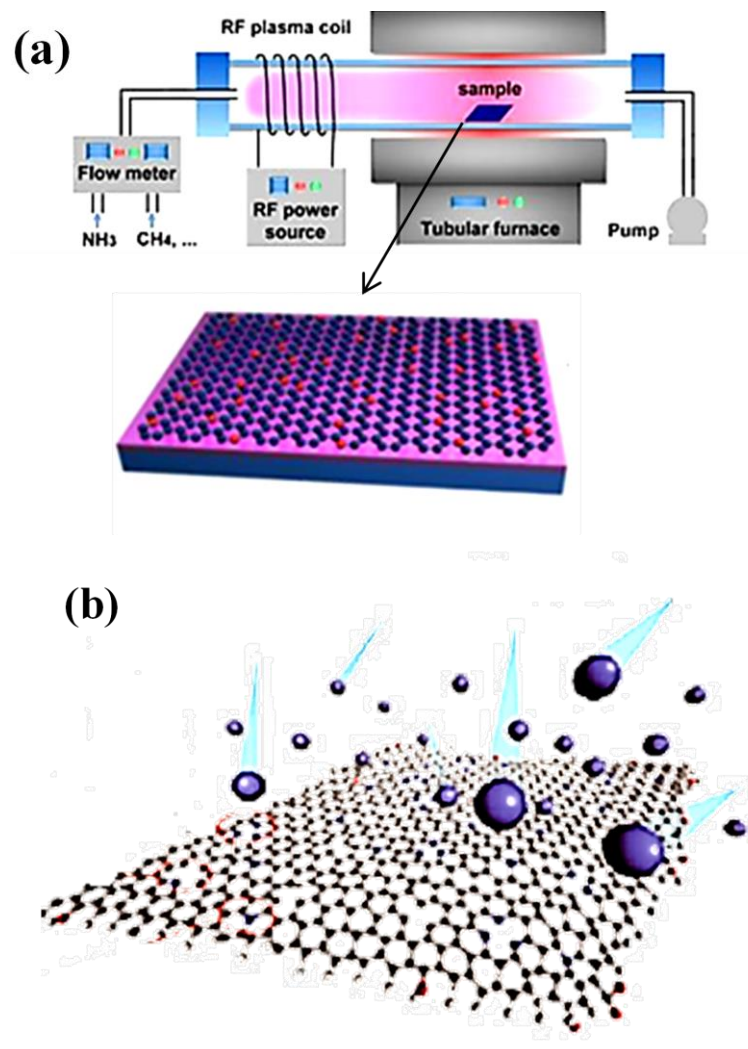


Figure 11. Schematic representations of (a) direct synthesis¹⁰² (b) post treatment methods⁷² used in production of N-graphene.

CHAPTER 2

CHARACTERIZATION TECHNIQUES

2.1. Optical Microscopy

Optical microscopy is a readily accessible and inexpensive tool for the microstructural analysis of a wide range of solid materials and it also offers the potential for rapid, non-destructive characterization of large-area samples. Although the use of optical microscopy is simple and easy in materials characterization, it can still provide valuable intellections into several materials such as metals, polymers and thin films ¹⁰³.

In this regard, characterization of graphene flakes at large scales is also possible by using optical microscopy. It basically supplies information about the number of layer of graphene flakes by contrast difference in the presence of white light ¹⁰⁴. As seen in Figure 12, in visible spectrum, thick graphene or graphite flakes can be seen more bluish; while few and single layer graphene are seen dark and light purple ¹⁰⁵.

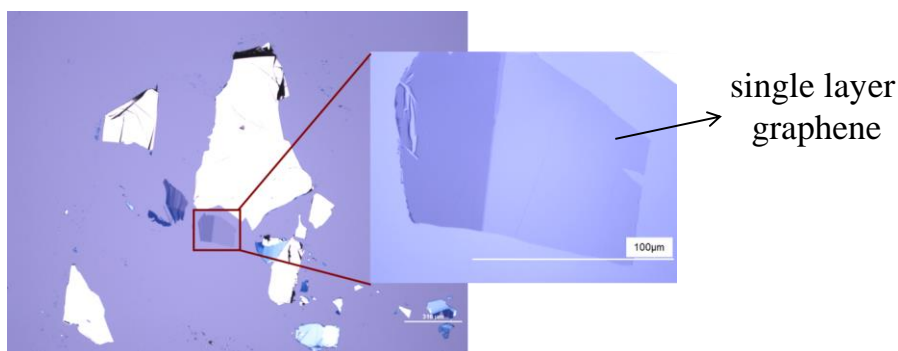


Figure 12. Optical image of the exfoliated graphene layers on SiO₂ (~290 nm)/Si substrate ¹⁰⁶.

As mentioned in Ref ¹⁰⁷, graphene flakes can be visible on the top of SiO₂ substrates with a thickness of the ~300 nm oxide layer. This oxide layer is critical, because when the white light interacts with monolayer surface, there is a change in

interference color with respect to the empty surface due to changing in the optical path of reflected light.

Optical microscope can also help to investigate the grains composed in during thermal annealing on Cu foil. In this work, Cu foil was used as a catalytic substrate for graphene growth. After graphene growth procedure, the change on surface of Cu foil was also examined by using optical microscopy technique and graphene layers can only be determined with the combination of Raman spectroscopy (Figure 13). This topic will be examined in Chapter 4.

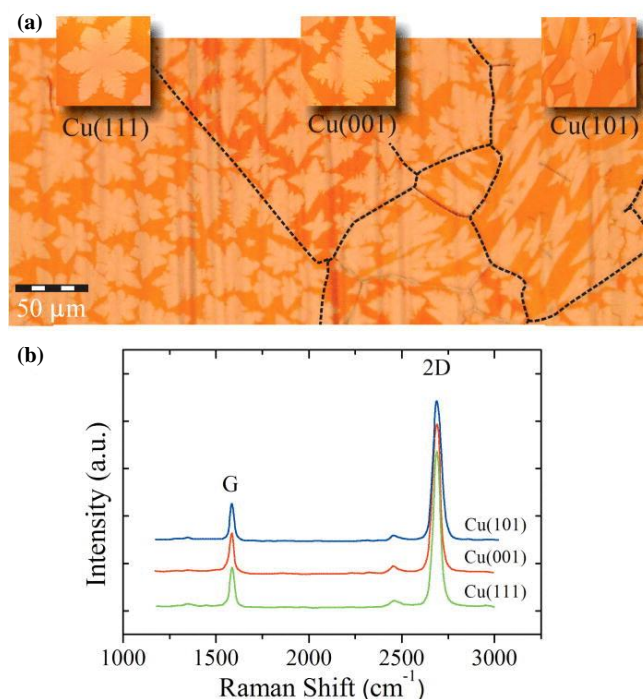


Figure 13. (a) Optical microscope images of graphene domains on Cu foil and (b) Raman spectra of graphene collected from different Cu faces. The fluorescence effect caused by Cu was subtracted from total spectra¹⁰⁸.

2.2. Raman Spectroscopy

Raman spectroscopy is the most preferred, handy, effective and non-destructive method to obtain information about solid, liquid and gaseous samples. The Raman effect was theoretically predicted in 1923 but the first experimental observation was made in 1928. Sir Chandrasekhara Venkata Raman, who has fulfilled the pioneering work in the field of light scattering¹⁰⁹, has won the Nobel Prize in Physics in 1930 for his work. After the introduction of the laser light, this method has started to be used

prevalently in materials research ¹¹⁰. Raman spectroscopy has developed into a powerful diagnostic technique which can provide information on the chemical structure, elemental composition and electronic states, namely rotational and vibrational modes of a sample.

This method relies on the scattering of incident monochromatic light with an atom or molecule by interacting with the vibrational modes of the atoms in a crystal. According to Raman theory, scatterings in material can be occurred in three ways. One is Rayleigh scattering. In this scattering, most photons are elastically scattered which means that the kinetic energy of scattered and incoming photons is conserved. Others contribute to Raman scatterings. These scatterings occur due to the inelastic scattered photons in material. Inelastic scatterings are divided into two as Stokes and anti-Stokes scattering. Stokes scattering process becomes when the frequency of the scattered photon is less than the frequency of the incident photon and the energy is added to the sample. In anti-Stokes, the frequency of the scattered photon is greater than the frequency of the incident photon and a phonon is annihilated from the sample (Figure 14). Both shifts in the energy of incoming photon and this information help to examine the vibrational, rotational and the other transitions in materials.

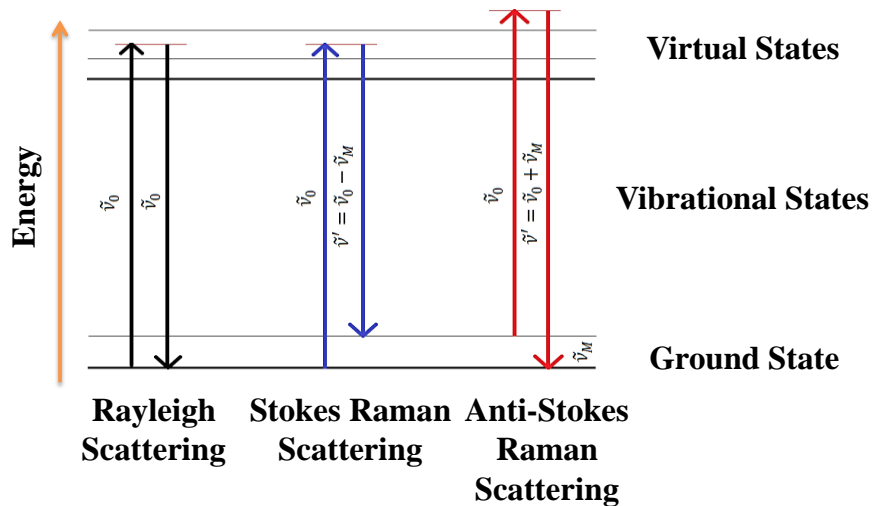


Figure 14. Schematic diagram of the energy transitions including Rayleigh, Stokes and Anti-Stokes scattering processes.

Since the Raman Effect appears with the interactive relation between the light and material including both incoming photon-electron and electron-phonon interactions, this effect on graphene can be understood easily with electron-phonon coupling and

phonon dispersion of graphene. In this context, Raman spectroscopy is considered an essential tool for identification and characterization in graphene research ¹¹¹.

The dispersion relation of graphene gives information about phonon modes as a function of frequency (Figure 15a). Typical Raman spectrum of defect-free or pristine graphene flake with exhibiting three distinct modes; the G, 2D or G' and 2D' peak are shown in Figure 15b. When defect or damage has been occurred in graphene flake, D, D', and their combination D+D' peaks appears in Raman spectra of graphene (Figure 15c) ¹¹². Despite Raman modes can be understood theoretically by using the dispersion relation curve, experimentally Raman spectroscopy is needed to show these phonon modes of graphene. In graphene, there are two different scattering modes; namely first and second order modes.

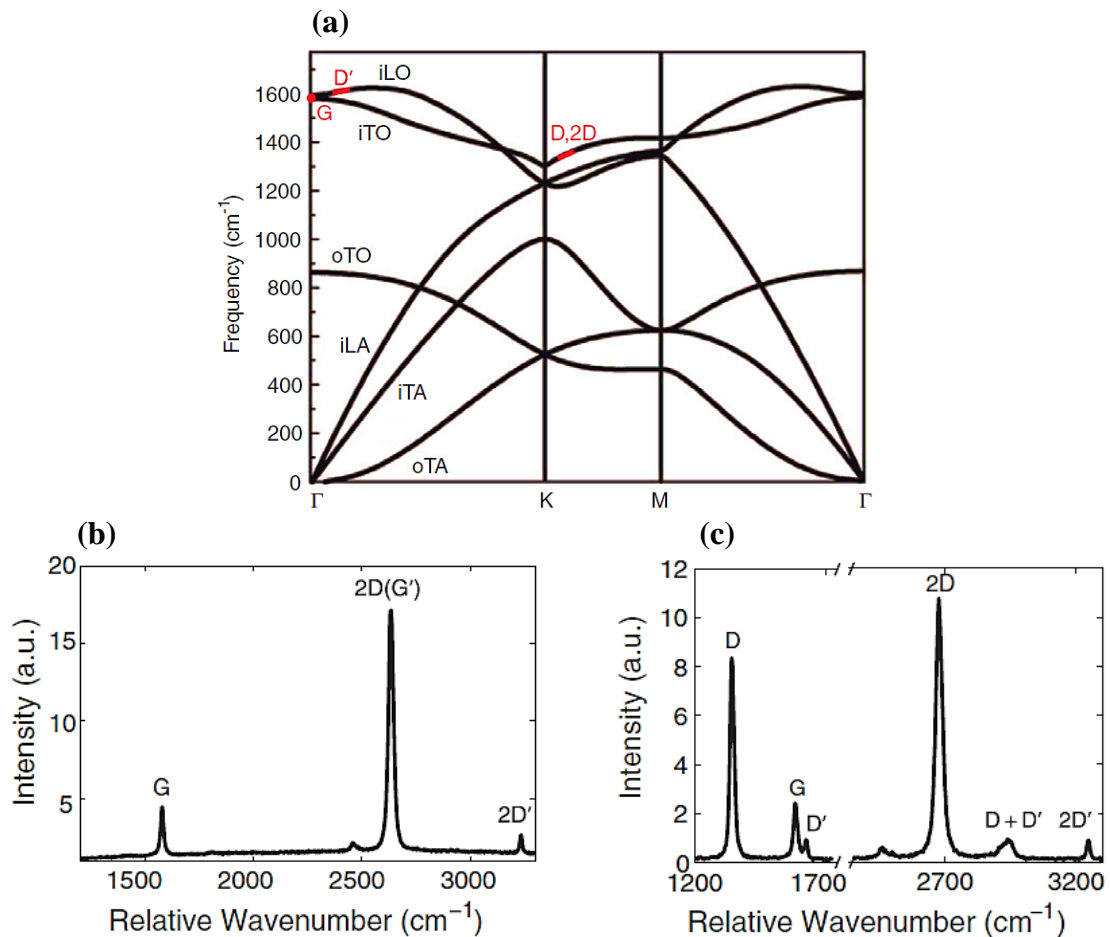


Figure 15. (a) Phonon dispersion relation and main Raman peaks of graphene which are corresponding to these phonon modes. Raman spectra of (b) pristine and (c) damaged or defect induced graphene with Raman active bands ¹¹².

The D, G, and 2D or G' peaks (bands) are dominant in the Raman spectra of N-graphene as in pristine graphene. They are represented by the peaks at around $1320\text{--}1350\text{ cm}^{-1}$, $1570\text{--}1585\text{ cm}^{-1}$, and $2640\text{--}2750\text{ cm}^{-1}$, respectively. The D' peak appears at $\sim 1602\text{--}1640\text{ cm}^{-1}$ and 2D' ($\sim 3240\text{ cm}^{-1}$) is a two phonon process and the overtone of the D' peak. This peak positions can be shifted in accordance with different wavelength excitations ¹¹³. Figure 16 shows the diagram of these dominant Raman modes of doped graphene. Especially, the G peak signifies the doubly degenerate E_{2g} phonons at the BZ. It arises from the first-order Raman scattering process. The G' and D peaks are all induced by the second-order, double-resonance process and related to zone-boundary phonons. Alternatively, the G' peak can also become a triple resonant process, in this circumstances, both carriers are scattered by iTO phonons from near the K to the K' point and reincorporate by emitting a photon ¹¹². The scattering process contains two zone-boundary phonons for G' peak; it contains one phonon and one defect for the D peak. While the D peak needs defects to activate it, the G' peak does not need the activation of defects. Therefore, the G' peak is always sighted in the Raman spectra of graphene and N-graphene, even when the D peak cannot be observed. In addition the D' peak originates in the intra-valley, defect-induced, double-resonance process ^{73, 114}.

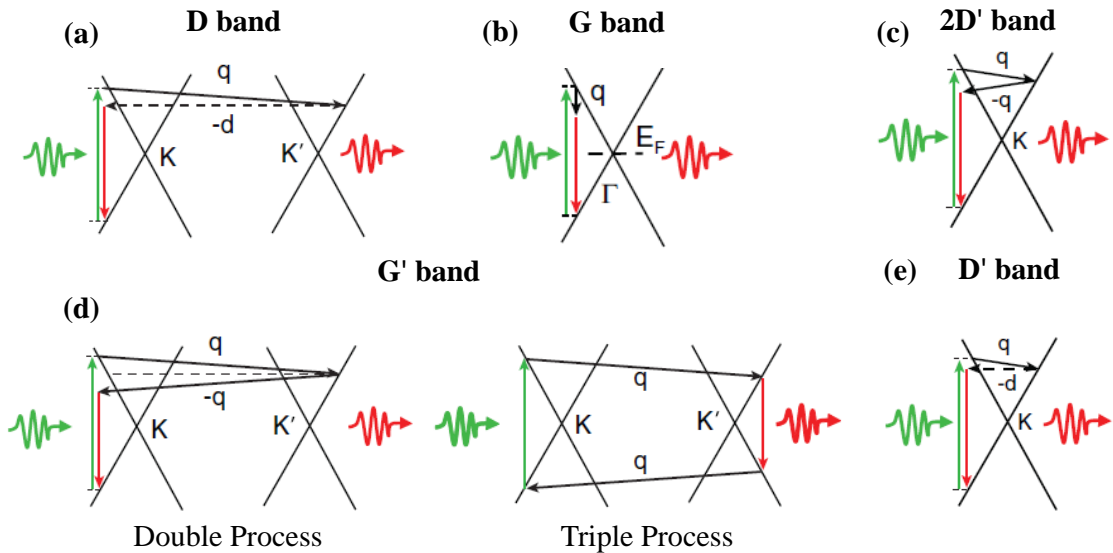


Figure 16. Illustration of the main Raman processes in defect induced graphene. (a) D band (peak) double resonant process containing a scattering from a defect (horizontal dotted line), (b) G band (d) G' band engendered through a second-order process that is either double resonant or triple resonant, (c) and (f) two intra-valley double resonance Raman bands, 2D' and D' ¹¹². Here 'q and d' stands for the magnitude of the phonon and defect wave vector, respectively.

For pristine graphene, the intensity ratio of G' and G peak is related with the number of layers in graphene flake ¹¹⁵ but in doped graphene, the intensity ratio of G' and G peaks ($I_{G'}/I_G$) indicates doping, the intensity ratio of D and D' peaks ($I_D/I_{D'}$) probes the nature of defects and the intensity ratio of D and G peaks (I_D/I_G) gives information on the relationship between the crystallite size and N doping level owing to the defects ^{74, 116}. The G and G' peaks are both exceedingly influenced by the carrier concentration.

In literature, N doping introduced n-doping in graphene owing to the extra one electron in valence band and hence should induce a blueshift of G peak and redshift of G' peak. Raman shift for G and G' peaks can give information about doping when compared before and after plasma treatment. The intensity of G' peak of graphene was much higher than that of N-graphene due to the extra scattering effect from the N induced electron doping. The change in the Raman shift for G and G' peaks and also their positions can change not only the doping concentration but also the graphene-substrate interaction induced by different thermal expansion coefficients of graphene and substrate ¹¹⁷⁻¹¹⁸.

The surface mapping of Raman spectroscopy provides information about deformation in graphitic lattice after doping process with plasma treatment. This technique is also commonly used to observe the number of layers of graphene ¹¹⁹⁻¹²⁰, the strain effect caused by graphene-substrate interaction ¹²¹, doping effect ^{116, 120} and surface defects ¹²² in graphene lattice. To conclude, Raman spectroscopy has been extensively studied for understanding changes in electronic structure of graphene after doping process.

2.3. X-Ray Photoelectron Spectroscopy

X-Ray photoelectron spectroscopy (XPS) utilizes the analysis of the kinetic energy distribution of the emitted photoelectrons to examine the composition and electronic state of the surface region of a sample. Besides, the surface chemistry of a material can be analyzed by using XPS. By this means, it is a standard technique to study the N doping effect in graphene lattice.

In the XPS spectrum of N-graphene, as seen in Figure 17a and b, the peaks at about 284 and 400 eV correspond to the C1s and N1s, respectively ^{59, 70}. In the research

about N-graphene, the N1s spectrum usually can be deconvoluted to several individual peaks that are named as pyridinic N (398.1–399.3 eV), pyrrolic N (399.8–401.2 eV), and quaternary N (401.1– 402.7 eV). In literature, it is indicated that the peak position of these N types varies in a relatively wide range in different studies (Figure 17c) ⁷⁴. When N atoms are introduced into graphitic lattice, peaks at the C1s spectrum will shift accordingly. In some cases, it may be difficult to determine the N1s peak in selected region because of the lowest N doping concentration ¹²³⁻¹²⁴.

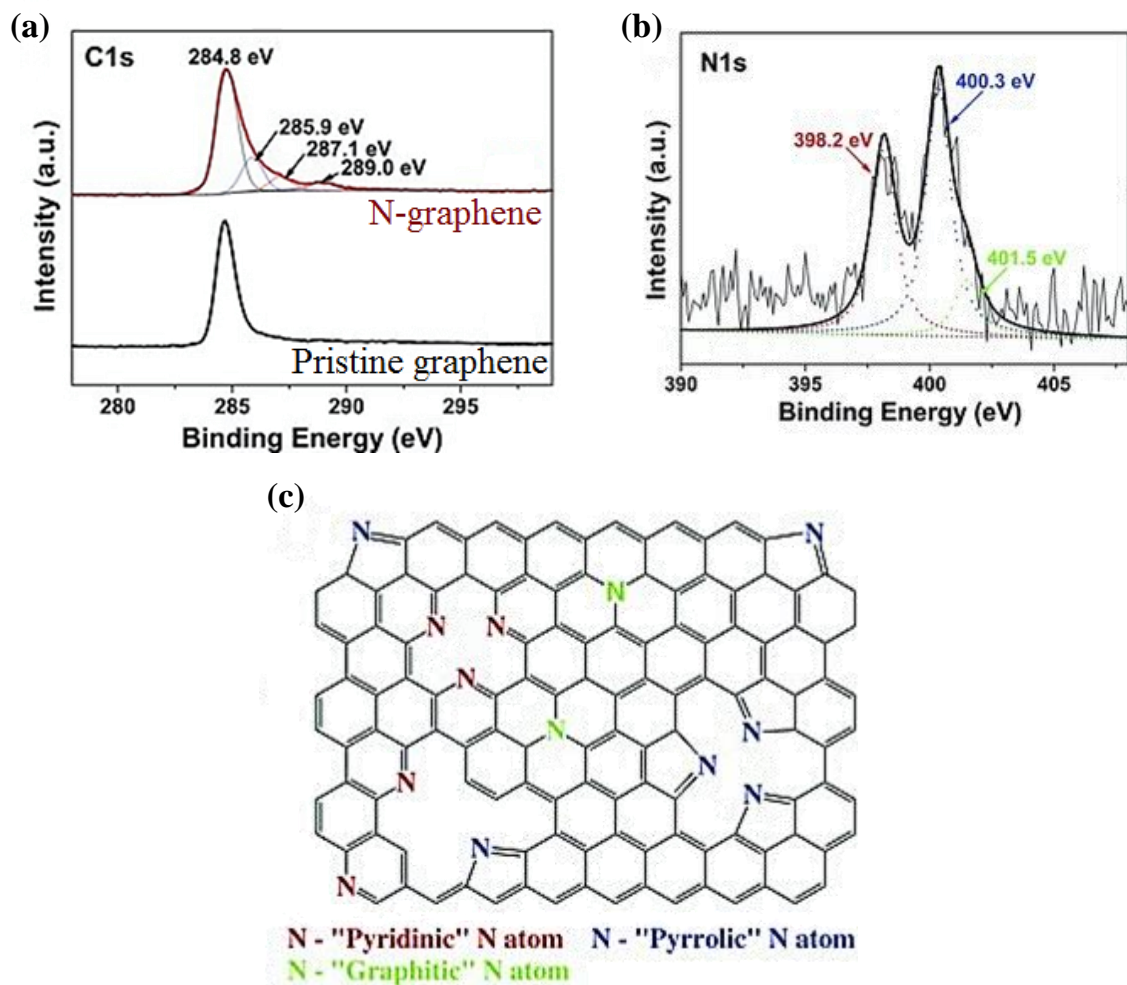


Figure 17. The XPS measurements of (a) C1s peaks of N-graphene and pristine graphene, (b) N1s peak of N-graphene and (c) schematic structure of N-graphene ⁷¹.

2.4. Scanning Tunneling Microscopy and Spectroscopy

Scanning tunneling microscope (STM) is an effective technique to study the electronic properties of a sample. Due to the sharp tip used in STM, it is possible to get topographic images with atomic resolution and observe the local electronic structures near lattice defects such as vacancies and impurities on atomic scale¹²⁵. Since it probes the charge density, scanning tunneling microscopy is an efficient method to demonstrate the electronic properties of N-graphene.

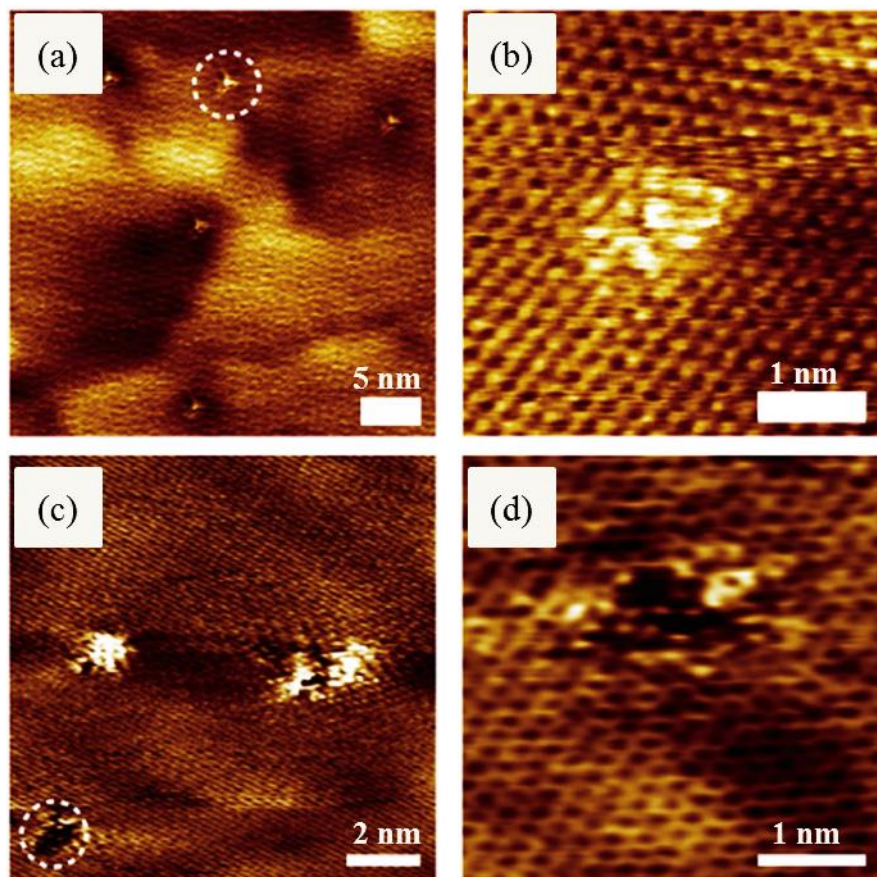


Figure 18. (a) Large-scale STM topographic image of graphitic N dominated graphene on Cu foil showing the presence of pointlike N dopants ($V_{\text{bias}} = -0.015$ V, $I_{\text{set}} = 0.3$ nA), (b) High-resolution STM image of graphitic N dopant ($V_{\text{bias}} = -0.015$ V, $I_{\text{set}} = 0.3$ nA), (c) Large-scale STM topographic image of pyrrolic N dominated graphene on Cu foil ($V_{\text{bias}} = -0.02$ V, $I_{\text{set}} = 0.3$ nA) and (d) High-resolution STM image of pyrrolic N dopant ($V_{\text{bias}} = -0.02$ V, $I_{\text{set}} = 0.3$ nA)¹²⁶.

STM is also used to investigate the possibility of dopant clustering with the dopant distribution in the N-N and C-N distance. In some studies, it is strongly recommended that theoretical simulations of different doping configurations allow catching the main features of the STM images and STS spectra to specify experimental results (Figure 18) ¹²⁷⁻¹²⁸. Furthermore, the charge-carrier type of N-graphene can be determined from a scanning tunneling spectroscopy (STS) study ¹²⁹. From the dI/dV (derivative of current with respect to the voltage) curves, the Dirac point of N-graphene can be measured and charge carrier type can be determined locally with the change in Dirac point of doped graphene ¹²⁰.

2.5. Kelvin Probe Force Microscopy

Kelvin probe force microscopy (KPFM), also named as surface potential microscopy, has been used in various applications for metals, semiconductors and insulators. While KPFM measures the work function in conducting materials, this method is used for non-conducting materials to measure the surface potential. KPFM has been used to provide information about charge distribution and surface potential of semiconducting materials.

Since KPFM was derived from existing atomic force microscopy, there is an electrostatic interaction between conducting tip and the surface of material. If this surface is metal, there becomes an interaction between two metals, namely two different Fermi levels. In the touching condition of these two metals, electron transfer starts to balance these Fermi levels. This electron flow situation between these surfaces is named as the contact potential difference (CPD). With applying bias voltage or external potential to the system, these electron flows can be finished and CPD balance is supplied. This process is called as Kelvin method. By the way, from the amount of applied external voltage, work function or surface potential of sample can be found (Figure 19) ¹³⁰.

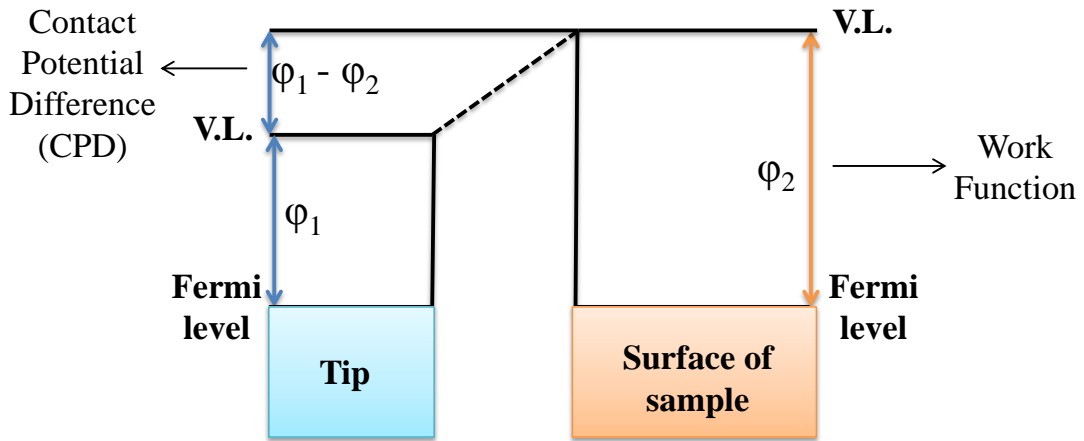


Figure 19. Band diagram of tip and sample in KPFM, V.L. represents the vacuum level.

Hence graphene is semi-metallic material; it is possible to measure the work function of graphene on different substrates. In literature, there are lots of study about work function of functionalized graphene layers by KPFM¹³¹⁻¹³². Since the work function is related to the Fermi level of substrate, with the comparing of pristine graphene and doped graphene, shift in Fermi level can be measured. This difference gives an idea about the carrier type after doping process^{88, 133}.

CHAPTER 3

EXPERIMENTAL

3.1. Materials

Graphene samples were grown on the Cu foil (25 μm thick, 99.8 purity, Alfa Aesar). Desired substrates used for graphene transfer were purchased: SiO_2 (300 nm)/n-Si (University Wafer, USA), Au (111) /mica (200 nm thick, Phasis, Switzerland) and sapphire (C plane (0001), Semiconductor wafer, Taiwan). The STM tip (Goodfellow, UK) was prepared from Pt/Ir wire cut under ambient conditions. All chemicals were used as received: Acetone (>99.9%, Sigma Aldrich), 2-Propanol ($\geq 99.5\%$, Sigma Aldrich), Microposit S1813 (Micro Resist Technology), Iron(III) Chloride (FeCl_3 , 0.2M, Norateks).

3.2. Sample Preparation

3.2.1 Synthesis of Large Area Graphene by CVD

Large area graphene samples were grown on 25 μm thick unpolished Cu foil by Low Pressure Chemical Vapor Deposition (LPCVD).



Figure 20. A picture of LPCVD setup at the department of Physics, IZTECH.

In this study, an oven (Lindberg/Blue TF55035C Split Mini tube Furnace) including a horizontally placed quartz tube with an outer diameter of 2.54 cm and length of 60 cm, equipped with various gas lines, mass flow controllers and roughing pump were used to grow graphene samples on Cu foil (Figure 20).

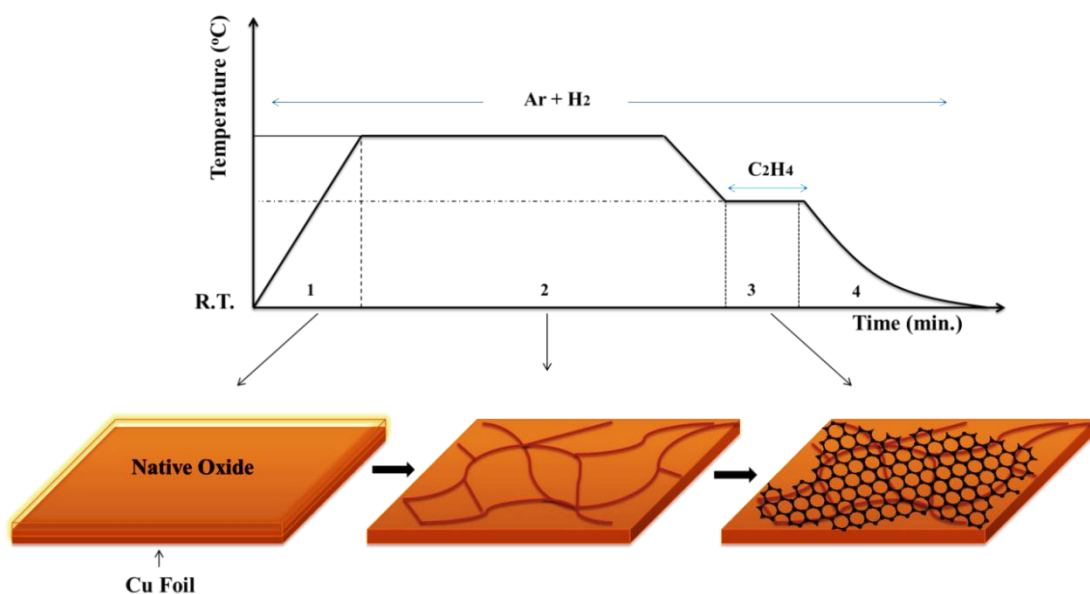


Figure 21. Heating (1), annealing (2), growth (3) and cooling (4) stages of graphene growth process on Cu foil with schematic representations by LPCVD.

Figure 21 shows the process of graphene growth in four stages. The process is started at room temperature and during all processes Ar and H₂ were utilized to reduce the native oxide layer on the Cu foil. Here, Ar was used as an inert gas to clean the impurities which stick onto the Cu foil and to increase the chamber pressure to unload the sample. The heating rate was always kept constant at 28 °C/min from room temperature (RT) to desired growth temperature. For increasing the grain size on Cu foil, the chamber was evacuated to a pressure of 10⁻³ Torr and annealing temperature of 990 °C for a duration of 80 min. For the growth stage, C₂H₄ decompose into C and H₂ with the help of growth temperature, H₂ flow and the catalytic activity of Cu surface. Besides, H₂ acts as etching reagent that controls the size and morphology of the graphene domains. After the growth was completed, the furnace is opened to the air for rapid cooling.

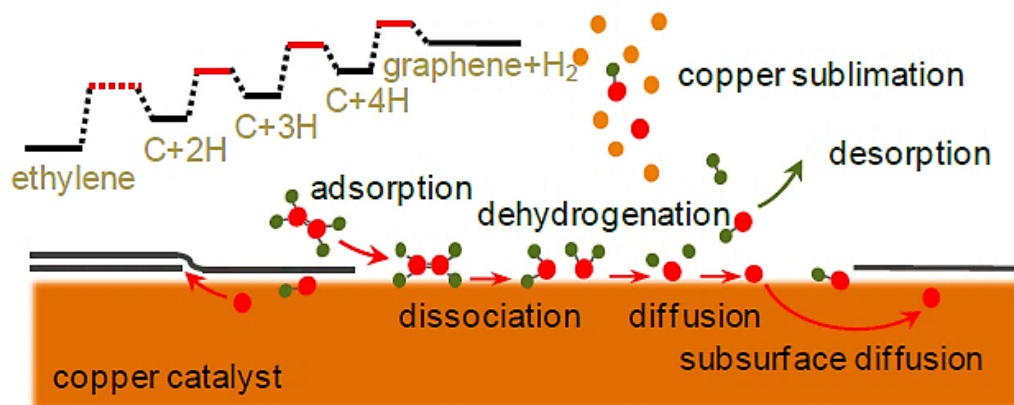


Figure 22. Graphene growth scheme under ethylene atmosphere and its associated formation mechanisms⁴⁹.

Formation of graphene on Cu foil was depicted in Figure 22. Different gas flow rates and growth temperatures were attempted to maintain the formation of graphene films on polycrystalline Cu foil by LPCVD. All the studied parameters are given in Table 2. All samples were labeled as GRP with number after the growth process.

Table 2. Graphene growth parameters on Cu foil by LPCVD.

Sample Name	Growth Pressure (Torr)	Growth Temperature (°C)	Ar (sccm)	H ₂ (sccm)	C ₂ H ₄ (sccm)	Growth Time (min.)
GRP406-421	1	990	100	10	10	10
GRP422	1	990	100	20	10	10
GRP423-495	1	990	100	10	10	10
GRP496	1	700	100	10	10	10
GRP497-499	1	990	100	10	10	10
GRP500	1	700	100	10	10	15
GRP501-505	1	990	100	10	10	10
GRP506	1	700	100	10	10	10
GRP507	1.5	700	100	20	10	10
GRP508	1.5	800	100	20	10	10
GRP509-511	1	990	100	10	10	10
GRP512	1.5	850	100	20	10	10
GRP513-520	1	990	100	10	10	10
GRP521	2	850	100	30	10	10
GRP522, 523	1	990	100	10	10	10
GRP524	2.4	850	200	30	10	10
GRP525	1	990	100	10	10	10
GRP526	2.4	850	200	30	10	15
GRP527	2.4	850	200	30	10	5
GRP528-534	1	900	100	10	10	10
GRP535	2.4	850	200	30	10	7
GRP536	2.4	800	200	30	10	15
GRP537	2.4	800	200	30	8	15
GRP538	2.4	850	200	30	8	15
GRP539-542	1	900	100	10	10	10
GRP543	2.6	850	200	30	15	10
GRP544	2.6	850	200	30	15	15
GRP545-591	2.6	850	200	30	15	20
GRP592-595	2.6	850	200	30	10	20
GRP596-599	2.4	850	150	30	10	20
GRP600-616	2.6	850	200	30	10	20
GRP617-649	2.4	850	150	30	10	20

3.2.2 Graphene Transfer Procedure

Substrate selection is of crucial importance for Raman, XPS and STM-STs measurements. After the growth, graphene films were transferred onto various substrates such as SiO₂, Au (111) and sapphire. Graphene was transferred onto desired substrates by using photoresist (PR) drop casting method (Figure 23). Thick droplets of S1813 photoresist was drop-casted on graphene holding Cu surfaces overnight in the oven at 70 °C to gently harden the PR. Then hardened PR on graphene holding Cu was put into the FeCl₃ solution for etching of Cu foils. When the Cu foil was completely etched away, graphene holding PR was put into DI water for 30 min. to remove the FeCl₃ residues. Next the sample was exposed to 70 °C for 30 sec and 120 °C for 2 min. to reflow the PR on graphene. During the reflow process, PR liquefies and releases the graphene layers on foil target substrate. Removing PR with acetone yields large area graphene on the desired substrate.

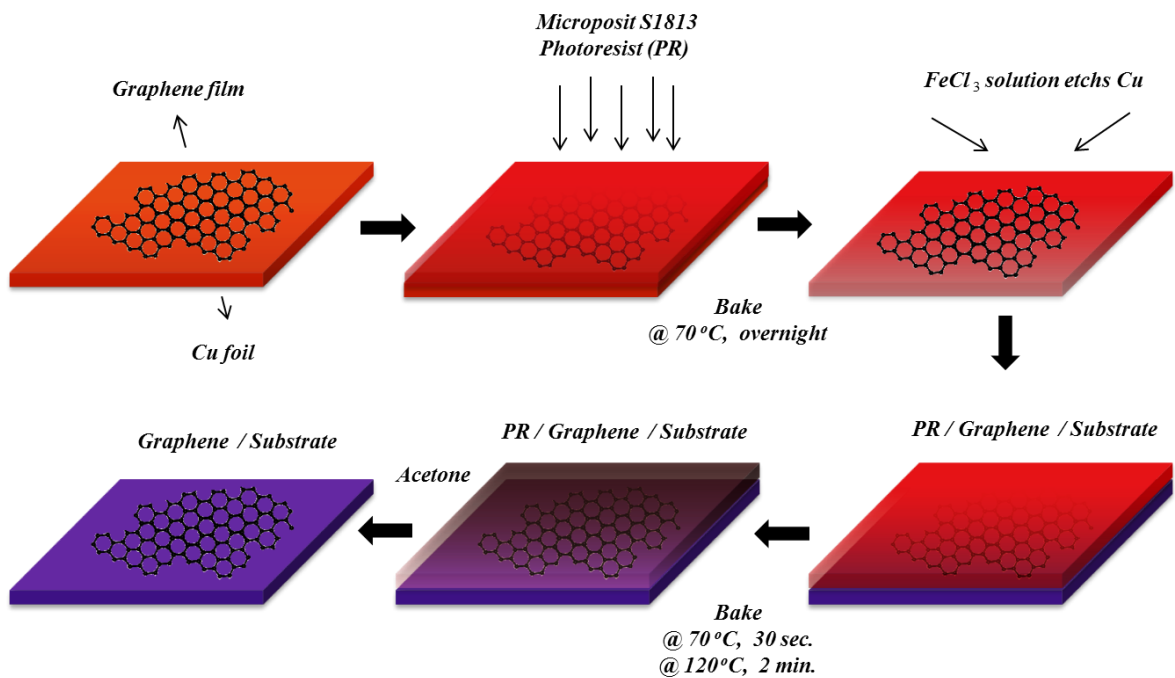


Figure 23. Schematic illustration of the graphene transfer procedure.

3.2.3 Nitrogen Plasma Treatment of Graphene

The graphene samples were treated by radio frequency (RF)-discharge plasma in N₂ gas. N doping processes were applied in a plasma chamber (PDC-002 (230V), Harrick Plasma Cleaner) shown in Figure 24. The process chamber was pumped down to a pressure of ~30 mTorr and then filled with N₂. After the pressure stabilization in the chamber at the desired value, the capacity coupled RF-discharge plasma was generated using the RF frequency generator. The RF generator was operated at the standard industrial frequency of 13.56 MHz and the controllable nominal power up to 30 W. The graphene sample was placed into the chamber using a high purity N₂ gas (99.999%) and a flow rate of 10 sccm to set the chamber pressure nearly 1060 mTorr. Finally, N₂ was introduced into the chamber to create plasma by applying a radio-frequency forward power of 7W, 10W and 30W.

Table 3. Growth parameters of N-graphene.

Substrate/Sample			N ₂ Plasma Parameters			
SiO ₂ (300nm)	Sapphire	Au (200nm)	N ₂ flow (mL/ min)	Pressure (mTorr)	Time (min.)	Power (Watt)
NGRP432			10	1045	5	10
NGRP452			10	1147	15	10
NGRP454		NGRP510	10	940	15	10
NGRP455			10	1036	15	7
NGRP457			10	1076	20	7
NGRP464	NGRP596		10	876	25	30
NGRP465	NGRP406		10	1049	10	7
NGRP466			10	976	10	30
NGRP493			10	1024	5	10
NGRP577	NGRP423	NGRP494	10	1053	15	10
NGRP511			10	864	79	30
NGRP513			10	1024	5	10
NGRP528			10	868	45	30
NGRP539		NGRP516	10	950	15	30
NGRP540	NGRP604		10	890	15	10
NGRP547	NGRP409		10	1015	5	30
NGRP603	NGRP601	NGRP432	10	898	15	10
NGRP617		NGRP519	10	1078	20	7
NGRP632	NGRP635		10	971	15	7

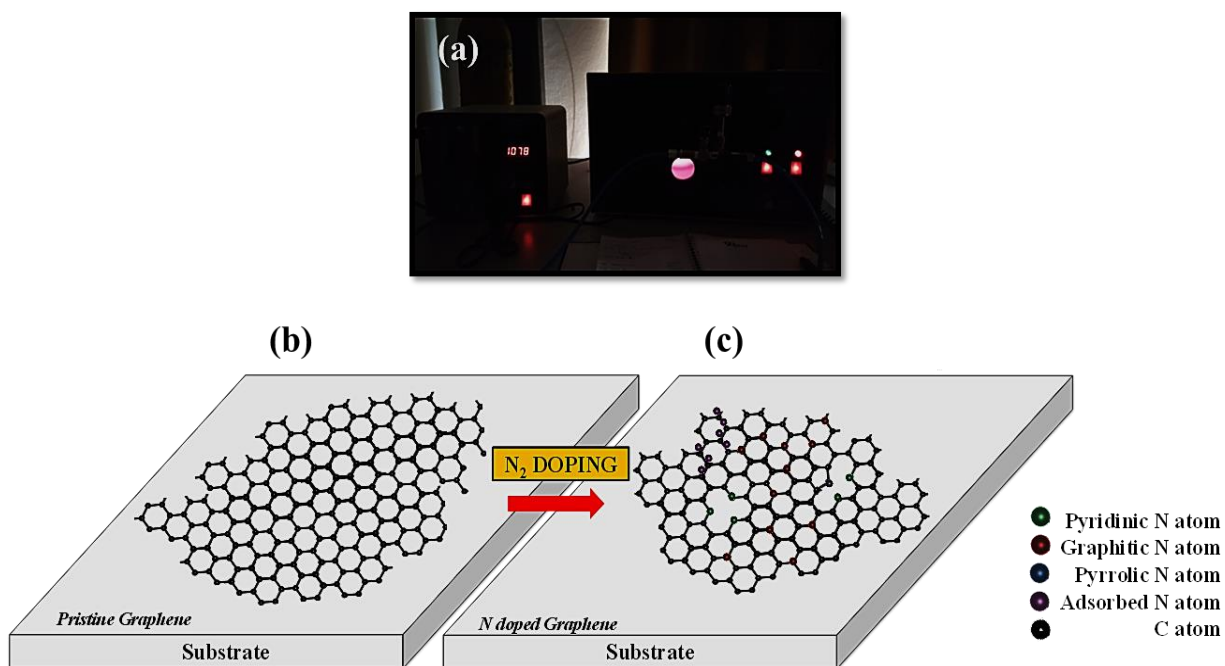


Figure 24. (a) Representation of N₂ plasma process, (b and c) schematic illustrations of N doping on graphene lattice.

The duration of plasma doping was varied between 5 and 79 min. All N₂ plasma treatment parameters are given in Table 3. Doping of graphene was realized on different substrates (samples given in the same row). After N₂ plasma process all samples were labeled as NGRP and corresponding graphene growth number.

CHAPTER 4

RESULTS AND DISCUSSION

4.1. Characterization of CVD grown Graphene

4.1.1. Optical Microscopy and Raman Spectroscopy Results

As seen in Table 2, the parameters including growth temperature, growth time and different gas ratios (Ar: H₂: C₂H₄) were studied at low pressure. The aim was to obtain homogenous and large area single layer (SLG) or few layer graphene (FLG) on Cu foil. In this regard, different annealing temperature was tried first while annealing time was kept constant. Annealing temperatures of 700, 850 and 990 °C were studied for constant annealing time. Grains on Cu foil becomes larger nearly at the melting point of the sample (~1085°C), however this temperature may lead nonuniform graphene growth on the edge sides of the Cu foil. Due to this fact, annealing temperature was determined as 990°C for a duration of 80 min to obtain largest grains (see Figure 25).



Figure 25. Change in grain size and formation based on different annealing temperatures; (a) 700 °C, (b) 850 °C and (c) 990 °C viewed by using 10x optical microscope.

In this study, Raman spectrometer Monovista (Princeton Instruments) was used in all the measurements. Raman signals were recorded in a spectral range between 1000 – 3100 cm^{-1} using Ar^+ ion laser 488 nm (2.54 eV) excitation (600 grooves/mm grating) to observe all D, G and G' peaks of graphene. The measurements were taken in combination with a 100X microscope objective. Each spectrum was analyzed using TriVista software.

As mentioned in Chapter 2, Raman spectroscopy technique was used to determine the number of graphene layers, the size and quality of graphene grown on the metal substrate by using the shift in the wavelength of scattered light from the substrate. Signal point Raman spectroscopy measurements were carried out on all the surface area of Cu substrate. The predominant peaks of pristine graphene are D, G, and G'. These peaks become apparent in the wavenumber range between 1320–1350 cm^{-1} , 1570–1610 cm^{-1} , and 2640–2710 cm^{-1} , respectively.

The number of layers for CVD grown graphene was determined only via Raman spectrum results. SLG on Cu foil can also be identified by analyzing the peak intensity ratio of the G' and G peaks ($I_G/I_{G'}$). The intensity ratio of these peaks is greater than, or equal to 0.5 for high-quality SLG. This ratio is also used to approve a defect-free graphene. The G' peak in the SLG is much more intense as compared in multi-layer graphene and this peak in SLG has a sharp line width on the order of $\sim 30 \text{ cm}^{-1}$ ¹³⁴. The number of layer of graphene is more than two layers with Full Width at Half Maximum (FWHM) $>50 \text{ cm}^{-1}$ when the $I_G/I_{G'} > 1$. On the other hand, for CVD grown graphene G' peak can be fitted well with a single Lorentzian, which induces a confusion to distinguish turbostratic graphene and SLG or bilayer graphene. This problem has been solved theoretically and experimental studies on this subject¹³⁵. In short, $I_G/I_{G'}$ was used to identify the graphene layers.

The G' peak of the graphene layers were fitted by the least squares (R^2) method with the minimum number of peak components to get a coefficient of determination ~ 0.99 ⁴⁶. Only one Lorentzian peak is sufficient for SLG or bilayer graphene, but four or more peaks are necessary to fit the G' peak for more than bilayer graphene. The FWHMs of G' peaks were widen and up-shifted with the increment in the layer number from SLG to graphite. Depending on the line shape, the G' peak is analyzed with the shift in layer number¹³⁶.

After the growth process, graphene samples on Cu foil were characterized by using Raman spectroscopy. All collected data were processed with Origin Lab program. The aim of the study was to obtain large area and homogenous SLG or FLG on unpolished, Cu foil by LPCVD. For that purpose, the effect of different growth parameters was investigated and the results are discussed as follows.

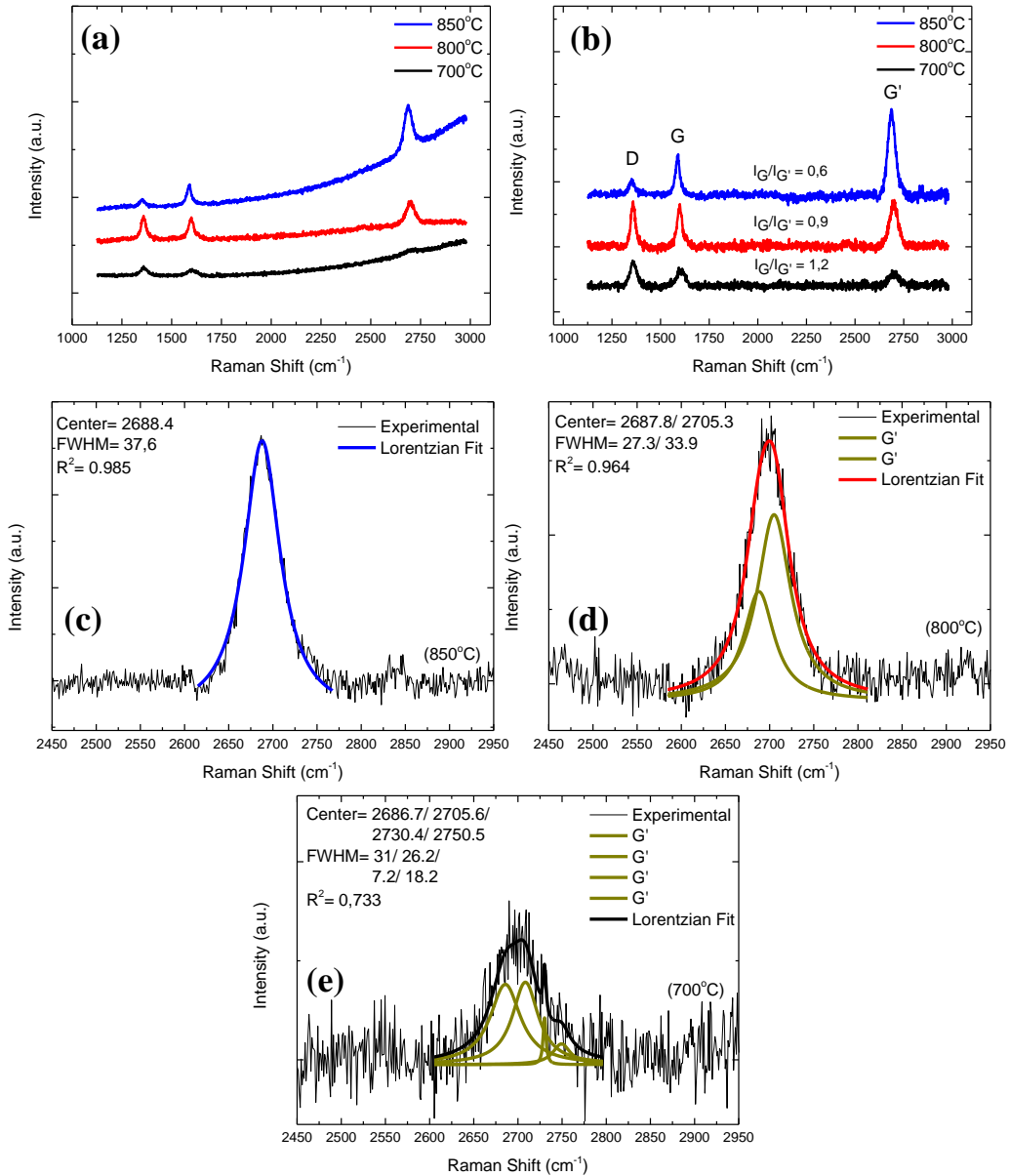


Figure 26. (a) and (b) Raman Spectra of graphene samples which were grown at different temperatures on Cu foil, (c-e) represents the center positions and FWHM values of fitted G' peaks of samples.

Graphene samples were grown on Cu foil with the parameters presented in Table 2. Raman spectrum of the samples were collected for random regions on Cu foil and the results were shown in Figure 26a. The fluorescence effect caused by Cu was eliminated and the spectra were reacquired as seen in Figure 26b. For optimizing large area and high quality graphene growth at low temperature (700-850°C), gas flow rates and growth time were kept constant and only growth temperature was changed for samples. Gas flow rates were Ar: H₂: C₂H₄ (100 sccm: 20 sccm: 10 sccm) and the

growth time was set to 10 min. According to the measurement results, graphene grown at 850°C; D, G and G' peak positions were defined as 1354.6, 1590.1 and 2688.4 cm⁻¹ while graphene grown at 800°C and 700°C these positions were found to be 1359.1, 1357.9, 1598.9, 1604.7 and 2699.3, 2704.9 cm⁻¹, respectively. Furthermore, FWHMs of G' peaks were determined to be 37.6, 47.5 and 61.5 cm⁻¹ (Figure 26c-e). Obtained results showed that C deposition on Cu foil was achieved for the samples grown at 700°C. However with increasing temperature up to 850°C, the number of graphene layers was decreased gradually and SLG was obtained.

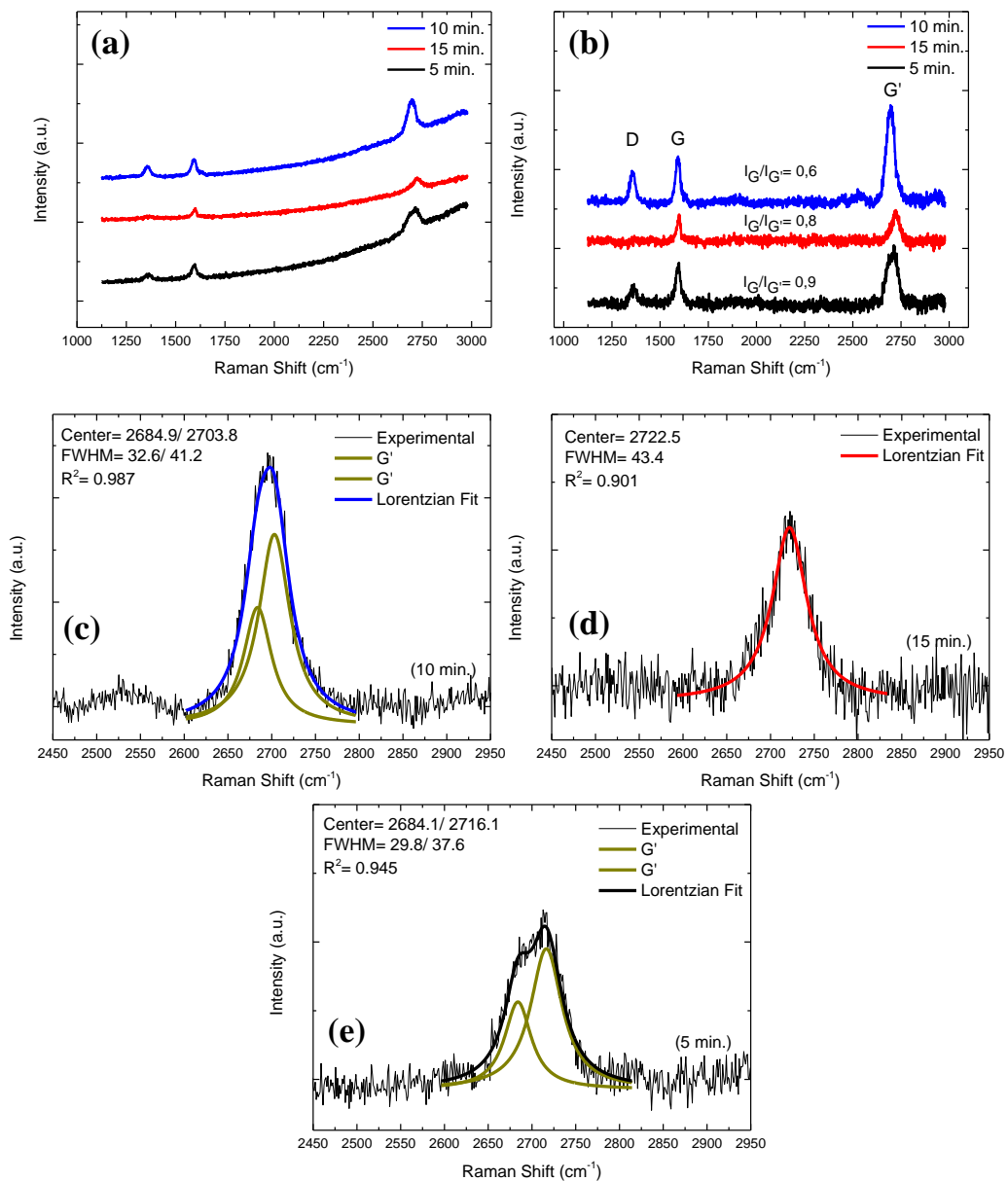


Figure 27. (a) and (b) Raman Spectra of graphene samples which were grown for different growth time on Cu foil, (c-e) represents the center positions and FWHM values of fitted G' peaks of samples.

After the optimization of growth temperature, we have changed the growth time for optimizing the number of graphene layer and homogeneity in large area on Cu foil. Three different growth times were applied while the other parameters (e.g., Growth Temperature: 850°C, Gas Flow rates: H₂ (30 sccm) and Ar (200 sccm) and C₂H₄ (10 sccm)) were kept constant. As seen in Figure 27a and b, the Raman spectra of the samples were collected in random region on Cu foil same as before. Moreover, G' peaks of the samples are broadened and upshifted than expected for the peak position of SLG. According to literature¹³⁴, this prediction shows the growth of turbostratic graphene. Turbostratic graphene is comprised of graphene layers which are stacked uncoupled. This type of stacking has single Lorentzian owing to the lack of an interaction between the graphene layers and it has a broaden G' linewidth (FWHM of ~45-60 cm⁻¹) in corporation with SLG.

Although disorder in graphene lattice (D peak) was not observed for the samples grown in a duration of 15 min., more than SLG was grown on Cu foil. The characteristic peaks (G and G' peaks), were seen at 1600.1 and 2722.5 cm⁻¹. The FWHM value of G' peak was 43.4 cm⁻¹ (Figure 27e). With decreasing growth time, disorder peak was also appeared and turbostratic graphene was attained as seen in the total spectra (Figure 27b). D, G and G' peaks of the samples, grown for 10 and 5 min, were observed at the peak positions of 1355.9, 1362.2, 1591.7, 1597.7 and 2697.2, 2716.2 cm⁻¹, respectively. The FWHM values of G' peaks were not narrow (46.3, 61.9 cm⁻¹) (Figure 27c and e). However, the intensity ratios of G and G' peaks ($I_G / I_{G'}$) are similar to each other. Because of the fact that, considering the fitted G' peaks and FWHM values, turbostratic graphene seemed to be grown on Cu foil with these growth parameters¹³⁷.

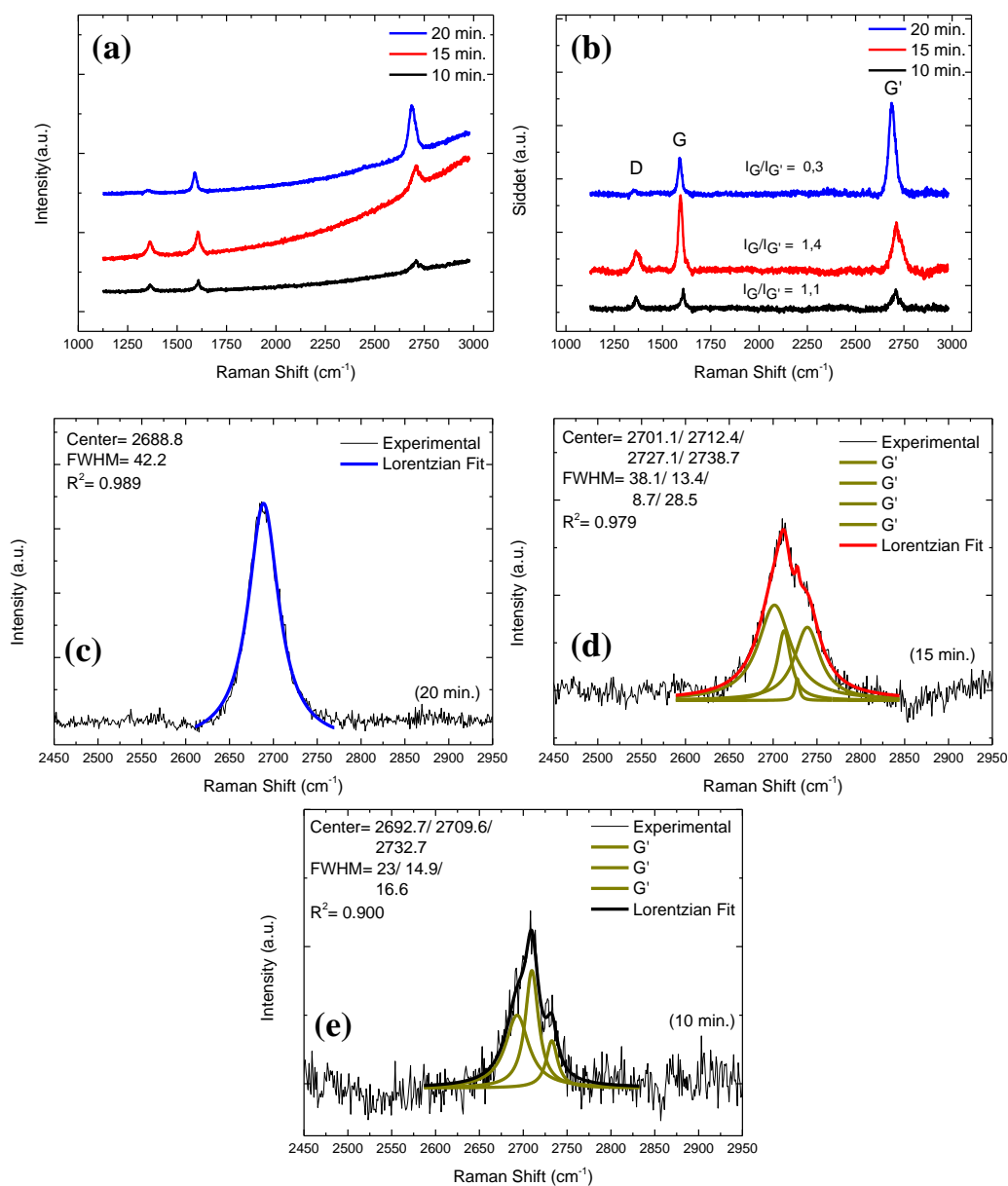


Figure 28. (a) and (b) Raman Spectrum of graphene samples which were grown for different growth time on Cu foil, (c-e) represents the center positions and FWHM values of fitted G' peaks of samples.

Up to now, growth temperature and growth time were studied to optimize the graphene growth parameters. Growth time and gas flow rates were altered to get defect-free, homogeneous and large area graphene. Three different growth times (10, 15 and 20 min.) were applied and gas flow rates were increased with respect to previous parameters; Ar: H₂: C₂H₄ (150 sccm: 30 sccm: 10 sccm). Similar to that applied previously, Raman spectra of the samples were collected in random regions on Cu foil Figure 28a. Fluorescence effect caused by Cu was again eliminated and the spectra were

acquired as seen in Figure 28b. After the subtraction of fluorescence effect, the peak positions were found to be as D ($1352.4, 1363.3, 1363.1 \text{ cm}^{-1}$), G ($1590.4, 1592.8, 1607.9 \text{ cm}^{-1}$) and G' ($2686.4, 2713.2, 2711.2 \text{ cm}^{-1}$). G' peaks were fitted by Lorentzian with one, four and three components and the FWHM values of G' peaks were determined as $42.2, 36.7$ and 51.4 cm^{-1} , respectively. Raman results showed that the growth in duration of 10 and 15 min. was not sufficient enough to decrease the graphene layer number at 850°C . When the growth time was increased to 20 min., defect-free and SLG was obtained on Cu foil.

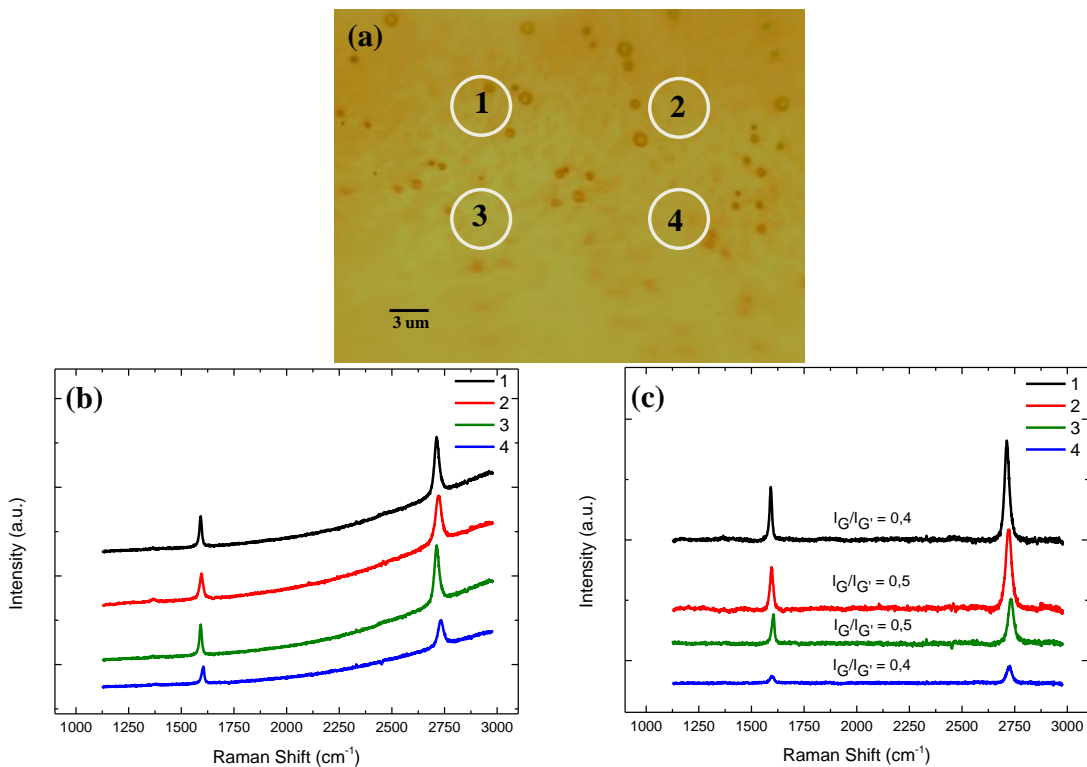


Figure 29. (a) Optical image and (b-c) Raman spectra of pristine graphene on Cu foil after optimizing of the growth parameters. Circles indicate where the Raman spectra were collected.

Figure 29 shows both the optical image taken in 100x magnification and Raman spectra of graphene. Large area graphene samples were grown on 25 μm thick unpolished Cu foil by LPCVD. For increasing the grain size on Cu foil, the chamber was pumped to a pressure of 10^{-5} Torr and an annealing temperature of 990°C was applied for a duration of 80 min. The process was started at room temperature and during the process; H_2 was utilized to reduce the native oxide layer on the Cu foil. The

graphene growth reaction was achieved in 20 min at 850 °C by introducing ethylene (C₂H₄), H₂ and Ar at a total pressure of about 1 Torr. The samples were grown with C₂H₄, H₂ and Ar flow rates of 10 sccm, 30 sccm and 150 sccm, respectively. Raman measurements were done in four different regions of the sample (Figure 29a). The Raman spectra which were taken in these regions show that 1L-graphene was obtained as large areas on Cu foil by using these growth parameters (Figure 29c). To sum up, repeatability of these optimized parameters to obtain large area, homogeneous and high quality graphene growth was ensured with these Raman spectra measurements.

4.2. Characterization of N-doped Graphene

4.2.1. Raman Spectroscopy Results

After the growth processes, graphene films were transferred onto different substrates such as SiO₂, Au (111) and sapphire to characterize the properties of graphene by different characterization techniques. Graphene was transferred onto desired substrates by using PR drop casting method. Details of the transfer procedure is presented in chapter 3. The most important step in the transfer procedure is to remove the polymer residues. Traditionally, PR drop casting method and other polymer-based methods¹³⁸ often produce residues on the graphene layer after the transfer. To remove PR residues, various strategies have been suggested in the literature, from using acetone or acetic acid¹³⁹ as a solvent to thermal annealing¹⁴⁰ in the presence of gas environment such as Ar¹⁴¹, N₂¹⁴² or Ar/H₂¹⁴³ under vacuum conditions. In addition to remaining polymer residues, some Cu particles may also be in contact to graphene after the transfer process. Although it is easy to remove the Cu particles by FeCl₃, it becomes difficult to separate these polymer residues from graphene. Despite intensive efforts involving high temperature treatment and extended annealing times, it turns out to be a great challenge to entirely remove the residues from the graphene layer¹⁴⁴. It has been shown that these residues could cause weak p-type doping of the graphene⁴⁹.

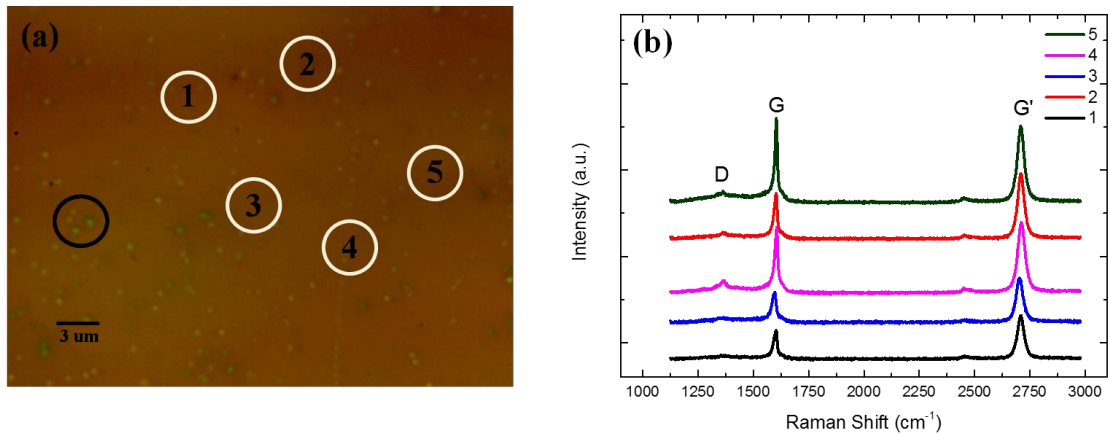


Figure 30. (a) Optical image and (b) Raman spectra of pristine graphene on SiO₂ substrate. As shown with black circle, greeny particles represent FeCl₃ residues and white circles indicate where the Raman spectra were collected.

The FeCl₃ residues were imaged by optical microscope as seen in Figure 30a and randomly collected Raman spectra of pristine graphene on SiO₂ substrate was shown in Figure 30b.

The Raman spectroscopy measurements were carried out to characterize the structural and electronic properties of pristine graphene and N-graphene. As mentioned previously, the D, G, and G' peaks are dominant in the Raman spectrum of N-graphene as in pristine graphene. The intensity ratio of G' and G peaks ($I_{G'}/I_G$) gives the information about doping, the intensity ratio of D and D' peaks ($I_D/I_{D'}$) corresponds to the defects and the intensity ratio of D and G peaks (I_D/I_G) give information about the relationship between the crystallite size and N doping level. These peaks are found at 1320–1350 cm⁻¹, 1570–1585 cm⁻¹, and 2640–2750 cm⁻¹, respectively. The D' peak appears at 1602–1640 cm⁻¹.

The doping uniformity is an important parameter that can be achieved by fine tuning of the doping parameters. The experiments conducted for doping homogeneously the graphitic lattice with N atoms, various plasma parameters were investigated for N₂ plasma treatment. The plasma period was varied from 5 min up to 79 min for the plasma powers 7W, 10W and 30W. All the samples were then analyzed in detail using Raman spectroscopy as shown in Figure 31. Raman spectra results were scrutinized with the corresponding doping parameters given in Table 3.

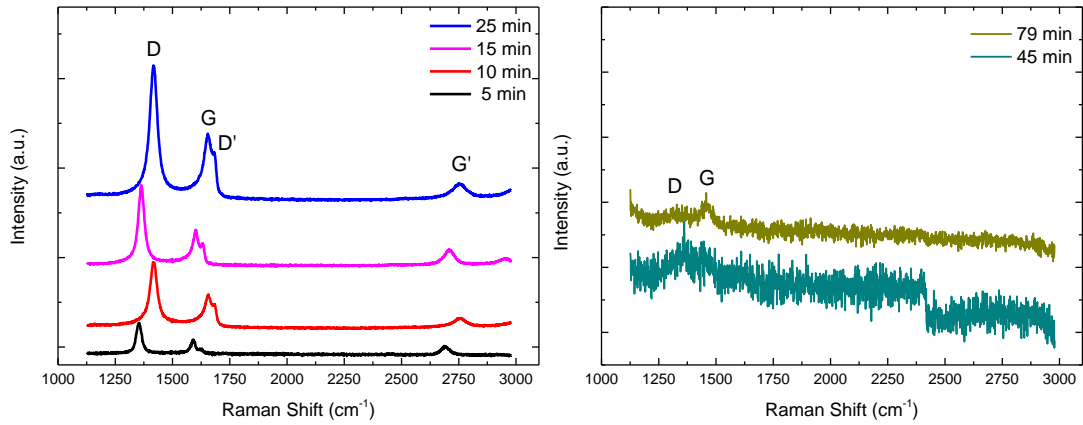


Figure 31. Raman spectra of N-graphene doped with different plasma times. The duration of plasma doping was varied between 5 and 79 min.

To understand the effect of plasma time in the doping process, plasma power and N_2 flow rate were kept constant. When plasma treatment period was above 30 min and the RF power was 30W, it was found that the graphene films were destroyed or partially removed from the substrate's surface without doping (Figure 31). The optimum plasma time was determined as less than 25 min.

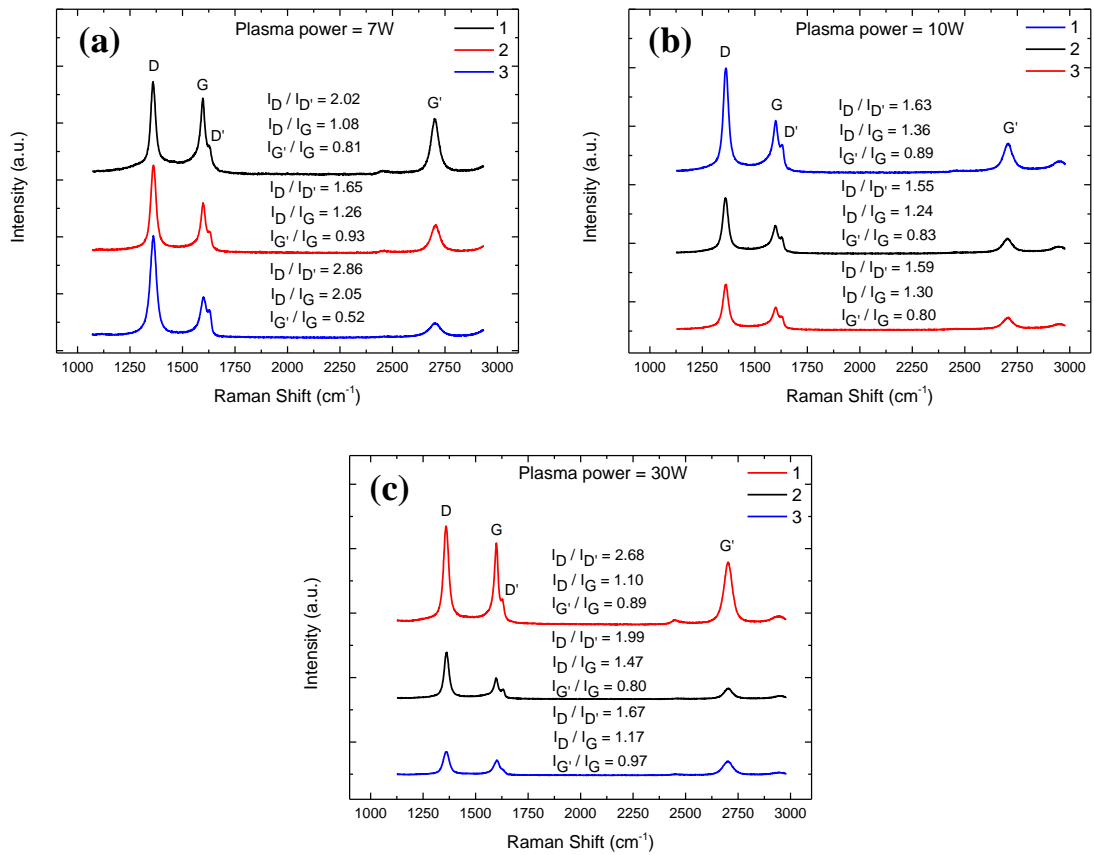


Figure 32. Raman spectra of N-graphene doped with different plasma powers. The intensity ratio of characteristics peaks was enclosed herewith.

After optimizing the plasma time, different plasma powers were studied to get homogenous doping parameter. N_2 plasma was created by applying a radio-frequency forward power of 7W, 10W and 30W, respectively. The Raman spectra of samples which were taken from three different regions were given in Figure 32. After analyzing I_G/I_G , $I_D/I_{D'}$ and I_D/I_G , the results obtained for 7W and 30W were compared with 10W. When a RF-power of 7 W and 30 W were applied, the I_D and $I_{G'}$ in Raman spectra were found to vary depending on the region (Figure 32a and c). Raman analysis revealed that the homogen and effective doping was obtained with an RF-power of 10 W and with a plasma duration of 15 min as determined by the change in the I_D and $I_{G'}$ as shown in Figure 32.

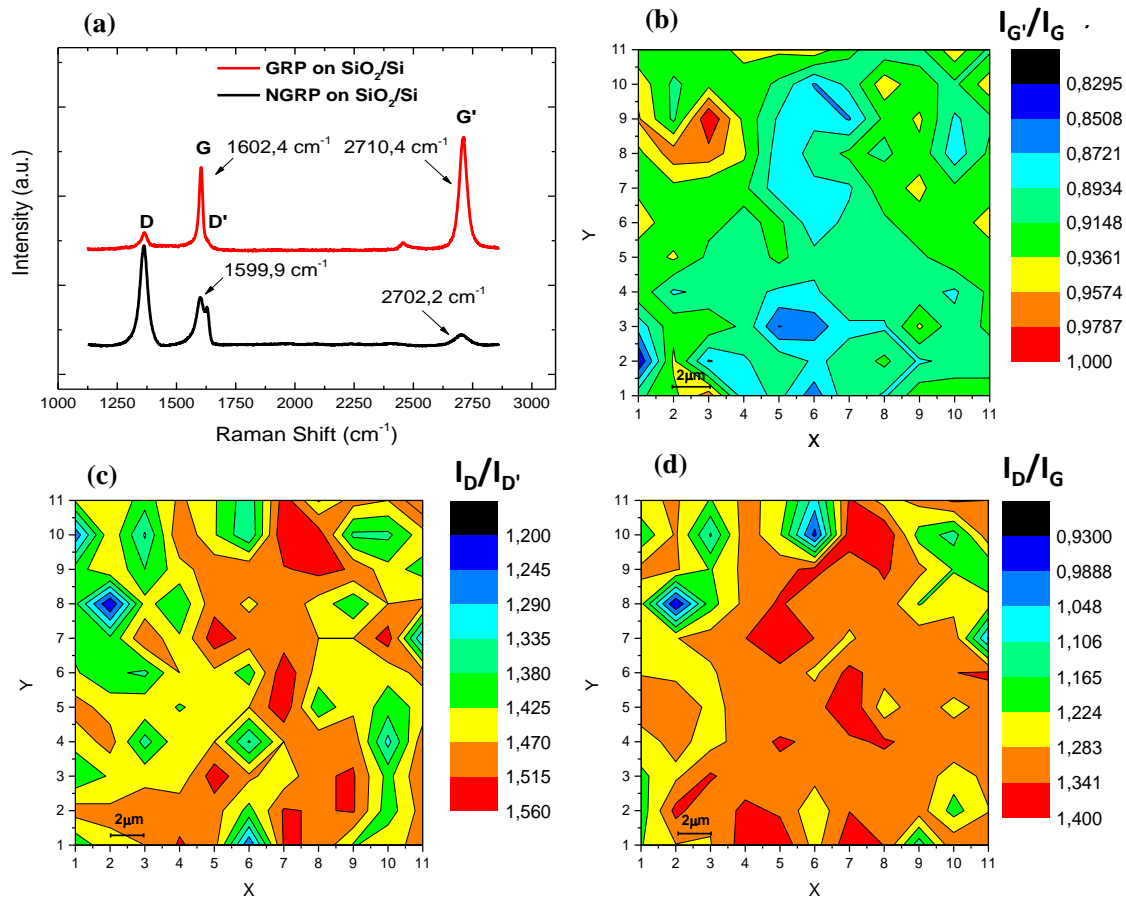


Figure 33. (a) Raman spectra of pristine graphene (GRP) and N-graphene (NGRP). Images (b), (c) and (d) show the Raman mapping of $I_{G'}/I_G$, $I_D/I_{D'}$ and I_D/I_G of NGRP on SiO₂/Si substrate with the selected region of 20 μm x 20 μm, respectively. N doping parameters: N₂ gas flow 10 sccm, effective RF-Power 10 W, plasma time 15 min, N₂ pressure 890 mTorr.

For the sample labeled as NGRP452, Raman mapping of N-graphene has also been carried out to show the homogeneity of the defect density in the graphitic lattice. Figure 33a shows the representative Raman spectra of graphene films on SiO₂/Si substrate before and after the plasma treatment for 15 min with an RF power of 10 W. It should be noted that graphene films on different substrates such as sapphire and Au (111) were also plasma-treated under the same conditions and yielded similar Raman spectra. In Figure 33a, the G and G' peaks can be clearly observed for graphene. The D peak was not clear before plasma treatment. However, after plasma process, the intensity of this peak was increased and became more significant.

The peak at 1630 cm⁻¹, the D' peak in the Raman spectrum of N-graphene was attributed to the inter-valley double resonance scattering process, emerged after plasma

process^{112, 116}. These results show that the amount of defects increased due to plasma treatment. In literature, it is claimed that homogeneous doping of graphene by N-plasma treatment method is challenging, because bombarded atoms in plasma environment damage all graphitic lattice randomly⁷⁴. According to our results, it is possible to prepare homogeneously N-graphene in large scale (20 μm x 20 μm) as proven by Raman surface mapping. By using Raman spectroscopy, 2D mapping of the substrate was studied at intervals of 2 μm and data were taken from 11 different points. After obtaining full Raman spectrum of N-graphene, baseline subtraction was done for all the data and then the map of $I_{G'}/I_G$, $I_D/I_{D'}$ and I_D/I_G was generated. As shown in Figure 33b, c and d, for a large area $I_{G'}/I_G$, $I_D/I_{D'}$ and I_D/I_G were about 0.83-1, 1.2-1.6, 0.93-1.4, respectively. These results were shown for the first time in literature that homogenous doping of N in graphene can be achieved using N- plasma treatment.

Raman spectroscopy analysis was also performed before and after the plasma treatment to observe the change in the Raman shift for G and G' peaks. The intensity of G' peak of graphene was much higher than that of N-graphene due to extra scattering events from the N induced electron doping. According to Table 4, the highest amount of blueshift for G peak was calculated as 8 cm^{-1} due to the effects of doping and compressive strain. The maximum ($I_D/I_{D'}$) of N-graphene was ~ 2 which is close to the boundary defects reported in literature¹¹⁶.

Table 4. Average Raman Peak Analysis of N-graphene.

Sample	Shift in G Peak (cm^{-1})	Shift in G' Peak (cm^{-1})	$I_{G'}/I_G$	$I_D/I_{D'}$	I_D/I_G
NGRP on Sapphire	-2 ± 0.25	10 ± 0.15	0.791	1.952	0.978
NGRP on SiO₂/Si	-3 ± 0.3	-8 ± 0.2	0.892	1.345	1.358
NGRP on Au/Mica	5 ± 0.2	-9 ± 0.15	1.317	1.685	1.427

As given in Table 4, the amount of the Raman shift for G and G' peaks and their positions change not only due to the doping concentration but also the graphene-substrate interaction caused by different thermal expansion coefficients of graphene and the substrate¹¹⁷⁻¹¹⁸. N induced n-type doping in graphene should cause a blueshift of G peak and redshift of 2D peak^{116, 128}. Therefore, as reported in literature¹¹⁶, the strong blueshifts of G and 2D peaks cannot be explained only by electron doping. Otherwise,

the other mechanisms such as compressive/tensile strain in graphene could cause a blue/red shift of these dominant peaks.

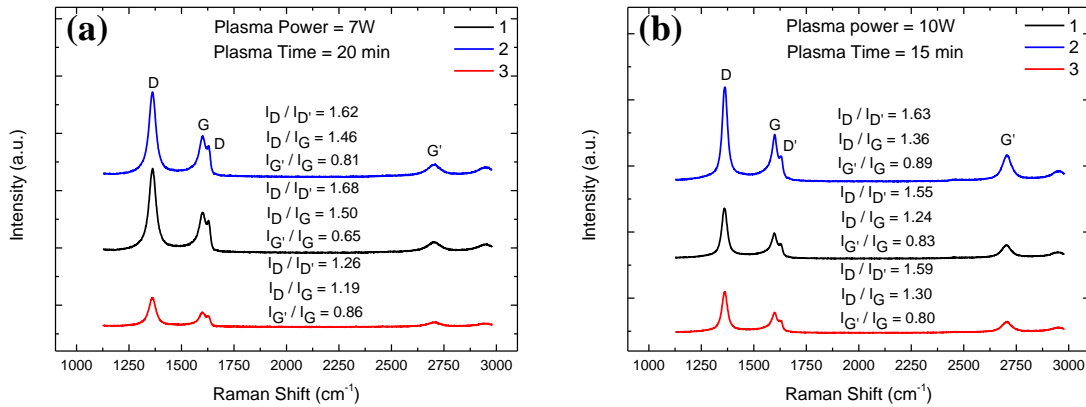


Figure 34. Raman spectra of N-graphene doped with different plasma powers and plasma times.

The effect of plasma time and plasma power on the doping concentration was also studied in this thesis. The doping process of RF-power of 10W and plasma duration of 15 min, plasma power was decreased to 7W and plasma time was increased to 20 min. The N_2 flow was regulated as 10 sccm and kept constant for two samples. Figure 34a and b shows the Raman spectra of the samples which were taken from different regions on the sample surface. The intensity ratio of characteristics peaks (I_G/I_G , $I_D/I_{D'}$ and I_D/I_G) was also determined and calculated for each samples. Although peak ratios were similar, the homogeneity was not achieved for the sample doped with RF-power of 7W and plasma duration of 20 min (Figure 34a). We found that the change in plasma power and plasma time did not alter the doping concentration. These results have also been verified by XPS measurements as discussed in the next section.

4.2.2. XPS Results

XPS measurements were done to determine the N configuration and concentration in graphitic lattice. In general the N1s spectrum of N-graphene samples can be deconvoluted to several individual peaks characteristic to pyridinic N (398.1–399.3 eV), pyrrolic N (399.8–401.2 eV), and quaternary N (401.1– 402.7 eV).

The XPS spectra of freshly prepared graphene samples we recorded before and after doping with N. Photoemission spectra were collected with a SPECS Phoibos 150 Hemispherical Analyzer furnished with monochromatized Al-K α x-ray source. N-graphene samples on SiO₂ were attached to the sample holder. The pressure of the vacuum chamber was $P < 10^{-9}$ mbar during the measurements. Large area focus and 40 eV pass energy was used to achieve the best signal-to-noise ratio in XPS spectra. The spectral fitting was performed with CASA XPS software and Shirley background type was used for subtraction of raw data. The XPS results of these samples have been presented in Figure 35. Among the process parameters only plasma power and treatment time were changed to observe the effect of N configuration in graphitic lattice.

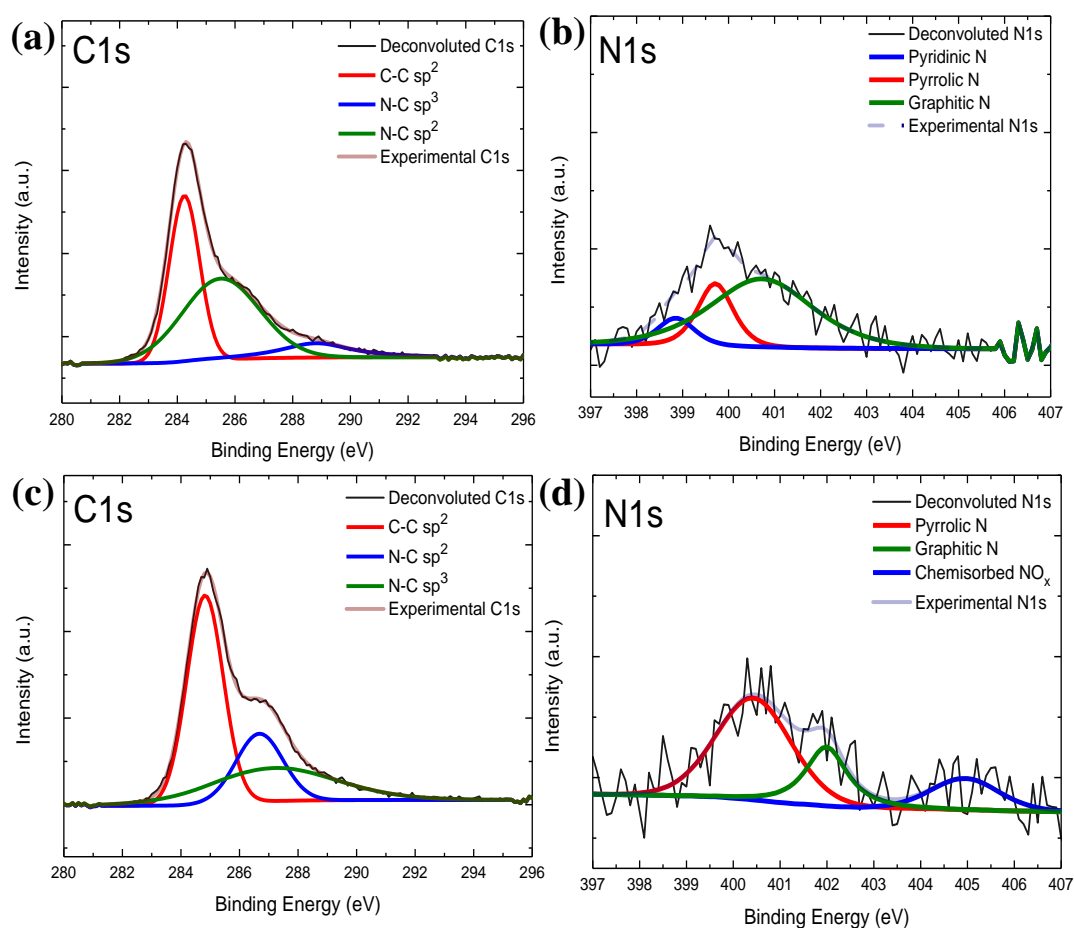


Figure 35. The XPS measurements of C1s and N1s band in N-graphene films on SiO₂/Si treated by N₂ plasma during (a-b) 15 min with RF-power of 10 W and (c-d) 20 min, with RF-power of 7W, respectively. The N₂ gas flow rate at plasma chamber was kept constant as 10 sccm.

As seen in Figure 35 a and c, the main signal in the C1s spectrum corresponds to C-C bond with sp^2 hybridization which has the binding energy around $284.5 \text{ eV} \pm 0.2 \text{ eV}$. These data confirms the presence of graphene. Other signals observed at $286 \pm 0.2 \text{ eV}$ and $287.8 \pm 0.2 \text{ eV}$ corresponds to sp^2 and sp^3 hybridized C-N bonding (C and N group structures), respectively ¹²⁴. These C and N group structures also increase the amount of defects in graphitic structure. On the other hand, the N1s signal with binding energy of 400 eV in XPS spectra of samples, treated by using different parameters, has revealed a redistribution of intensities of all components of the band. Figure 35 b and d show the N1s spectra of N-graphene. The signals with energies $398.7 \pm 0.2 \text{ eV}$, $400.1 \pm 0.2 \text{ eV}$ and $402.0 \pm 0.2 \text{ eV}$ correspond to pyridinic-N, pyrrolic-N and quaternary N or graphitic-N, respectively ⁷⁴. The signal seen at $405 \pm 0.2 \text{ eV}$ (blue colored in Figure 35d) was attributed to the adsorbed N species or chemisorbed N oxide ¹⁴⁵.

As shown in Figure 35 b and d, the pyridinic-N configuration was not formed when the plasma time is increased and RF-power is decreased. However pyrrolic-N and graphitic-N were formed in either case. Increasing the RF-power and decreasing the plasma time, pyrrolic-N configuration became more dominant. It should be noted that the N_2 plasma treatment resulted in the predominant pyrrolic type of N doping in graphitic lattice.

As reported in literature ¹²³, when RF-discharged with lower effective power was used, the concentration of N increased with the treatment time. For example, graphene treatment using an effective RF-power of 7 W and a plasma treatment time of 20 min provided a N concentration of 1.8 atomic %, while the treatment of graphene film using an RF-power of 10 W for 15 min led to 1.7 atomic % of N atoms in graphitic lattice. The N/C atomic ratio of samples was calculated by taking the ratio of the total areas under the N1s and C1s spectrum. We found that the concentration of N atoms in graphitic lattice could be the same with different plasma time and different types of N configurations.

4.2.3. STM-STS Results

The local topographic structure of n-type doped graphene sheets and its sublattices were studied by using STM. STS measurements were also conducted to measure the density of states (DOS) and carrier concentration at the atomic scale. The STM and

STS measurements were performed over different regions of N-doped and pristine graphene samples for reference on Au (111) surface to investigate the configuration of N atoms. STM images were acquired from the graphene films transferred onto Au (111) substrates under ambient conditions by using a Nanosurf Easyscan system. STM piezoelectric scanners were calibrated laterally, with graphite and Au (111)¹⁴⁶. The STM tip was prepared from a Pt/Ir (90%/10%) 0.25–0.2 mm wire cut under ambient conditions. All images were acquired in constant-current mode. The typical imaging conditions were a bias voltage of 25 to 70 mV and a tunneling current of 1 nA. The images shown in this thesis are the raw data unless stated otherwise. The obtained images were processed with Scanning Probe Image Processor software.

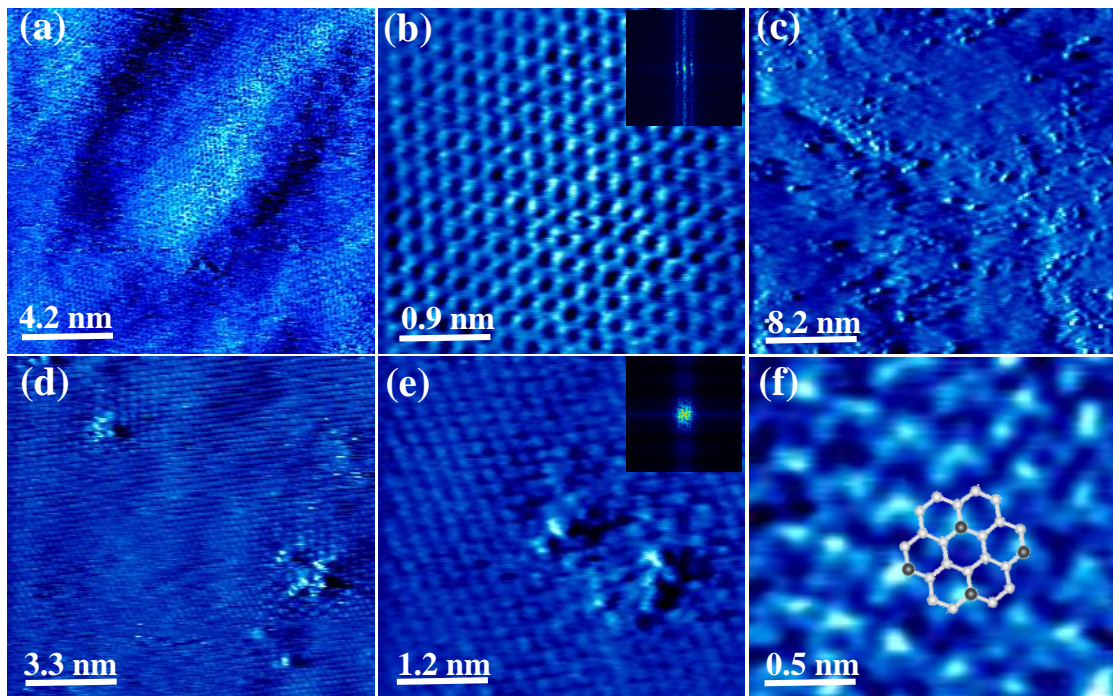


Figure 36. STM images of graphene (a-b) and N-graphene (c-f) on Au (111) substrate. In Figure f, simulated N and C atoms are shown as black and white colors, respectively. The STM images were recorded under constant-current mode with bias voltage varying between 25 and 70 mV and a 1 nA tunneling current.

STM image of graphene is shown in Figure 36a. As seen in Figure 36b, the STM image of graphene with honeycomb lattice infers that the graphene layer on Au/Mica is one layer. After N doping, STM images of N-graphene are shown in Figure 36c-f. It is clearly seen that the bombarded N atoms deformed the honeycomb structure and yields

small clusters on the graphitic lattice. The presence of brighter sites in the selected region showed that the doping of N atoms is smooth and this was also proven by Fast Fourier Transform (inset of Figure 36b and e). High magnification STM image of N-graphene (Figure 36f) showed that N atoms have one unoccupied electron in valence band, were shaped in a triangular pattern on graphitic surface. As seen in Figure 36f, these free electrons in C-N bonding cause an electron cloud around C atoms. The observed change in the morphology is due to the electronic configuration of N atom on graphene layer.

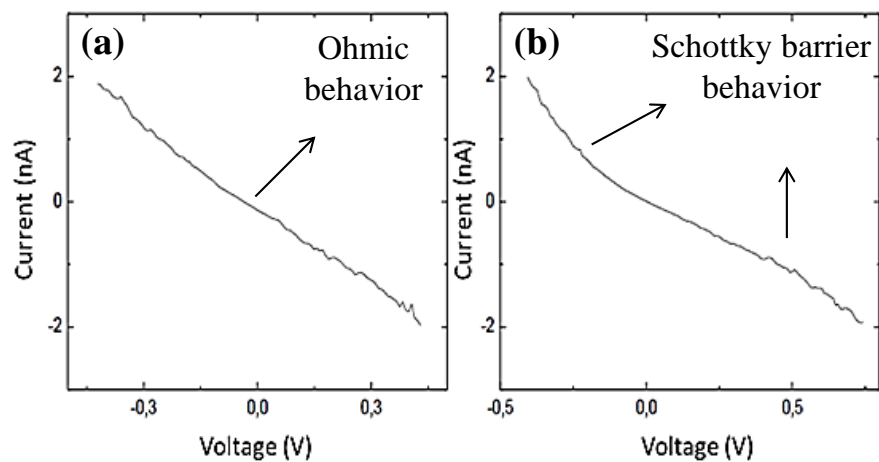


Figure 37. STS curves of (a) pristine and (b) N-graphene, respectively.

STS results of pristine and doped graphene was also investigated. The results showed that pristine graphene has ohmic behavior in current vs voltage curve. After doping due to the N_2 dopants this linear curve was bended and it showed like a metal-semiconductor behavior (Figure 37).

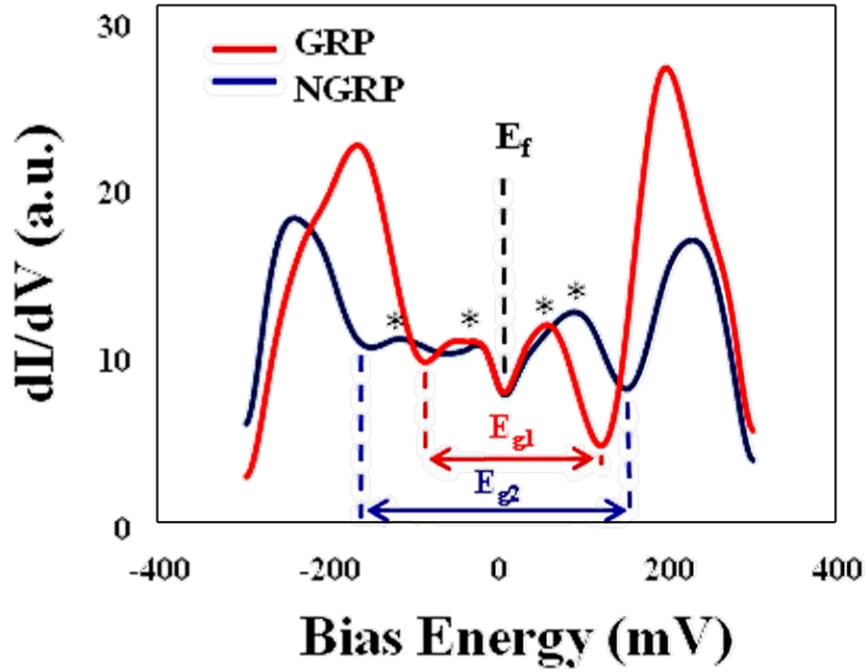


Figure 38. dI/dV characteristics of pristine (red line) and N-graphene (blue line) on Au (111).

We also investigated the electronic behavior of pristine (red) and N-graphene (blue) via STS measurements (Figure 38). Based on the dI/dV measurements, the average energy gap for pristine graphene (E_{g1}) and N-graphene (E_{g2}) were determined as 205 meV and 317 meV, respectively. This was in good agreement with the calculated gap values. There is a gap in pristine graphene on Au (111). This gap may be occurred due to the defect states in the honeycomb lattice, the weak graphene-Au (111) interaction or the intervalley scattering observed around a point defect in the graphene layer on the Au (111) surface¹⁴⁷. After N doping, the difference in energy gap can be easily observed. Since the Dirac point of graphene on the Au (111) surface is located at E_F ¹⁴⁷, there is no signature that could be associated with the presence of Dirac point in any particular position as seen in the STS measurements on graphene/ Pt (111)¹⁴⁸. This result may indicate that insufficient doping of graphene exists for graphene/Au or no significant change expected in the energy position of the Dirac point. Fermi level is located at 0 meV as done in Refs¹⁴⁹⁻¹⁵¹. There are some peaks near Fermi level which are shown with asterisk in the dI/dV curve. These can be attributed to the presence of defect states which cause the change in electronic state of pristine graphene after plasma treatment.

4.2.4. Methodology of DFT Simulations

In order to understand the STM analysis shown in Figure 36f, we used density-functional theory (DFT) calculations. For structural and electronic relaxation of N-graphene structures first-principles calculations were performed by employing the plane-wave basis projector augmented wave (PAW) method in the framework of DFT. As exchange-correlation potential, Perdew-Burke-Ernzerhof (PBE)¹⁵²⁻¹⁵³ form of generalized gradient approximation (GGA) implemented in the Vienna Ab Initio Simulation Package (VASP)¹⁵⁴⁻¹⁵⁵ is used. The energy cutoff value for the plane-wave basis set was taken to be 500 eV. The total energy was minimized until the energy variation in successive steps became less than 10^{-5} eV in the structural relaxation and the convergence criterion for the Hellmann-Feynman forces was taken to be 10^{-4} eV/Å. The minimum energy was obtained by varying the lattice constant and the pressure was reduced below 1 kbar. $25 \times 25 \times 1$ gamma-centered k-point sampling is used for the primitive unit cell. In DOS calculations of N-graphene, the Gaussian broadening for the DOS calculation was taken to be 0.05. The van der Waals (vdW) correction to the GGA functional was included by using the DFT-D2 method of Grimme¹⁵⁶. Analysis of the charge transfers in the structures was performed by employing Bader analysis¹⁵⁷.

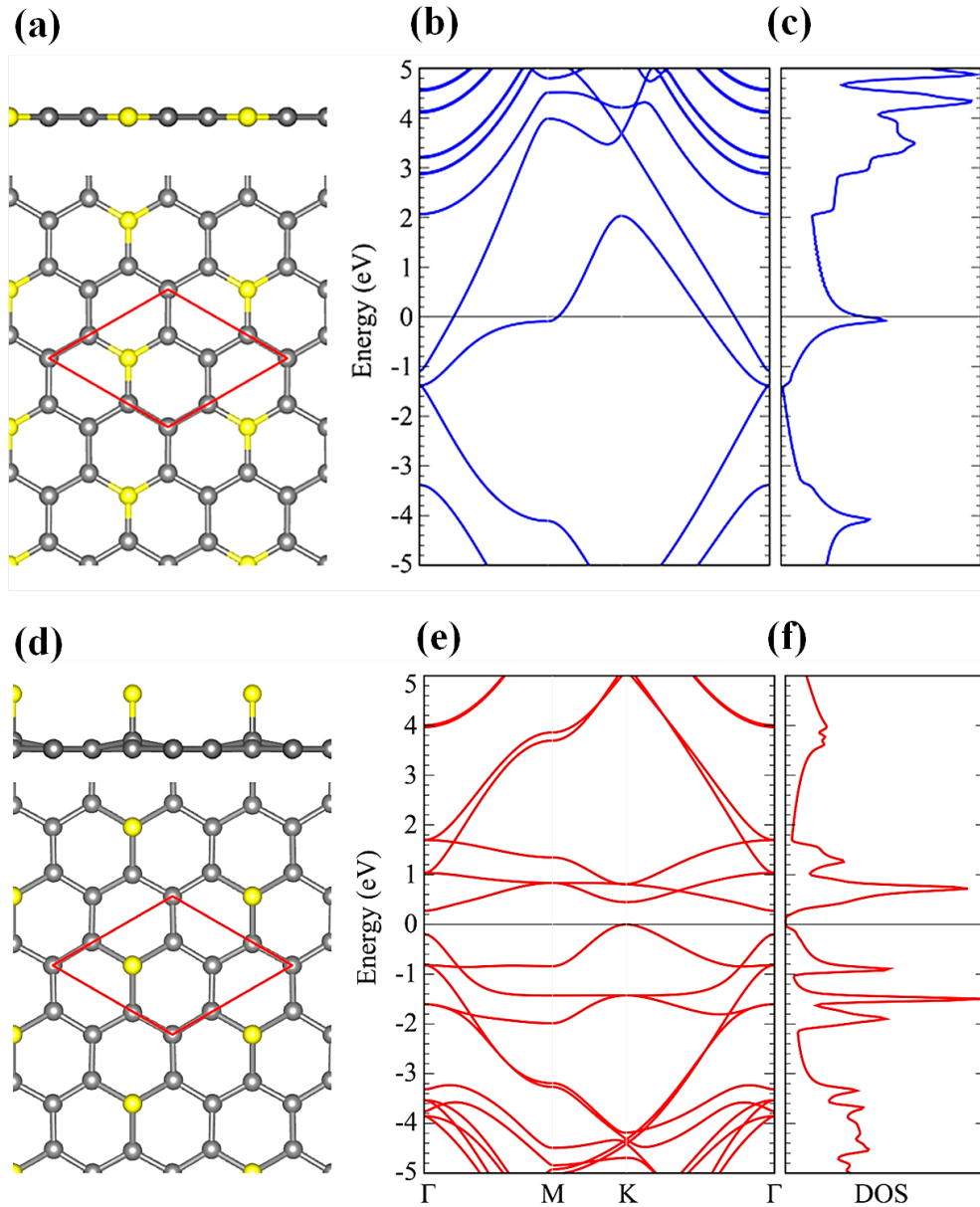


Figure 39. (a, d) The top and side views, (b, e) the energy band structure, and (c, f) density of states of N substituted and N adsorbed graphene, respectively.

The experimental results show that the well-patterned regions formed by nitrogenation have a trigonal lattice periodicity that corresponds to a graphene supercell $\sqrt{3} \times \sqrt{3} \times 1$ with one doping. Moreover, another question is whether the doping occurs by adsorption of N atoms on graphene host or N atoms are substituted by C atoms. Our careful structural relaxation calculation reveals that both substitution and adsorption of N atoms on graphene may take place. For the substitution case, the structural calculation shows that the substituted N is localized as C in lattice and the hexagonal symmetry is

conserved as shown in Figure 39a. The N-C bond length was found to be 1.40 Å which is slightly lower than C-C bond in bare graphene. Consequently, the lattice constant reduces from bare graphene lattice constant of 4.27 to 4.23 Å. In addition, Bader charge transfer analysis shows that C atoms donated 1.2e per N atom. In the adsorption case, N prefers to localize over the C atom with bond length of 1.46 Å as shown in Figure 39 d. The C atom slightly shifts towards the N atom which is donated 0.4e. The C-C bonds in the vicinity of N slightly increases hence the lattice constant is extended to 4.32 Å.

In addition, the electronic structure analysis reveals that substitution and adsorption of N result different modification in the electronic property of graphene. In the substitution case, the system has metallic property. As shown in Figure 39 b and c the Fermi level of the well-known graphene like band and DOS dispersions is shifted towards positive energy region. This indicates that the graphene is n-type doped when the N is substituted. On the other hand, the adsorption of N opens an indirect band gap of 0.28 eV which are shown in Figure 39e and f. The valance band maximum and conduction band minimum appears at K and Γ , respectively.

The experimental band gap measurement indicates that the band gap of N-graphene increases compared to that of pristine graphene as shown in Figure 38. According to these results, graphene on Au (111) presented a semiconductor like behavior due to the presence of N dopants. Experimental and theoretical results indicate that this further gap opening stems from adsorption of N on C sites in our measurement.

4.2.5. Kelvin Probe Force Microscopy (KPFM) Results

Kelvin Probe Force Microscopy (KPFM) was used to define the work functions of graphene and N-graphene to determine the carrier type after the doping process. KPFM technique was performed using commercial Scanning Probe Microscopy instrument (Solver Pro 7 from NT-MDT, Russia). Contact potential difference (CPD) between tip and sample ($CPD = \Phi_{SAMPLE} - \Phi_{TIP}$) was measured with this technique. Conductive TiN coated tip with thickness of 35 nm (NT-MDT, Russia) was used to obtain CPD signals and calibrated with HOPG ($\Phi_{HOPG} = 4.6$ eV) as reference due to the constant work function in air and inert nature¹⁵⁸. Therefore, the work functions of the

samples were calculated as follows where the CPD_{HOPG} is the work function of HOPG relative to the probe ¹⁵⁹.

$$\Phi_{SAMPLE} = 4.6 \text{ eV} + CPD_{HOPG} - CPD_{SAMPLE} \quad (4.1)$$

After getting XPS results (see Figure 35), KPFM measurements were also done for these two samples to determine the difference in the work function related with the different plasma treatment parameters. Akada *et al.* was indicated that graphitic-N decreases the work function, whereas pyridinic-N and pyrrolic-N increase the work function ¹⁶⁰.

Figure 40 shows the cantilever oscillation amplitude (Mag) versus bias voltage. When Mag signal is close to zero due to feedback in the SPM system, interaction forces between tip and samples become zero and applied dc voltage to the tip equals to CPD. These measurements were taken locally and three different region on the sample surface. The CPD of HOPG which is commonly used for the calibration in KPFM measurement was around 0.26V. The CPD values of GRP, NGRP457 and NGRP452 were measured as 0, -0.091 and -0.114V (Figure 40). Additionally, the calculated work functions were around 4.34, 4.24 and 4.22 eV for GRP, NGRP457 and NGRP452, respectively (see the Table 5). The differences of CPD reflect the doping effect on the N-graphene sample surfaces.

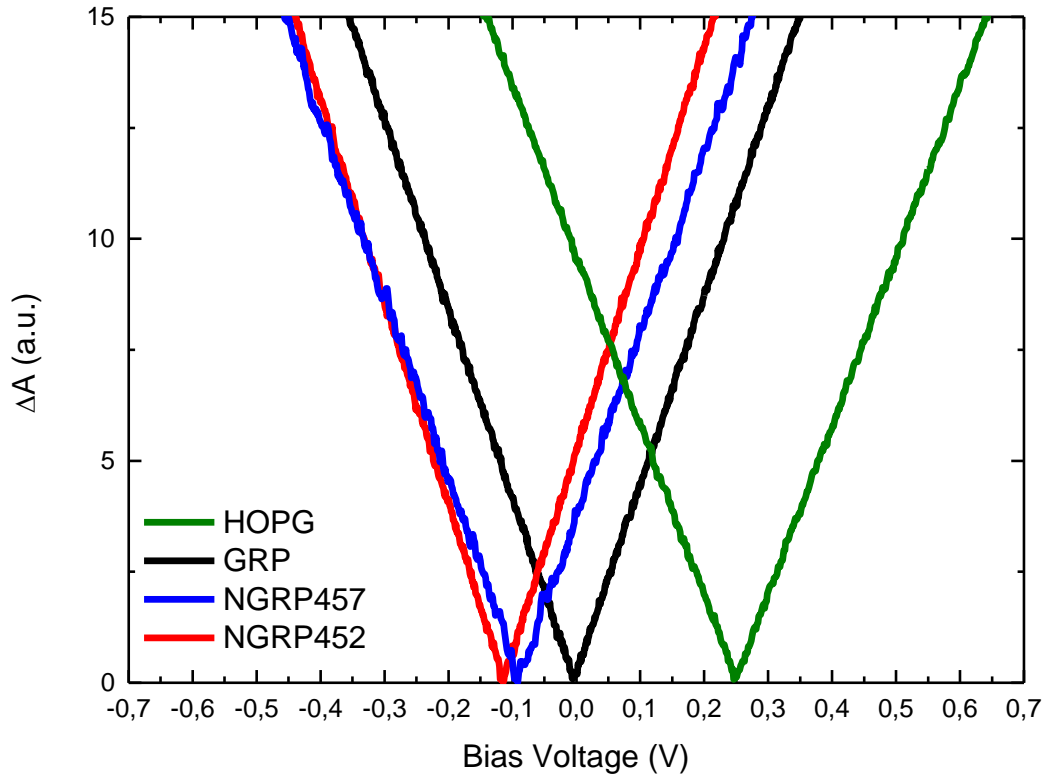


Figure 40. Surface potential differences of graphene (GRP) and N-graphene (NGRP) with various doping parameters. N-graphene films on SiO₂/Si treated by N₂ plasma during (red color) 15 min with RF-power of 10 W and (blue color) 20 min with RF-power of 7W, respectively. The N₂ gas flow rate at plasma chamber was kept constant as 10 sccm. HOPG (green color) is used as reference .

All values of mean CPD and mean Φ are summarized in Table 5. The work-function value of graphene without N₂ plasma treatment is smaller than the reference value (4.60 eV) , indicating a p-type behavior, as reported in the literature ¹⁶¹ .

Table 5. The values of mean CPD and mean Φ .

Sample	Mean Φ (eV)	Mean CPD (V)
HOPG	4.6	0.26
GRP	4.34	0
NGRP457	4.24	-0.091
NGRP452	4.22	-0.114

After N doping of graphene samples, the CPD values showed a downshift trends. This indicates that there is an electron donation from the graphitic N atom to the graphene lattice which causes n-type doping. In addition, the reason for the lowest downshift in surface potential of doped samples is due to the lowest N doping concentration in graphene layer which was supported by the XPS results. It should be noted that KPFM measurement results are in good agreement with the XPS results.

CHAPTER 5

CONCLUSIONS

The main aim of this thesis was to develop an effective method for achieving homogeneously doped graphene by using N_2 plasma treatment. In this study, a two-steps procedure was applied in the following manner: Firstly, large-area graphene was successfully grown by using C_2H_4 gas on Cu foil at low pressure, followed by its transfer onto a desired substrate. The next step was the treatment of synthesized graphene film using RF discharge in N_2 gas. These steps were crucial for controlling the process precisely. This method also allowed the control of N doping level in graphitic lattice. Both graphene samples, grown on Cu foil and transferred on desired substrates were characterized by Raman spectroscopy. The doping process was controlled by plasma power and time under constant N_2 flow rate. The homogeneous N-doping of graphene was further analyzed by Raman spectroscopy, XPS, STM/STS and KPFM measurements.

After the graphene growth by CVD, Raman spectroscopy was utilized in order to determine the number of the layers and quality of graphene growth over Cu foil. This method was applied for all the samples before and after plasma treatment to observe the change in Raman shift for G and G' peaks. We found that the intensity of G' peak of graphene was much higher than that of N-graphene due to the enhanced scattering from the nitrogen induced electron doping. It was observed that the graphene films were partially removed from the surface for plasma duration of 30 min. and RF power of 30W. When plasma duration was decreased to 15 min and RF-power was set to 7W and 30W was applied to the graphene samples, I_D and $I_{G'}$ were found to vary from region to region on the surfaces. The optimum homogeneous doping parameter was obtained with an RF-power of 10W and plasma duration of 15 min indicated by the change in I_D/I_G . Raman mapping of N-graphene was also performed to show the homogeneity of defect density in the graphitic lattice. This study showed that it becomes possible to prepare homogeneously doped N-graphene in large scale ($20\ \mu\text{m} \times 20\ \mu\text{m}$) as proven by Raman surface mapping. By using Raman spectroscopy, 2D mapping of substrate was studied at intervals of $2\ \mu\text{m}$ and data were taken from 11 different points. After getting full

Raman spectrum of N-graphene, baseline subtraction was done for all data and colored maps of I_G/I_G , I_D/I_D and I_D/I_G were generated.

XPS measurements were used to determine the nitrogen configuration and concentration in graphitic lattice. According to the obtained results, an effective RF-power of 7W with a plasma treatment time of 20 min. yields a nitrogen concentration of about 1.8 atomic %, while the treatment of graphene film using an RF-power of 10W for 15 min led to 1.7 atomic % of nitrogen atoms in graphitic lattice. The most favorable doping parameters for homogeneous doping were determined and at these optimized parameters, 1.7 atomic % of nitrogen atoms were introduced to the graphitic lattice. When RF-discharged with low power was used, the concentration of nitrogen is increased with the treatment time. The increment of N_2 plasma time and decrement of N_2 plasma power, the pyridinic-N configuration was found to disappear and pyrrolic-N became more dominant. It should be noted that the N plasma treatment resulted in the predominant pyrrolic type of N doping in graphitic lattice. We also found that the concentration of N atoms in graphitic lattice could be same with different plasma time and different types of nitrogen configurations.

STM measurements were done on homogeneously doped graphene sample to understand the local atomic structure in the vicinity of a N dopant in the graphene sheets and in their sub-lattices. STS results showed an increase of nearly 100 meV in the band gap after doping the graphene on Au (111). In addition, for further understanding of STM/STS results and DFT based calculations were performed. It was concluded that the periodic adsorption of N atoms on the top of C atoms rather than substitution of them is the dominant doping mechanism in our N-graphene samples.

KPFM measurements were also conducted for pristine graphene and for two different N doped samples to determine the difference in the work function related with the different plasma treatment parameters. The average work functions and CPD values were estimated respectively. These measurements were taken locally on three different regions of the sample surface. After N doping of graphene samples, the CPD values showed a downshift (negative) trend, indicating the n-type doping. To conclude, KPFM measurement results are in good agreement with XPS results.

REFERENCES

1. Geim, A. K.; Novoselov, K. S., The rise of graphene. *Nature Materials* 2007, 6 (3), 183-191.
2. Novoselov, K.; Jiang, D.; Schedin, F.; Booth, T.; Khotkevich, V.; Morozov, S.; Geim, A., Two-dimensional atomic crystals. *Proceedings of the National Academy of Sciences of the United States of America* 2005, 102 (30), 10451-10453.
3. Geim, A. K., Graphene: status and prospects. *Science* 2009, 324 (5934), 1530-1534.
4. Neto, A. C.; Guinea, F.; Peres, N. M.; Novoselov, K. S.; Geim, A. K., The electronic properties of graphene. *Reviews of Modern Physics* 2009, 81 (1), 109.
5. Boehm, H. P.; Setton, R.; Stumpp, E., Nomenclature and terminology of graphite intercalation compounds (IUPAC Recommendations 1994). *Pure and Applied Chemistry* 1994, 66 (9), 1893-1901.
6. Pierson, H., Handbook of carbon, graphite, diamond and fullerenes. Properties, processing and applications, 1993. NY: William Andrew Publishing/Noyes.
7. Mostofizadeh, A.; Li, Y.; Song, B.; Huang, Y., Synthesis, properties, and applications of low-dimensional carbon-related nanomaterials. *Journal of Nanomaterials* 2011, 2011, 16.
8. Kuc, A., Low-dimensional transition-metal dichalcogenides. *Chem. Modell.* 2014, 11, 1-29.
9. Gumbs, G.; Huang, D., Electronic and photonic properties of graphene layers and carbon nanoribbons. *Philosophical Transactions of the Royal Society of London A: Mathematical, Physical and Engineering Sciences* 2010, 368 (1932), 5353-5354.
10. Katsnelson, M. I., Graphene: carbon in two dimensions. *Materials today* 2007, 10 (1), 20-27.
11. Novoselov, K. S.; Geim, A. K.; Morozov, S. V.; Jiang, D.; Zhang, Y.; Dubonos, S. V.; Grigorieva, I. V.; Firsov, A. A., Electric field effect in atomically thin carbon films. *Science* 2004, 306 (5696), 666-669.
12. Wang, F.; Zhang, Y.; Tian, C.; Girit, C.; Zettl, A.; Crommie, M.; Shen, Y. R., Gate-variable optical transitions in graphene. *Science* 2008, 320 (5873), 206-209.
13. Pop, E.; Varshney, V.; Roy, A. K., Thermal properties of graphene: Fundamentals and applications. *MRS Bulletin* 2012, 37 (12), 1273-1281.

14. Ovid'ko, I., Mechanical properties of graphene. *Rev. Adv. Mater. Sci* 2013, 34, 1-11.
15. Bolotin, K. I.; Sikes, K.; Jiang, Z.; Klima, M.; Fudenberg, G.; Hone, J.; Kim, P.; Stormer, H., Ultrahigh electron mobility in suspended graphene. *Solid State Communications* 2008, 146 (9), 351-355.
16. Morozov, S.; Novoselov, K.; Katsnelson, M.; Schedin, F.; Elias, D.; Jaszczak, J. A.; Geim, A., Giant intrinsic carrier mobilities in graphene and its bilayer. *Physical Review Letters* 2008, 100 (1), 016602.
17. Blake, P.; Brimicombe, P. D.; Nair, R. R.; Booth, T. J.; Jiang, D.; Schedin, F.; Ponomarenko, L. A.; Morozov, S. V.; Gleeson, H. F.; Hill, E. W., Graphene-based liquid crystal device. *Nano Letters* 2008, 8 (6), 1704-1708.
18. Ado, J., Raman Spectroscopy in Graphene-Based Systems: Prototypes for Nanoscience and Nanometrology." *ISRN Nanotechnology* 2012, 16. doi: 10.5402/2012/234216
19. Kumar, N.; Kumbhat, S., *Essentials in Nanoscience and Nanotechnology*. John Wiley & Sons: 2016.
20. Gomez de Arco, L. M., *Graphene and carbon nanotubes: synthesis, characterization and applications for beyond silicon electronics*. 2010.
21. Reich, S.; Maultzsch, J.; Thomsen, C.; Ordejon, P., Tight-binding description of graphene. *Physical Review B* 2002, 66 (3), 035412.
22. Enoki, T.; Ando, T., *Physics and chemistry of graphene: graphene to nanographene*. CRC Press: 2013.
23. Tománek, D.; Jorio, A.; Dresselhaus, M. S.; Dresselhaus, G., Introduction to the important and exciting aspects of carbon-nanotube science and technology. In *Carbon Nanotubes*, Springer: 2007; pp 1-12.
24. Kumar, P.; Singh, A. K.; Hussain, S.; Hui, K. N.; San Hui, K.; Eom, J.; Jung, J.; Singh, J., Graphene: synthesis, properties and application in transparent electronic devices. *Reviews in Advanced Sciences and Engineering* 2013, 2 (4), 238-258.
25. Novoselov, K.; Geim, A. K.; Morozov, S.; Jiang, D.; Katsnelson, M.; Grigorieva, I.; Dubonos, S.; Firsov, A., Two-dimensional gas of massless Dirac fermions in graphene. *Nature* 2005, 438 (7065), 197-200.
26. Zhang, Y.; Tang, T.-T.; Girit, C.; Hao, Z.; Martin, M. C.; Zettl, A.; Crommie, M. F.; Shen, Y. R.; Wang, F., Direct observation of a widely tunable bandgap in bilayer graphene. *Nature* 2009, 459 (7248), 820-823.
27. Zhang, Y.; Tan, Y.-W.; Stormer, H. L.; Kim, P., Experimental observation of the quantum Hall effect and Berry's phase in graphene. *Nature* 2005, 438 (7065), 201-204.

28. Chen, J.-H.; Jang, C.; Xiao, S.; Ishigami, M.; Fuhrer, M. S., Intrinsic and extrinsic performance limits of graphene devices on SiO₂. *Nature Nanotechnology* 2008, 3 (4), 206-209.
29. Saito, R.; Dresselhaus, G.; Dresselhaus, M. S., *Physical properties of carbon nanotubes*. World Scientific: 1998; Vol. 35.
30. Cooper, D. R.; D'Anjou, B.; Ghattamaneni, N.; Harack, B.; Hilke, M.; Horth, A.; Majlis, N.; Massicotte, M.; Vandsburger, L.; Whiteway, E., Victor Yu. *Experimental review of graphene* 2011.
31. Georgakilas, V., *Functionalization of graphene*. John Wiley & Sons: 2014.
32. Gomez De Arco, L.; Zhang, Y.; Schlenker, C. W.; Ryu, K.; Thompson, M. E.; Zhou, C., Continuous, highly flexible, and transparent graphene films by chemical vapor deposition for organic photovoltaics. *ACS Nano* 2010, 4 (5), 2865-2873.
33. Kusdemir, E.; Özkendir, D.; Fırat, V.; Çelebi, C., Epitaxial graphene contact electrode for silicon carbide based ultraviolet photodetector. *Journal of Physics D: Applied Physics* 2015, 48 (9), 095104.
34. Tian, M.; Qu, L.; Zhang, X.; Zhang, K.; Zhu, S.; Guo, X.; Han, G.; Tang, X.; Sun, Y., Enhanced mechanical and thermal properties of regenerated cellulose/graphene composite fibers. *Carbohydrate polymers* 2014, 111, 456-462.
35. Novoselov, K. S.; Fal, V.; Colombo, L.; Gellert, P.; Schwab, M.; Kim, K., A roadmap for graphene. *Nature* 2012, 490 (7419), 192-200.
36. Choi, W.; Lahiri, I.; Seelaboyina, R.; Kang, Y. S., Synthesis of graphene and its applications: a review. *Critical Reviews in Solid State and Materials Sciences* 2010, 35 (1), 52-71.
37. Novoselov, K.; Neto, A. C., Two-dimensional crystals-based heterostructures: materials with tailored properties. *Physica Scripta* 2012, 2012 (T146), 014006.
38. Çelebi, C.; Yanık, C.; Demirkol, A. G.; Kaya, I. I., The effect of a SiC cap on the growth of epitaxial graphene on SiC in ultra high vacuum. *Carbon* 2012, 50 (8), 3026-3031.
39. Al-Temimy, A.; Riedl, C.; Starke, U., Low temperature growth of epitaxial graphene on SiC induced by carbon evaporation. *Applied Physics Letters* 2009, 95 (23), 231907.
40. Hass, J.; De Heer, W.; Conrad, E., The growth and morphology of epitaxial multilayer graphene. *Journal of Physics: Condensed Matter* 2008, 20 (32), 323202.

41. Muñoz, R.; Gómez- Aleixandre, C., Review of CVD synthesis of graphene. *Chemical Vapor Deposition* 2013, *19* (10-11-12), 297-322.
42. Shelton, J.; Patil, H.; Blakely, J., Equilibrium segregation of carbon to a nickel (111) surface: A surface phase transition. *Surface Science* 1974, *43* (2), 493-520.
43. Ueta, H.; Saida, M.; Nakai, C.; Yamada, Y.; Sasaki, M.; Yamamoto, S., Highly oriented monolayer graphite formation on Pt (111) by a supersonic methane beam. *Surface Science* 2004, *560* (1), 183-190.
44. Rut'kov, E.; Tontegode, A. Y., Interaction of silver atoms with iridium and with a two-dimensional graphite film on iridium: Adsorption, desorption, and dissolution. *Physics of the Solid State* 2004, *46* (2), 371-377.
45. Kumar, A.; Lee, C. H., Synthesis and biomedical applications of graphene: present and future trends. *Advances in Graphene Science* 2013, 5772-5578.
46. Reina Ceeco, A. Single-and few-layer graphene by ambient pressure chemical vapor deposition on nickel. Massachusetts Institute of Technology, 2010.
47. Yu, Q.; Lian, J.; Siriponglert, S.; Li, H.; Chen, Y. P.; Pei, S.-S., Graphene segregated on Ni surfaces and transferred to insulators. *Applied Physics Letters* 2008, *93* (11), 113103.
48. Celebi, K.; Cole, M.; Teo, K.; Park, H., Observations of early stage graphene growth on copper. *Electrochemical and Solid-State Letters* 2011, *15* (1), K1-K4.
49. Celebi, K. Chemical vapor deposition of graphene on copper. Diss., Eidgenössische Technische Hochschule ETH Zürich, Nr. 21458, 2013, 2013.
50. Gonçalves, R. V.; Wojcieszak, R.; Wender, H.; Sato B. Dias, C.; Vono, L. L.; Eberhardt, D.; Teixeira, S. R.; Rossi, L. M., Easy access to metallic copper nanoparticles with high activity and stability for CO oxidation. *ACS Applied Materials & Interfaces* 2015, *7* (15), 7987-7994.
51. Levendorf, M. P.; Ruiz-Vargas, C. S.; Garg, S.; Park, J., Transfer-free batch fabrication of single layer graphene transistors. *Nano Letters* 2009, *9* (12), 4479-4483.
52. Wood, J. D.; Schmucker, S. W.; Lyons, A. S.; Pop, E.; Lyding, J. W., Effects of polycrystalline Cu substrate on graphene growth by chemical vapor deposition. *Nano Letters* 2011, *11* (11), 4547-4554.
53. Yao, Y.; Feng, C.; Zhang, J.; Liu, Z., "Cloning" of single-walled carbon nanotubes via open-end growth mechanism. *Nano Letters* 2009, *9* (4), 1673-1677.
54. Tao, L.; Lee, J.; Chou, H.; Holt, M.; Ruoff, R. S.; Akinwande, D., Synthesis of high quality monolayer graphene at reduced temperature on hydrogen-enriched evaporated copper (111) films. *ACS Nano* 2012, *6* (3), 2319-2325.

55. Trinsoutrot, P.; Dardenne, L.; Vergnes, H.; Caussat, B., Graphene synthesis on copper from ethylene by Catalytic Chemical Vapor Deposition. *Surface and Coatings Technology, Elsevier* 2013, 230, 87-92.
56. Vlassiouk, I.; Regmi, M.; Fulvio, P.; Dai, S.; Datskos, P.; Eres, G.; Smirnov, S., Role of hydrogen in chemical vapor deposition growth of large single-crystal graphene. *ACS Nano* 2011, 5 (7), 6069-6076.
57. Wirtz, C.; Lee, K.; Hallam, T.; Duesberg, G. S., Growth optimisation of high quality graphene from ethene at low temperatures. *Chemical Physics Letters* 2014, 595, 192-196.
58. Agnoli, S.; Favaro, M., Doping graphene with boron: a review of synthesis methods, physicochemical characterization, and emerging applications. *Journal of Materials Chemistry A* 2016, 4 (14), 5002-5025.
59. Wang, X.; Li, X.; Zhang, L.; Yoon, Y.; Weber, P. K.; Wang, H.; Guo, J.; Dai, H., N-doping of graphene through electrothermal reactions with ammonia. *Science* 2009, 324 (5928), 768-771.
60. Wang, X.; Ouyang, Y.; Li, X.; Wang, H.; Guo, J.; Dai, H., Room-temperature all-semiconducting sub-10-nm graphene nanoribbon field-effect transistors. *Physical review letters* 2008, 100 (20), 206803.
61. Peres, N., Colloquium: The transport properties of graphene: An introduction. *Reviews of Modern Physics* 2010, 82 (3), 2673.
62. Tikhonenko, F.; Kozikov, A.; Savchenko, A.; Gorbachev, R., Transition between electron localization and antilocalization in graphene. *Physical Review Letters* 2009, 103 (22), 226801.
63. Zhang, J.; Li, J.; Wang, Z.; Wang, X.; Feng, W.; Zheng, W.; Cao, W.; Hu, P., Low-temperature growth of large-area heteroatom-doped graphene film. *Chemistry of Materials* 2014, 26 (7), 2460-2466.
64. Poh, H. L.; Šimek, P.; Sofer, Z. k.; Pumera, M., Sulfur-doped graphene via thermal exfoliation of graphite oxide in H₂S, SO₂, or CS₂ gas. *ACS Nano* 2013, 7 (6), 5262-5272.
65. Panchakarla, L.; Subrahmanyam, K.; Saha, S.; Govindaraj, A.; Krishnamurthy, H.; Waghmare, U.; Rao, C., Synthesis, structure and properties of boron and nitrogen doped graphene. *arXiv preprint arXiv:0902.3077* 2009.
66. Deifallah, M.; McMillan, P. F.; Corà, F., Electronic and structural properties of two-dimensional carbon nitride graphenes. *The Journal of Physical Chemistry C* 2008, 112 (14), 5447-5453.
67. Lin, Y.-C.; Lin, C.-Y.; Chiu, P.-W., Controllable graphene N-doping with ammonia plasma. *Applied Physics Letters* 2010, 96 (13), 133110.

68. Reddy, A. L. M.; Srivastava, A.; Gowda, S. R.; Gullapalli, H.; Dubey, M.; Ajayan, P. M., Synthesis of nitrogen-doped graphene films for lithium battery application. *ACS Nano* 2010, 4 (11), 6337-6342.
69. Wang, H.; Zhang, C.; Liu, Z.; Wang, L.; Han, P.; Xu, H.; Zhang, K.; Dong, S.; Yao, J.; Cui, G., Nitrogen-doped graphene nanosheets with excellent lithium storage properties. *Journal of Materials Chemistry* 2011, 21 (14), 5430-5434.
70. Wang, Y.; Shao, Y.; Matson, D. W.; Li, J.; Lin, Y., Nitrogen-doped graphene and its application in electrochemical biosensing. *ACS Nano* 2010, 4 (4), 1790-1798.
71. Zhang, C.; Fu, L.; Liu, N.; Liu, M.; Wang, Y.; Liu, Z., Synthesis of Nitrogen-Doped Graphene Using Embedded Carbon and Nitrogen Sources. *Advanced materials* 2011, 23 (8), 1020-1024.
72. Jeong, H. M.; Lee, J. W.; Shin, W. H.; Choi, Y. J.; Shin, H. J.; Kang, J. K.; Choi, J. W., Nitrogen-doped graphene for high-performance ultracapacitors and the importance of nitrogen-doped sites at basal planes. *Nano Letters* 2011, 11 (6), 2472-2477.
73. Bao, J. F.; Kishi, N.; Soga, T., Synthesis of nitrogen-doped graphene by the thermal chemical vapor deposition method from a single liquid precursor. *Materials Letters* 2014, 117, 199-203.
74. Wang, H.; Maiyalagan, T.; Wang, X., Review on recent progress in nitrogen-doped graphene: synthesis, characterization, and its potential applications. *ACS Catalysis* 2012, 2 (5), 781-794.
75. Iqbal, M.; Singh, A. K.; Iqbal, M.; Eom, J., Raman fingerprint of doping due to metal adsorbates on graphene. *Journal of Physics: Condensed Matter* 2012, 24 (33), 335301.
76. Das, A.; Pisana, S.; Chakraborty, B.; Piscanec, S.; Saha, S.; Waghmare, U.; Novoselov, K.; Krishnamurthy, H.; Geim, A.; Ferrari, A., Monitoring dopants by Raman scattering in an electrochemically top-gated graphene transistor. *Nature Nanotechnology* 2008, 3 (4), 210-215.
77. Khan, M. F.; Iqbal, M. Z.; Iqbal, M. W.; Eom, J., Improving the electrical properties of graphene layers by chemical doping. *Science and Technology of Advanced Materials* 2016.
78. Derycke, V.; Martel, R.; Appenzeller, J.; Avouris, P., Controlling doping and carrier injection in carbon nanotube transistors. *Applied Physics Letters* 2002, 80 (15), 2773-2775.
79. Schedin, F.; Geim, A.; Morozov, S.; Hill, E.; Blake, P.; Katsnelson, M.; Novoselov, K., Detection of individual gas molecules adsorbed on graphene. *Nature materials* 2007, 6 (9), 652-655.

80. Chen, W.; Chen, S.; Qi, D. C.; Gao, X. Y.; Wee, A. T. S., Surface transfer p-type doping of epitaxial graphene. *Journal of the American Chemical Society* 2007, *129* (34), 10418-10422.
81. Lin, T.; Huang, F.; Liang, J.; Wang, Y., A facile preparation route for boron-doped graphene, and its CdTe solar cell application. *Energy & Environmental Science* 2011, *4* (3), 862-865.
82. Yang, Z.; Yao, Z.; Li, G.; Fang, G.; Nie, H.; Liu, Z.; Zhou, X.; Chen, X. a.; Huang, S., Sulfur-doped graphene as an efficient metal-free cathode catalyst for oxygen reduction. *ACS Nano* 2011, *6* (1), 205-211.
83. Liu, H.; Liu, Y.; Zhu, D., Chemical doping of graphene. *Journal of Materials Chemistry* 2011, *21* (10), 3335-3345.
84. Qu, L.; Liu, Y.; Baek, J.-B.; Dai, L., Nitrogen-doped graphene as efficient metal-free electrocatalyst for oxygen reduction in fuel cells. *ACS Nano* 2010, *4* (3), 1321-1326.
85. Li, Y.; Zhao, Y.; Cheng, H.; Hu, Y.; Shi, G.; Dai, L.; Qu, L., Nitrogen-doped graphene quantum dots with oxygen-rich functional groups. *Journal of the American Chemical Society* 2011, *134* (1), 15-18.
86. Wei, D.; Liu, Y.; Wang, Y.; Zhang, H.; Huang, L.; Yu, G., Synthesis of N-doped graphene by chemical vapor deposition and its electrical properties. *Nano Letters* 2009, *9* (5), 1752-1758.
87. Gao, H.; Song, L.; Guo, W.; Huang, L.; Yang, D.; Wang, F.; Zuo, Y.; Fan, X.; Liu, Z.; Gao, W., A simple method to synthesize continuous large area nitrogen-doped graphene. *Carbon* 2012, *50* (12), 4476-4482.
88. Schiros, T.; Nordlund, D.; Pálová, L.; Prezzi, D.; Zhao, L.; Kim, K. S.; Wurstbauer, U.; Gutiérrez, C.; Delongchamp, D.; Jaye, C., Connecting dopant bond type with electronic structure in N-doped graphene. *Nano Letters* 2012, *12* (8), 4025-4031.
89. Lu, Y.-F.; Lo, S.-T.; Lin, J.-C.; Zhang, W.; Lu, J.-Y.; Liu, F.-H.; Tseng, C.-M.; Lee, Y.-H.; Liang, C.-T.; Li, L.-J., Nitrogen-doped graphene sheets grown by chemical vapor deposition: Synthesis and influence of nitrogen impurities on carrier transport. *ACS Nano* 2013, *7* (8), 6522-6532.
90. Wu, T.; Shen, H.; Sun, L.; Cheng, B.; Liu, B.; Shen, J., Nitrogen and boron doped monolayer graphene by chemical vapor deposition using polystyrene, urea and boric acid. *New Journal of Chemistry* 2012, *36* (6), 1385-1391.
91. Lambin, P.; Amara, H.; Ducastelle, F.; Henrard, L., Long-range interactions between substitutional nitrogen dopants in graphene: electronic properties calculations. *Physical Review B* 2012, *86* (4), 045448.

92. Nxumalo, E. N.; Coville, N. J., Nitrogen doped carbon nanotubes from organometallic compounds: a review. *Materials* 2010, 3 (3), 2141-2171.
93. Jin, Z.; Yao, J.; Kittrell, C.; Tour, J. M., Large-scale growth and characterizations of nitrogen-doped monolayer graphene sheets. *Acs Nano* 2011, 5 (5), 4112-4117.
94. Wang, C.; Yuen, M. F.; Ng, T. W.; Jha, S. K.; Lu, Z.; Kwok, S. Y.; Wong, T. L.; Yang, X.; Lee, C. S.; Lee, S. T., Plasma-assisted growth and nitrogen doping of graphene films. *Applied Physics Letters* 2012, 100 (25), 253107.
95. Luo, Z.; Lim, S.; Tian, Z.; Shang, J.; Lai, L.; MacDonald, B.; Fu, C.; Shen, Z.; Yu, T.; Lin, J., Pyridinic N doped graphene: synthesis, electronic structure, and electrocatalytic property. *Journal of Materials Chemistry* 2011, 21 (22), 8038-8044.
96. Park, S. H.; Chae, J.; Cho, M.-H.; Kim, J. H.; Yoo, K.-H.; Cho, S. W.; Kim, T. G.; Kim, J. W., High concentration of nitrogen doped into graphene using N₂ plasma with an aluminum oxide buffer layer. *Journal of Materials Chemistry C* 2014, 2 (5), 933-939.
97. Geng, D.; Chen, Y.; Chen, Y.; Li, Y.; Li, R.; Sun, X.; Ye, S.; Knights, S., High oxygen-reduction activity and durability of nitrogen-doped graphene. *Energy & Environmental Science* 2011, 4 (3), 760-764.
98. Li, X.; Wang, H.; Robinson, J. T.; Sanchez, H.; Diankov, G.; Dai, H., Simultaneous nitrogen doping and reduction of graphene oxide. *Journal of the American Chemical Society* 2009, 131 (43), 15939-15944.
99. Jafri, R. I.; Rajalakshmi, N.; Ramaprabhu, S., Nitrogen doped graphene nanoplatelets as catalyst support for oxygen reduction reaction in proton exchange membrane fuel cell. *Journal of Materials Chemistry* 2010, 20 (34), 7114-7117.
100. Shao, Y.; Zhang, S.; Engelhard, M. H.; Li, G.; Shao, G.; Wang, Y.; Liu, J.; Aksay, I. A.; Lin, Y., Nitrogen-doped graphene and its electrochemical applications. *Journal of Materials Chemistry* 2010, 20 (35), 7491-7496.
101. Kinoshita, K., Carbon: electrochemical and physicochemical properties. 1988.
102. Wei, D.; Peng, L.; Li, M.; Mao, H.; Niu, T.; Han, C.; Chen, W.; Wee, A. T. S., Low temperature critical growth of high quality nitrogen Doped graphene on dielectrics by plasma-enhanced chemical vapor deposition. *ACS Nano* 2015, 9 (1), 164-171.
103. Mukhopadhyay, S. M., Sample preparation for microscopic and spectroscopic characterization of solid surfaces and films. *Sample Preparation Techniques in Analytical Chemistry* 2003, 162 (9), 377-411.

104. Blake, P.; Hill, E.; Neto, A. C.; Novoselov, K.; Jiang, D.; Yang, R.; Booth, T.; Geim, A., Making graphene visible. *Applied Physics Letters* 2007, *91* (6), 063124.
105. Yi, C. Graphene Based Flexible Gas Sensors. Duke University, 2013.
106. Zan, R.; Ramasse, Q. M.; Jalil, R.; Bangert, U., Atomic structure of graphene and h-BN layers and their interactions with metals. *Advances in graphene science* 2013, 63.
107. Ferrari, A.; Meyer, J.; Scardaci, V., The Raman fingerprint of graphene [J]. *Physical Review Letters* 2006, *97*, 187401-187406.
108. Cunha, T.; Ek-Weis, J.; Lacerda, R.; Ferlauto, A., Graphene chemical vapor deposition at very low pressure: The impact of substrate surface self-diffusion in domain shape. *Applied Physics Letters* 2014, *105* (7), 073104.
109. Raman, C. V.; Krishnan, K. S., A new type of secondary radiation. *Nature* 1928, *121*, 501-502.
110. Friedbacher, G.; Bubert, H., *Surface and Thin Film Analysis: A Compendium of Principles, Instrumentation, and Applications*. John Wiley & Sons: 2011.
111. Ferrari, A. C., Raman spectroscopy of graphene and graphite: disorder, electron-phonon coupling, doping and nonadiabatic effects. *Solid State Communications* 2007, *143* (1), 47-57.
112. Beams, R.; Cançado, L. G.; Novotny, L., Raman characterization of defects and dopants in graphene. *Journal of Physics: Condensed Matter* 2015, *27* (8), 083002.
113. Ferrari, A. C.; Basko, D. M., Raman spectroscopy as a versatile tool for studying the properties of graphene. *Nature Nanotechnology* 2013, *8* (4), 235-246.
114. Pimenta, M.; Dresselhaus, G.; Dresselhaus, M. S.; Cancado, L.; Jorio, A.; Saito, R., Studying disorder in graphite-based systems by Raman spectroscopy. *Physical Chemistry Chemical Physics* 2007, *9* (11), 1276-1290.
115. Malard, L.; Pimenta, M.; Dresselhaus, G.; Dresselhaus, M., Raman spectroscopy in graphene. *Physics Reports* 2009, *473* (5), 51-87.
116. Zafar, Z.; Ni, Z. H.; Wu, X.; Shi, Z. X.; Nan, H. Y.; Bai, J.; Sun, L. T., Evolution of Raman spectra in nitrogen doped graphene. *Carbon* 2013, *61*, 57-62.
117. Tsukamoto, T.; Yamazaki, K.; Komurasaki, H.; Ogino, T., Effects of surface chemistry of substrates on Raman spectra in graphene. *The Journal of Physical Chemistry C* 2012, *116* (7), 4732-4737.

118. Wang, Y. Y.; Ni, Z. H.; Yu, T.; Shen, Z. X.; Wang, H. M.; Wu, Y. H.; Chen, W.; Shen Wee, A. T., Raman studies of monolayer graphene: the substrate effect. *The Journal of Physical Chemistry C* 2008, *112* (29), 10637-10640.
119. Graf, D.; Molitor, F.; Ensslin, K.; Stampfer, C.; Jungen, A.; Hierold, C.; Wirtz, L., Raman mapping of a single-layer to double-layer graphene transition. *The European Physical Journal Special Topics* 2007, *148* (1), 171-176.
120. Lv, R.; Li, Q.; Botello-Méndez, A. R.; Hayashi, T.; Wang, B.; Berkdemir, A.; Hao, Q.; Elías, A. L.; Cruz-Silva, R.; Gutiérrez, H. R., Nitrogen-doped graphene: beyond single substitution and enhanced molecular sensing. *Scientific Reports* 2012, *2*.
121. Yu, T.; Ni, Z.; Du, C.; You, Y.; Wang, Y.; Shen, Z., Raman mapping investigation of graphene on transparent flexible substrate: The strain effect. *The Journal of Physical Chemistry C* 2008, *112* (33), 12602-12605.
122. Seo, H.-K.; Kim, T.-S.; Park, C.; Xu, W.; Baek, K.; Bae, S.-H.; Ahn, J.-H.; Kim, K.; Choi, H. C.; Lee, T.-W., Value-added synthesis of graphene: recycling industrial carbon waste into electrodes for high-performance electronic devices. *Scientific Reports* 2015, *5*.
123. Rybin, M.; Pereyaslavtsev, A.; Vasilieva, T.; Myasnikov, V.; Sokolov, I.; Pavlova, A.; Obraztsova, E.; Khomich, A.; Ralchenko, V.; Obraztsova, E., Efficient nitrogen doping of graphene by plasma treatment. *Carbon* 2016, *96*, 196-202.
124. Zhao, R.; Afaneh, T.; Dharmasena, R.; Jasinski, J.; Sumanasekera, G.; Henner, V., Study of nitrogen doping of graphene via in-situ transport measurements. *Physica B: Condensed Matter* 2016, *490*, 21-24.
125. Fujimoto, Y., Formation, Energetics, and Electronic Properties of Graphene Monolayer and Bilayer Doped with Heteroatoms. *Advances in Condensed Matter Physics* 2015, *2015*.
126. Zhang, J.; Zhao, C.; Liu, N.; Zhang, H.; Liu, J.; Fu, Y. Q.; Guo, B.; Wang, Z.; Lei, S.; Hu, P., Tunable electronic properties of graphene through controlling bonding configurations of doped nitrogen atoms. *Scientific Reports* 2016, *6*.
127. Tison, Y.; Lagoute, J. r. m.; Repain, V.; Chacon, C.; Girard, Y.; Rousset, S.; Joucken, F.; Sharma, D.; Henrard, L.; Amara, H., Electronic interaction between nitrogen atoms in doped graphene. *ACS Nano* 2015, *9* (1), 670-678.
128. Zhao, L.; He, R.; Rim, K. T.; Schiros, T.; Kim, K. S.; Zhou, H.; Gutiérrez, C.; Chockalingam, S.; Arguello, C. J.; Pálová, L.; Nordlund, D. ; Hybertsen, M. ; Reichman D. ; Heinz, T.; Kim, P. ; Pinczuk, A. ; Flynn, K. ;and Pasupathy, A., Visualizing individual nitrogen dopants in monolayer graphene. *Science* 2011, *333* (6045), 999-1003.

129. Joucken, F.; Tison, Y.; Le Fèvre, P.; Tejada, A.; Taleb-Ibrahimi, A.; Conrad, E.; Repain, V.; Chacon, C.; Bellec, A.; Girard, Y., Charge transfer and electronic doping in nitrogen-doped graphene. *Scientific Reports* 2015, 5.
130. Nonnenmacher, M.; o'Boyle, M.; Wickramasinghe, H., Kelvin probe force microscopy. *Applied Physics Letters* 1991, 58 (25), 2921-2923.
131. Yu, Y.-J.; Zhao, Y.; Ryu, S.; Brus, L. E.; Kim, K. S.; Kim, P., Tuning the graphene work function by electric field effect. *Nano Letters* 2009, 9 (10), 3430-3434.
132. Ziegler, D.; Gava, P.; Güttinger, J.; Molitor, F.; Wirtz, L.; Lazzeri, M.; Saitta, A.; Stemmer, A.; Mauri, F.; Stampfer, C., Variations in the work function of doped single-and few-layer graphene assessed by Kelvin probe force microscopy and density functional theory. *Physical Review B* 2011, 83 (23), 235434.
133. Zeng, J.-J.; Lin, Y.-J., Tuning the work function of graphene by nitrogen plasma treatment with different radio-frequency powers. *Applied Physics Letters* 2014, 104 (23), 233103.
134. Reina, A.; Jia, X.; Ho, J.; Nezich, D.; Son, H.; Bulovic, V.; Dresselhaus, M. S.; Kong, J., Large area, few-layer graphene films on arbitrary substrates by chemical vapor deposition. *Nano Letters* 2008, 9 (1), 30-35.
135. Park, J.; Reina, A.; Saito, R.; Kong, J.; Dresselhaus, G.; Dresselhaus, M., G' band Raman spectra of single, double and triple layer graphene. *Carbon* 2009, 47 (5), 1303-1310.
136. Özçeri, E., Influence of Ni thin flim structural properties over graphene growth by CVD. 2013.
137. Lenski, D. R.; Fuhrer, M. S., Raman and optical characterization of multilayer turbostratic graphene grown via chemical vapor deposition. *Journal of Applied Physics* 2011, 110 (1), 013720.
138. Ren, Y.; Zhu, C.; Cai, W.; Li, H.; Hao, Y.; Wu, Y.; Chen, S.; Wu, Q.; Piner, R. D.; Ruoff, R. S., An improved method for transferring graphene grown by chemical vapor deposition. *Nano* 2012, 7 (01), 1150001.
139. Her, M.; Beams, R.; Novotny, L., Graphene transfer with reduced residue. *Physics Letters A* 2013, 377 (21), 1455-1458.
140. Lin, Y.-C.; Lu, C.-C.; Yeh, C.-H.; Jin, C.; Suenaga, K.; Chiu, P.-W., Graphene annealing: how clean can it be? *Nano Letters* 2011, 12 (1), 414-419.
141. Hu, B.; Wei, Z.; Ago, H.; Jin, Y.; Xia, M.; Luo, Z.; Pan, Q.; Liu, Y., Effects of substrate and transfer on CVD-grown graphene over sapphire-induced Cu films. *Science China Chemistry* 2014, 57 (6), 895-901.

142. Jang, C. W.; Kim, J. H.; Kim, J. M.; Shin, D. H.; Kim, S.; Choi, S.-H., Rapid-thermal-annealing surface treatment for restoring the intrinsic properties of graphene field-effect transistors. *Nanotechnology* 2013, 24 (40), 405301.
143. Dan, Y.; Lu, Y.; Kybert, N. J.; Luo, Z.; Johnson, A. C., Intrinsic response of graphene vapor sensors. *Nano Letters* 2009, 9 (4), 1472-1475.
144. Demirbaş, T.; Baykara, M. Z., Nanoscale tribology of graphene grown by chemical vapor deposition and transferred onto silicon oxide substrates. *Journal of Materials Research* 2016, (31), 1914-1923.
145. Podila, R.; Chacón-Torres, J.; Spear, J.; Pichler, T.; Ayala, P.; Rao, A. M., Spectroscopic investigation of nitrogen doped graphene. *Applied Physics Letters* 2012, 101 (12), 123108.
146. Tomak, A.; Bacaksiz, C.; Mendirek, G.; Sahin, H.; Hur, D.; Görgün, K.; Senger, R.; Birer, Ö.; Peeters, F.; Zareie, H., Structural changes in a Schiff base molecular assembly initiated by scanning tunneling microscopy tip. *Nanotechnology* 2016, 27 (33), 335601.
147. Gao, L., Probing Electronic Properties of Graphene on the Atomic Scale by Scanning Tunneling Microscopy and Spectroscopy. *Graphene and 2D Materials* 2014, 1 (1).
148. Sławińska, J.; Zasada, I., Fingerprints of Dirac points in first-principles calculations of scanning tunneling spectra of graphene on a metal substrate. *Physical Review B* 2011, 84 (23), 235445.
149. Jung, S.; Rutter, G. M.; Klimov, N. N.; Newell, D. B.; Calizo, I.; Hight-Walker, A. R.; Zhitenev, N. B.; Stroscio, J. A., Evolution of microscopic localization in graphene in a magnetic field from scattering resonances to quantum dots. *Nature Physics* 2011, 7 (3), 245-251.
150. Nirmalraj, P.; Thompson, D.; Molina-Ontoria, A.; Sousa, M.; Martín, N.; Gotsmann, B.; Riel, H., Nanoelectrical analysis of single molecules and atomic-scale materials at the solid/liquid interface. *Nature materials* 2014, 13 (10), 947-953.
151. Barja, S.; Wickenburg, S.; Liu, Z.-F.; Zhang, Y.; Ryu, H.; Ugeda, M. M.; Hussain, Z.; Shen, Z.-X.; Mo, S.-K.; Wong, E., Charge density wave order in 1D mirror twin boundaries of single-layer MoSe₂. *Nature Physics* 2016.
152. Perdew, J. P.; Burke, K.; Ernzerhof, M., Generalized gradient approximation made simple. *Physical Review Letters* 1996, 77 (18), 3865.
153. Perdew, J. P.; Burke, K.; Ernzerhof, M., Emission in symmetric heavy ion reactions at subthreshold energies. *Physical Review Letters* 1997, 78, 1396.

154. Kresse, G.; Hafner, J., Ab initio molecular dynamics for open-shell transition metals. *Physical Review B* 1993, 48 (17), 13115.
155. Kresse, G.; Hafner, J., Ab initio molecular-dynamics simulation of the liquid-metal–amorphous-semiconductor transition in germanium. *Physical Review B* 1994, 49 (20), 14251.
156. Grimme, S., Semiempirical GGA- type density functional constructed with a long- range dispersion correction. *Journal of computational chemistry* 2006, 27 (15), 1787-1799.
157. Henkelman, G.; Arnaldsson, A.; Jónsson, H., A fast and robust algorithm for Bader decomposition of charge density. *Computational Materials Science* 2006, 36 (3), 354-360.
158. Beerbom, M.; Lägél, B.; Cascio, A.; Doran, B.; Schlaf, R., Direct comparison of photoemission spectroscopy and in situ Kelvin probe work function measurements on indium tin oxide films. *Journal of electron spectroscopy and related phenomena* 2006, 152 (1), 12-17.
159. Yu, T.; Wang, F.; Xu, Y.; Ma, L.; Pi, X.; Yang, D., Graphene Coupled with Silicon Quantum Dots for High- Performance Bulk- Silicon- Based Schottky- Junction Photodetectors. *Advanced Materials* 2016, 28 (24), 4912-4919.
160. Akada, K.; Terasawa, T.-o.; Imamura, G.; Obata, S.; Saiki, K., Control of work function of graphene by plasma assisted nitrogen doping. *Applied Physics Letters* 2014, 104 (13), 131602.
161. Tongay, S.; Lemaitre, M.; Miao, X.; Gila, B.; Appleton, B.; Hebard, A., Rectification at graphene-semiconductor interfaces: zero-gap semiconductor-based diodes. *Physical Review X* 2012, 2 (1), 011002.